

---

Electronic Thesis and Dissertation Repository

---

12-11-2017 1:30 PM

## Optical Fibre-based Force Sensing Needle Driver for Minimally Invasive Surgery

Pouya Soltani Zarrin, *The University of Western Ontario*

Supervisor: Trejos, Ana Luisa, *The University of Western Ontario*

: Patel, Rajni V., *The University of Western Ontario*

A thesis submitted in partial fulfillment of the requirements for the Master of Engineering Science degree in Biomedical Engineering

© Pouya Soltani Zarrin 2017

Follow this and additional works at: <https://ir.lib.uwo.ca/etd>



Part of the [Biomedical Devices and Instrumentation Commons](#)

---

### Recommended Citation

Soltani Zarrin, Pouya, "Optical Fibre-based Force Sensing Needle Driver for Minimally Invasive Surgery" (2017). *Electronic Thesis and Dissertation Repository*. 5065.

<https://ir.lib.uwo.ca/etd/5065>

This Dissertation/Thesis is brought to you for free and open access by Scholarship@Western. It has been accepted for inclusion in Electronic Thesis and Dissertation Repository by an authorized administrator of Scholarship@Western. For more information, please contact [wlsadmin@uwo.ca](mailto:wlsadmin@uwo.ca).

# Optical Fibre-based Force Sensing Needle Driver for Minimally Invasive Surgery

Pouya Soltani Zarrin

Master's Thesis, 2017

Department of Biomedical Engineering  
The University of Western Ontario

## Abstract

Minimally Invasive Surgery (MIS) has been limited from its inception by insufficient haptic feedback to surgeons. The loss of haptic information threatens patient's safety and results in longer operation times. To address this problem, various force sensing systems have been developed to provide information about tool-tissue interaction forces. However, the provided results for axial and grasping forces have been inaccurate in most of these studies due to considerable amount of error and uncertainty in their force acquisition method. Furthermore, sterilizability of the sensorized instruments plays a pivotal role in accurate measurement of forces inside a patient's body. Nonetheless, none of the force sensing devices described in the literature can be fully cleaned or sterilized for use inside a patient's body during a surgery.

The objective of this thesis was to develop a sterilizable needle-driver type grasper using fibre Bragg gratings. In order to measure more accurate and reliable tool-tissue interaction forces, optical force sensors were integrated in the grasper jaw to measure axial and grasping forces directly at their exertion point on the tool tip. Two sets of sensor prototypes were developed to prove the feasibility of the proposed concept. Implementation of this concept into a needle-driver instrument resulted in the final proposed model of the sensorized laparoscopic instrument. Fibre Bragg gratings were used for measuring forces due to their many advantages for this application such as small size, sterilizability and high sensitivity. Visual force feedback was provided for users based on the acquired real-time force data. Improvement and consideration points related to the current work were identified and potential areas to continue this project in the future are discussed.

**Keywords:** Sterilizable force sensing instrument, minimally invasive surgery; force sensing; fibre Bragg gratings.

*Dedicated to:*  
*My father,*  
*who never hesitated to sacrifice himself for our family.*

# Acknowledgements

I would like to express my sincerest gratitude to my supervisors Dr. Ana Luisa Trejos and Dr. Rajni V. Patel for their countless support and help with this project. With their help, I learned the fundamental principles of doing research and I was able to expand my knowledge in the field of engineering. Without their encouragement and guidance, this journey would never have had an ending.

This work was supported by the Ontario Research Fund—Research Excellence Grant RE-05-049, by the Natural Sciences and Engineering Research Council (NSERC) of Canada under grant RGPIN-2014-03815 and RGPIN-2012-1345; and by infrastructure grants from the Canada Foundation for Innovation awarded to the London Health Sciences Centre (Canadian Surgical Technologies & Advanced Robotics (CSTAR)) and to The University of Western Ontario (Western).

I have been fortunate to be part of CSTAR lab at Western University with its outstanding personnel and long history of academic and research excellence. This work would have not been possible without facilities and resources provided for researchers at CSTAR. I have had the full support from my colleagues with technical and administrative issues the whole time. Therefore, I would like to thank all of the staff at CSTAR for their help and support, especially Dr. Michael Naish, Dr. Ran Xu, Christopher Ward for their priceless help with the instrument design.

Finally, my special thanks go out to Abelardo Escoto, who assisted me with various parts of this project including the mechanical development of the instrument, as well as programming. His endless support and help throughout this work is truly appreciated. I would like to acknowledge Kevin Barker for his precious help with micro-welding of the instrument prototypes. His help, wisdom and enthusiasm during this project was heart-warming and it is really appreciated.



# Contents

<b>Abstract</b>	<b>ii</b>
<b>Acknowledgements</b>	<b>iv</b>
<b>Table of Contents</b>	<b>v</b>
<b>List of Figures</b>	<b>ix</b>
<b>List of Tables</b>	<b>xii</b>
<b>Nomenclature and Acronyms</b>	<b>xiii</b>
<b>1 Introduction</b>	<b>1</b>
1.1 Motivation . . . . .	1
1.2 Research Objectives . . . . .	2
1.3 Scope of Research . . . . .	3
1.4 Overview of the Thesis . . . . .	3
<b>2 Literature Review</b>	<b>5</b>
2.1 Introduction . . . . .	5
2.2 Force Sensing in MIS . . . . .	7
2.3 Required Force Information in MIS . . . . .	8
2.3.1 The sensor location . . . . .	10

---

2.3.2	Essential force directions in MIS . . . . .	13
2.3.2.1	Grasping force sensing in MIS . . . . .	14
2.3.2.2	Axial force sensing in MIS . . . . .	17
2.3.2.3	Lateral forces and bending moment sensing in MIS . . . . .	19
2.3.2.4	Torsion sensing in MIS . . . . .	21
2.4	Force Sensing Technologies in MIS . . . . .	22
2.4.1	Strain gauges . . . . .	23
2.4.2	Capacitive Sensors . . . . .	23
2.4.3	Piezoelectric Sensors . . . . .	24
2.4.4	Optical Fibre-based Sensors . . . . .	24
2.4.4.1	FBG Working and Sensing Principle . . . . .	26
2.4.4.2	FBG Temperature Compensation Methods . . . . .	27
2.4.4.3	Optical Interrogation System . . . . .	29
2.4.4.4	Manufacturing Methods of Sensing System . . . . .	29
2.5	Different Feedback Methods . . . . .	30
2.6	Mechatronics and Robotics in MIS . . . . .	31
2.7	FDA and Health Canada Medical Device Regulation . . . . .	31
2.8	Force Sensor Design Specifications . . . . .	35
2.9	Research Motivation and Objectives . . . . .	38
<b>3</b>	<b>First Generation of Sensor Prototype</b>	<b>40</b>
3.1	Introduction . . . . .	40
3.2	Design Specifications . . . . .	40
3.3	Mechanical Design of the Partial Prototype . . . . .	41
3.4	Finite Element Simulation . . . . .	44
3.5	Sensor Fabrication and Prototyping . . . . .	46
3.6	Data Acquisition . . . . .	49
3.7	Calibration . . . . .	50
3.7.1	Calibration Setup . . . . .	50

---

3.7.2	Calibration Method . . . . .	51
3.8	Sensor Performance Assessment . . . . .	53
3.9	Results and Discussion . . . . .	53
3.9.1	Conclusion . . . . .	55
<b>4</b>	<b>Second Generation of Sensor Prototype</b>	<b>57</b>
4.1	Introduction . . . . .	57
4.2	Design Solutions . . . . .	57
4.2.1	Introduction . . . . .	57
4.2.2	Finite Element Analysis . . . . .	61
4.3	Sensor Fabrication and Prototyping . . . . .	64
4.4	Calibration Setup Solutions . . . . .	66
4.4.1	Introduction . . . . .	66
4.4.2	Grasping Setup . . . . .	67
4.4.3	Axial Setup . . . . .	68
4.5	Results and Discussion . . . . .	69
4.5.1	Conclusion . . . . .	70
<b>5</b>	<b>Integration of the Novel Force Sensing Design into the Full Instrument Prototype</b>	<b>73</b>
5.1	Introduction . . . . .	73
5.2	Design Specifications . . . . .	73
5.3	Mechanical Design of the Partial Prototype . . . . .	74
5.4	Sensor Fabrication and Prototyping . . . . .	76
5.5	Results and Discussion . . . . .	77
<b>6</b>	<b>Conclusion and Future Work</b>	<b>79</b>
6.1	Introduction . . . . .	79
6.2	Contributions . . . . .	80
6.3	Future Work . . . . .	81
	<b>Bibliography</b>	<b>82</b>

<b>Appendices</b>	<b>100</b>
<b>A Expanded Views and Technical Drawings</b>	<b>100</b>
<b>B Permissions and Approvals</b>	<b>114</b>
<b>Curriculum Vitae</b>	<b>127</b>

# List of Figures

2.1	MIS vs. Open surgery . . . . .	6
2.2	Force sensing instruments in MIS . . . . .	9
2.3	Forces acting on minimally invasive instruments . . . . .	11
2.4	The transmitted light source through the FBG . . . . .	27
2.5	The substantial equivalence process flow chart . . . . .	33
2.6	Evaluation of automatic Class III designation process . . . . .	34
3.1	Mechanical behavior of various materials . . . . .	41
3.2	CAD model of the sensorized grasper . . . . .	43
3.3	The deformable part to slide over the fixed part . . . . .	43
3.4	FEA in 2D-ANSYS. . . . .	45
3.5	FEA in 3D-ANSYS . . . . .	45
3.6	SLM printed parts . . . . .	46
3.7	EDM machining . . . . .	47
3.8	Assembly of EDM fabricated pieces . . . . .	47
3.9	The welded grasper . . . . .	48
3.10	Assembled and welded parts . . . . .	49
3.11	Custom-made user interface . . . . .	50
3.12	Setup for calibrating the grasping and axial force sensors. . . . .	51
3.13	Relationship between the FBG wavelength and the F/T sensor values . . . . .	52
3.14	Comparison of force data obtained by the ATI force sensor and FBG sensors . . . . .	54

---

4.1	CAD model of the second generation of the grasper . . . . .	59
4.2	Synchronous sliding of the top and bottom graspers . . . . .	60
4.3	An I-shaped grasper . . . . .	61
4.4	Strain generated by a 5 N force on the grasper . . . . .	62
4.5	Strain generated over the axial FBGs . . . . .	63
4.6	The FEA results for strain and stress . . . . .	64
4.7	Installation of FBG fibres . . . . .	65
4.8	Adhesives and superglue . . . . .	66
4.9	Linear regression fitted line . . . . .	67
4.10	Calibration setups . . . . .	68
4.11	Setup for exerting forces on different locations on the grasper jaw . . . . .	69
4.12	Comparison of the results from the FBGs and the F/T sensors . . . . .	72
5.1	CAD model of the sensorized laparoscopic needle-driver . . . . .	75
5.2	Mechanism and working principles of the final sensorized instrument . . . . .	76
5.3	Sensorized needle-driver with an I-shaped grasper . . . . .	77
5.4	3 FBG sensors at 120° arrangements . . . . .	78
A.1	1st prototype of the sensorized grasper . . . . .	101
A.2	Expanded view of the 1st prototype of the sensorized grasper . . . . .	101
A.3	Lower jaw handle of 1st sensorized grasper . . . . .	102
A.4	Fixed part of the lower jaw of the 1st sensorized grasper . . . . .	103
A.5	Moving part of the lower jaw of the 1st sensorized grasper . . . . .	104
A.6	2nd prototype of the sensorized grasper . . . . .	105
A.7	Expanded view of the 2nd prototype of the sensorized grasper . . . . .	105
A.8	Fixed part of the lower jaw of the 2nd sensorized grasper . . . . .	106
A.9	Moving part of the lower jaw of the 2nd sensorized grasper . . . . .	107
A.10	Final prototype of the sensorized instrument . . . . .	108
A.11	Expanded view of the final prototype of the sensorized instrument . . . . .	108
A.12	Fixed part of the lower jaw of the final sensorized instrument . . . . .	109

---

A.13	Moving part of the lower jaw of the final sensorized instrument . . . . .	110
A.14	Actuation shaft of the lower jaw of the final sensorized instrument . . . . .	111
A.15	Connection link for the crank-slider mechanism . . . . .	112
A.16	Upper jaw of the final sensorized instrument . . . . .	113
B.1	Online permission for Figure 2.1 . . . . .	115
B.2	Online permission for Figure 2.2 (a) . . . . .	116
B.3	Online permission for Figure 2.2 (b) . . . . .	117
B.4	Online permission for Figure 2.2 (c) . . . . .	118
B.5	Online permission for Figure 2.2 (d) . . . . .	119
B.6	Online permission for Figure 2.2 (e) . . . . .	120
B.7	Online permission for Figure 2.2 (f) . . . . .	121
B.8	Online permission for Figure 2.2 (g) . . . . .	122
B.9	Online permission for Figure 2.2 (h) . . . . .	123
B.10	Online permission for Figure 2.3 . . . . .	124
B.11	Online permission for Figure 2.4 . . . . .	125
B.12	Online permission for Figures 3.2 – 3.14 . . . . .	126

# List of Tables

- 2.1 Average mechanical efficiency (ME) of four commercialized laparoscopic instruments . . . 12
- 3.1 Summary of design specifications . . . . . 42
- 3.2 Performance of the first generation of the sensorized grasper . . . . . 55
- 4.1 Performance of the second generation of the sensorized grasper . . . . . 71



# Nomenclature and Acronyms

## Acronyms

2D	Two-Dimensional
3D	Three-Dimensional
ADEISS	Additive Design in Surgical Solutions
CAD	Computer Aided Design
CNC	Computer Numerical Control
CSTAR	Canadian Surgical Technologies and Advanced Robotics
DOF	Degrees of Freedom
EDM	Electrical Discharge Machining
EM	Electro Magnetic
FBG	Fiber Bragg Grating
FDA	Food and Drug Administration
FDAMA	FDA Modernization Act
FEA	Finite Element Analysis
FOS	Fiber Optic Sensors
FPI	Fabry–Perot Interference
F/T	Force/Torque
GFRP	Glass Fibre Reinforced Plastic

---

GUI	Graphical User Interface
ID	Inner Diameter
ME	Mechanical Efficiency
MIS	Minimally Invasive Surgery
MRI	Magnetic Resonance Imaging
NSE	Not Substantially Equivalent
OD	Outer Diameter
OR	Operation Room
PCF	Photonic Crystal Fiber
PDP	Product Development Protocol
PMA	Premarket Approval
PVDF	Polyvinylidene Fluoride
SDM	Shape Deposition Manufacturing
SG	Strain Gauges
SLM	Selective Laser Melting
RMS	Root Mean Square
UV	Ultraviolet
VF	Virtual Fixtures

## Variables

$y$	Distance from the surface of the neutral surface
$I$	Moment of inertia
$M$	Moment
$L$	Distance of the strain measurement location from the tip
$F$	Force

---

$E$	Modulus of elasticity (Young's Modulus)
$K_\varepsilon$	Strain bulk modulus
$K_t$	Temperature bulk modulus
$G$	Shear modulus
$\varphi$	Angle of twist
$\Delta\lambda_i$	Wavelength shift induced by temperature change
$k$	Slope of the linear dependence between temperature gradient and wavelength change
$J$	Polar moment of inertia
$r$	Shaft radius
$T$	Torque
$\tau$	Shear stress
$\eta$	Strain transfer ratios from the surface to fibers
$\varepsilon_a$	Axial strain
$\varepsilon_{max}$	Maximum bending strain
$\sigma$	Stress
$\sigma_{max}$	Maximum stress
$R$	Radius of curvature
$Ra$	Surface finish roughness ( $\mu m$ )
$\alpha$	Angle of rotation
$\varepsilon_t$	Thermal strain
$h$	Helix design pitch
$b$	Bending radius of fibers
$C$	Capacitance
$A$	Overlapping area
$\varepsilon_0$	Relative permittivity of free space
$\varepsilon_r$	Relative permittivity of the dielectric material

---

$d$	Distance between capacitor plates
$\lambda_B$	Reflectivity of Bragg wavelength
$n_{eff}$	Effective refractive index
$\Lambda$	Grating pitch
$\Delta\lambda_B$	Wavelength shift
$\varepsilon$	Mechanical strain
$x, y, z$	Cartesian coordinates corresponding to bending (x, y) and axial (z)
$t$	Temperature

## Units

cm	centimeters
mm	millimeters
$\mu\text{m}$	micrometers
nm	nanometers
Nm	Newton-meters
Kg	Kilograms
KPa	KiloPascals
GPa	GigaPascals
Hz	Hertz
mN	milinewtons
N	Newtons
s	Seconds
$^{\circ}\text{C}$	degree celsius
$\mu\varepsilon$	microstrain

# Chapter 1

## Introduction

### 1.1 Motivation

Minimally Invasive Surgery (MIS) is a modern method of surgery performed via small incisions on a patient's body. MIS has been proven to be a desirable alternative to traditional open surgery due to its considerable benefits. The advantages of MIS for patients are less trauma, faster recovery, shorter hospital stay, better cosmesis and less post-operative pain [1]. However, all of these benefits come at the cost of significant difficulties for surgeons during surgical operations. Disadvantages of this method are the complexity and difficulty of conducting MIS, caused by the challenging removal of bulky organs, the degraded dexterity, the reversal of hand movements and the loss of the sense of touch (diminished haptic feedback). These drawbacks result in longer operation times, make it difficult for novice surgeons to learn, and cause discomfort for expert surgeons [2]. In particular, the lack of kinesthetic and tactile information significantly impairs the performance of surgeons [3]. For instance, the absence of proper force information makes it difficult to assess anatomical structures of body organs to detect abnormalities, such as tumours. Excessive force exertion during MIS can cause tissue trauma and internal bleeding [2, 4]. On the other hand, applying insufficient force can cause needle slippage during suturing and tissue slippage during tissue dissection [2, 5]. Therefore, providing information on tool–tissue interaction forces can notably increase patient safety and make MIS easier for surgeons [6]. In addition, the availability of force information may be used to develop automated surgical robots and virtual reality simulators for training and skills assessment [3, 5, 7].

## 1.2 Research Objectives

Over the past few decades, several researchers have investigated sensorization of MIS instruments to provide tool–tissue interaction force information to users. Although clinical studies to determine what force information is required in different MIS procedures have yet to be performed, it is recognized that the main degrees of freedom (DOF) to sensorize are grasping, the three Cartesian forces (axial and the two lateral forces) and torsion about the instrument axis. However, information on grasping and axial forces play a pivotal role to make MIS operations easier for surgeons [8]. Grasping force information may be used for tissue dissection and palpation purposes. For the suturing and knot tying tasks, integrating axial and grasping force sensors into needle drivers would help surgeons to ensure that knots are tightened properly, and prevent suture breakage and needle slippage [9]. The specific size constraint of the entry port for MIS instruments, the trocar, limits the size of the sensors that can be used for this application. In addition, sterilizability requirements, such as those needed to autoclave sterilization, should be considered in sensor selection. Furthermore, the location of the sensors on the instrument affects the authenticity of the measured force information. The internal friction inside the instruments, friction between the tool and the trocar, and forces and torques generated by the surrounding organs and the abdominal wall affect any force measurement outside of the trocar. Any force measurement acquired from outside of a patient’s body is an inaccurate indicator of the real tool–tissue interaction forces. As a result, integrating force sensors on the tool tip is necessary to achieve the most accurate results. However, size constraints on the instrument tip make the fabrication process of the instrument very complex and challenging. By taking into account the aforementioned issues, the objectives of this thesis are as follows:

- To design and develop a sterilizable laparoscopic grasper capable of measuring axial and grasping forces at the tool tip.
- To use optical fibre force sensors for the instrument sensorization due to their high sensitivity, small size and sterilizability.
- To test the developed prototypes in order to evaluate their performance in providing accurate force information and to identify areas of improvement and points of consideration regarding the concept of direct force measurement.

- To develop a user-friendly interface for sensor calibration and performance assessment.
- To implement the novel direct force sensing concept into a complete laparoscopic instrument.

### 1.3 Scope of Research

Current research projects at Canadian Surgical Technologies and Advanced Robotics (CSTAR) are scrutinizing the importance of presence of haptic feedback in surgical operations. It has been identified that providing tool–tissue interaction forces notably enhances surgeons’ performance during MIS operations. Moreover, the acquired force information is used to develop surgical simulators and skill assessment metrics. This thesis however investigates the possibility of acquiring grasping and axial force information at their exertion point. The specific focus of this thesis is on mechanically development of a sensorized laparoscopic needle-driver to provide real-time grasping and axial force information. In this work, design and fabrication limitations regarding the integration of force sensors inside a restricted needle-driver grasper have been studied and solved. In previous projects conducted in CSTAR, laparoscopic instruments were sensorized using strain gauge sensors [8]. However, implementation of strain gauges on the tool tip was not possible due to their bulky size. As a result, this thesis investigates the development process for a 5-DOF laparoscopic needle-driver equipped with Fibre Bragg Grating (FBG) sensors. Although this work relies on literature that providing force information on axial and grasping directions is of a great importance for surgeons [8], upon the completion of this instrument further trials could be conducted to elaborate the impact of the presence of this information on surgeons’ performance.

### 1.4 Overview of the Thesis

The structure of this thesis is summarized in the outline below:

**Chapter 1** Introduction: The introductory chapter.

**Chapter 2** Literature Review: Introduces the state-of-the-art in sensorized laparoscopic instruments and background work on optical fibre-based sensing systems.

**Chapter 3** First Generation of Sensing Prototype: Presents the mechanical development of the first partial prototype and its performance evaluation, as well as calibration process.

**Chapter 4** Second Generation of Sensing Prototype: Presents the mechanical development of the second partial prototype and its performance evaluation, as well as calibration process.

**Chapter 5** Final Generation of Sensing Prototype: Presents the mechanical modeling of the final 5-DOF instrument.

**Chapter 6** Concluding Remarks: Highlights the contributions of this work and the expected developments and modifications as future work.

**Appendix I** CAD Modeling and Evaluated Design Concepts

**Appendix II** Permissions and Approvals



## Chapter 2

# Literature Review

### 2.1 Introduction

Since the dawn of surgical operations, bleeding, infection and pain have been an inevitable part of every surgical procedure. Conventional open surgery requires a large incision to provide enough space for the surgery to take place. Large wounds that result from open surgery cause a great deal of post-operative pain and longer healing time for the patients. Furthermore, there is a greater possibility of infection caused by the exposure of the internal organs and tissue to the surrounding air [10].

In recent decades, new surgical techniques have been developed to address these issues and to decrease the side-effects of surgical operations. The focus of the new generation of surgeries has been to reduce the size and number of incisions made on a patient's body [11]. Hence, Minimally Invasive Surgery (MIS) has been introduced as a method of accessing internal body organs through several small incisions, Figure 2.1. In general, 3 to 5 small incisions (5 or 10 mm diameter), based on the nature of the surgery, are made on a patient's body and long slender surgical instruments are used to conduct surgical operations. An endoscopic camera is inserted through one of the openings to provide visual feedback from the operative site inside the patient's body. The resulting images are displayed to surgeons on monitors in operating rooms. In this method, surgical tools such as laparoscopic instruments are used for dissecting, grasping and cutting tissues to access internal features and organs and to diagnose diseases [12].

MIS has been accepted as a favorable alternative to open surgery for most types of surgeries [1]. Due to the smaller incisions, this method reduces the infection rate and decreases blood loss during surgery.

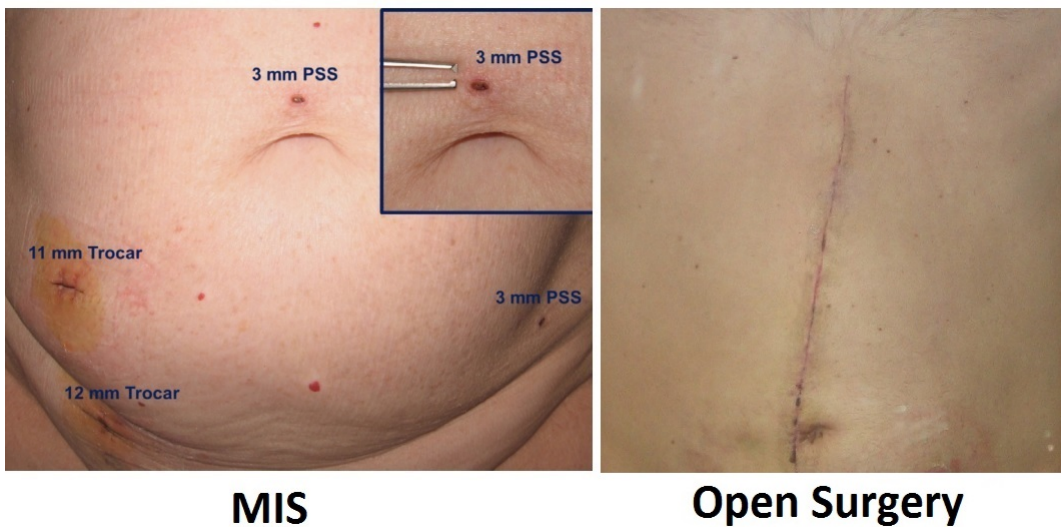


Figure 2.1: MIS incisions made by PSS (Percutaneous Surgical Set) vs. Open surgery (used with permission) [11]

Moreover, patients experience less postoperative pain, faster healing time and better cosmesis. While MIS has all of these advantages, it also faces several obstacles that have affected MIS from its infancy, such as longer operating times, difficulty in removing bulky organs, reduction in dexterity, reversal of hand motion, steep learning curves for novice surgeons, and reduced haptic feedback [2, 4, 13]. Haptics is the sense of touch, which helps surgeons to feel the body organs and tissue they are operating on and to determine their features. From a scientific point of view, haptics has three main components: kinesthetic, tactile and proprioception. The two main categories that help surgeons in effectively performing a conventional surgery are the ability to sense force and position using muscle receptors (kinesthetic) and the ability of the human skin to recognize the shapes and textures of touched objects (tactile). The absence of sufficient tactile and kinesthetic information in MIS significantly affects the efficiency and performance of surgeons [14]. In open surgery, surgeons identify the abnormalities of tissue based on the sensed stiffness differences. For instance, they can localize and extract a tumor buried under the tissue surface by palpating it [15]. However, due to the absence of tactile sensation in MIS, it is no longer possible to feel the hardness or stiffness of tissues or to evaluate anatomical structures such as nerves, vessels, and ducts. Furthermore, applying excessive amounts of force in MIS can cause tissue trauma. In contrast, insufficient force exertion leads to needle slippage during grasping, loose knots and the inability to perform specific tasks such as driving a needle during suturing [2, 16]. Consequently, laparoscopic suturing demands complex surgical techniques

and longer operating times compared to open procedures [5]. Therefore, providing haptic feedback in an MIS suturing task may significantly impact needle grasp control and patient safety [6, 17].

Additionally, the lack of proper haptic feedback is a significant barrier to develop surgical robots and telerobotic technologies. Providing force information about tool–tissue interaction is necessary to prevent potential damage in a robotic master–slave surgery and it is essential for successfully conducting tasks such as tissue manipulation, retraction, and dissection. Apart from surgical applications, force information can be used to develop virtual reality simulators for training and skills assessment purposes [3, 5, 7].

## 2.2 Force Sensing in MIS

In the last few years, researchers have tried to address the haptic deficiency problem by implementing force sensors into surgical instruments [18, 19]. In a work by Trejos *et al.*, a sensorized instrument capable of measuring force and torque in 5 degrees of freedom (DOF) was developed for MIS, as is shown in Figure 2.2 (a). The developed instrument is able to track the position in 6-DOF using an electromagnetic tracking system. Additionally, it provides all of the acquired force and position information to users through a computer user-interface. The provided information was used for training purposes and to evaluate the skill level of novice surgeons [20–22]. In [23], a 6-DOF force/torque sensor was developed for acquiring force and torque data in minimally invasive robotic surgery applications. This sensor is suitable for measuring forces in cable driven manipulators such as daVinci master–slave robot, as it is illustrated in Figure 2.2 (b). A miniaturized 6-DOF optical force/torque sensor was also presented in [24], as shown in Figure 2.2 (c). A theoretical model of this sensor was developed to study its usability in MIS applications. Yurkewich *et al.* designed a low-cost arthroscopic grasper, which is capable of measuring axial and bending forces on the instrument shaft and the grasping force at the instrument handle. Fibre optic sensors were used for sensor development due to their high sensitivity and ease of installation [13, 25]. As depicted in Figures 2.2 (d) and (e), multiple work have done in developing force-sensing instruments for retinal surgery applications [26–30]. For example, a 2-DOF force sensing micro-forceps was developed for robot assisted retinal surgery by Kuru *et al.*. This instrument measures applied forces on the retina directly at the tool tip. Therefore, it aims to prevent the exertion of excessive forces on the retina and its potential damages [26]. A 3-DOF force sensing micro-forceps obtains lateral and axial force information at the distal end of the instrument

developed in [28], as depicted in Figure 2.2 (e). Figure 2.2 (f) illustrates a 3-DOF force sensor, which was designed and developed in [31] for tissue palpation in MIS. This sensor is capable of identifying tissue stiffness variations in the axial and radial directions. This Magnetic Resonance Imaging (MRI) compatible instrument is used to localize relatively stiff tissue lesions such as tumors. Peirs *et al.*, has equipped a laparoscopic needle-driver with strain gauges in order to record exerted forces in an *in-vivo* test, as shown in Figure 2.2 (g). An optical version of the sensor was developed to acquire force data in axial and radial directions. The developed sensor was planned to be mounted on a laparoscopic robot to provide force feedback [32]. In [33], a multi-axial contact force sensor was proposed for robotic surgery graspers. The capacitive sensor is able to measure normal and shear forces exerted on a grasping plate in 3-DOF, as shown in Figure 2.2 (h).

Although, various work aimed to measure forces in different DOFs, consideration must be given to determine what force information can best meet the clinical applications requirements of the designed instrument.

### 2.3 Required Force Information in MIS

Several factors determine the required force information in MIS. First, different force information is needed based on the type of surgical tasks being conducted [9]. For instance, providing grasping force information in needle-based tasks is necessary to prevent needle slippage. Likewise, axial force information is needed in a knot tying task to ensure tight knots [8]. Similarly, palpation and other identical tasks require force information in different directions to help users in identifying tissue properties and stiffness differences [34–36]. Therefore, the requirements of force information in MIS are very much task dependent.

Second, the type of the MIS surgery, i.e. robotic or laparoscopic, determines the need for providing force information in different DOFs. In a work by Bholt *et al.*, it was indicated that although the haptic feedback in laparoscopic surgery is altered, it is not completely eliminated [37]. Although the existing sense of touch in laparoscopic instruments is not the exact indicator of tool–tissue interaction forces, it is still helpful enough to conduct some tasks [38]. In contrast, there is absolutely no sense of touch in robotic master–slave surgery. Therefore, incorporating haptic feedback technologies into surgical robotic systems can significantly influence the performance and efficiency of users [39].

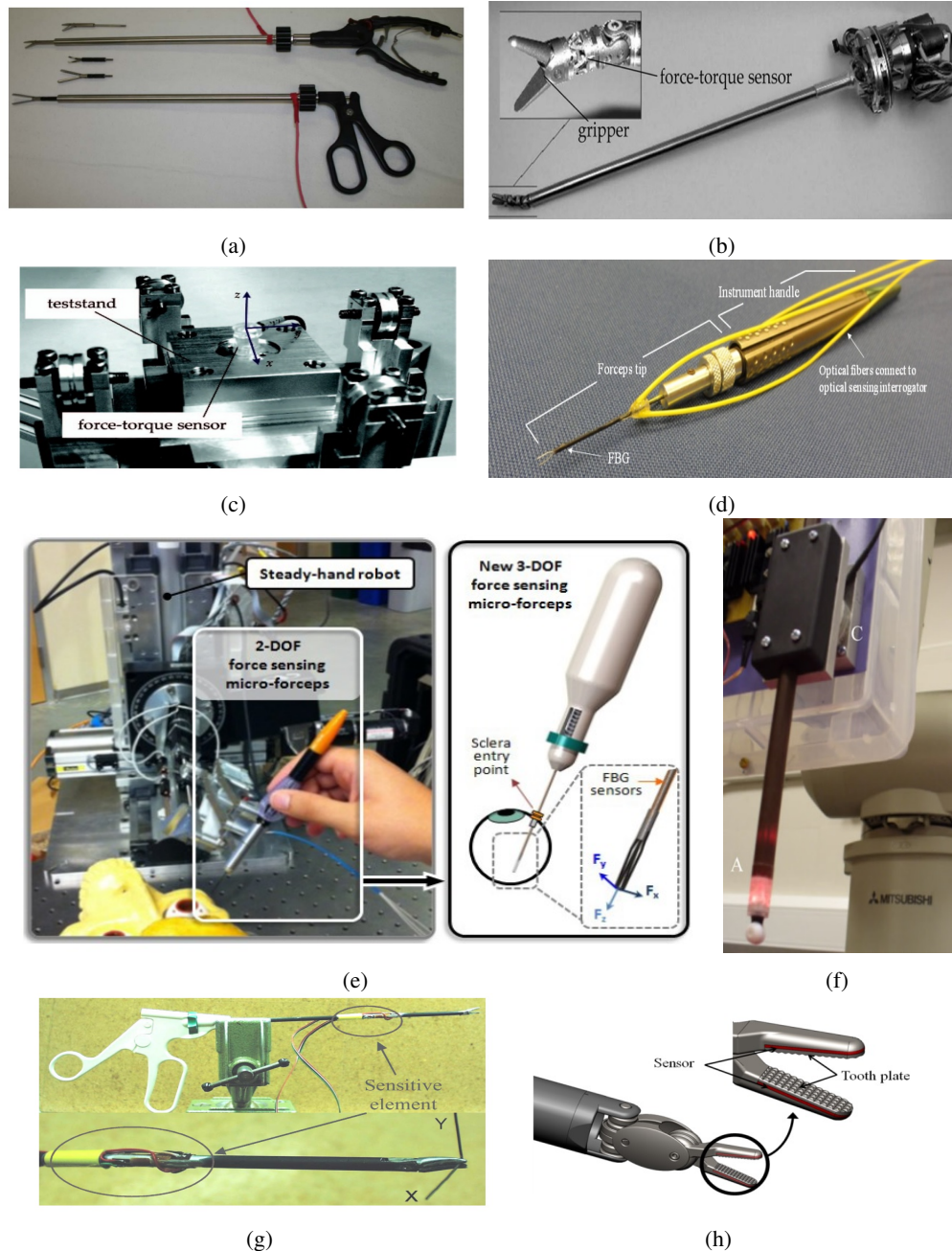


Figure 2.2: a) A 5-DOF sensorized laparoscopic needle-driver [22]; b) A 6-DOF force/torque sensor for minimally invasive robotic surgery [23]; c) A miniaturized 6-DOF optical force/torque sensor [24]; d) A force-sensing instrument for retinal surgery [27]; e) A 3-DOF force sensing micro-forceps [28]; f) A 3-DOF force sensor for tissue palpation [19]; g) A laparoscopic needle-driver sensorized using strain gauges [32]; h) A 3-DOF capacitive force sensor for surgical graspers [33] (used with permission).

As it is discussed in [40], 6 out of 15 subjects claimed that they performed better with a conventional laparoscopic instrument rather than the developed sensorized instrument and only 40% of the operators found the developed sensorized laparoscopic instrument in this work more efficient. Likewise, in a study by Delft Institute of Technology, more than 70% of investigated laparoscopic surgeons have indicated the need for providing haptic feedback for the sake of surgical performance improvement [41]. Thus, the effectiveness of the provided force feedback varies for different subjects.

In conclusion, different surgeries and different tasks require force feedback in various directions. The instruments and devices used determine the users' need for different force data. Moreover, providing haptic information in surgical operations does not essentially improve the performance of all operators.

After assessing the need to measure force information in MIS, it is important to determine what is the best location on the instrument to locate force sensors. Measuring tool–tissue interaction forces inside of a patient's body is more challenging and at the same time more accurate compared to force measurements conducted outside of a patient's body. Therefore, the next section outlines the advantages and disadvantages of measuring forces on different locations on an instrument.

### 2.3.1 The sensor location

Placement of force sensors in proper locations on the instrument has a pivotal role in increasing measurement accuracy. In a laparoscopic surgery, casual interactions of surgical instruments with the surgical environment affect the haptic perception of operators. As illustrated in Figure 2.3, the forces acting on MIS instruments result from the interactions of the tool with the abdominal wall, the trocar, and the organs [38]. For this reason, the perceived haptic sensation at the handle of the instrument is an inaccurate indicator of the real tool–tissue interaction forces. The work presented in [42] indicates that the average values of forces sensed at an instrument handle are approximately 4 times greater than their actual value at the tool tip. The magnitude of kinetic friction in different trocars has been studied in [38,43]. Results show that the amount of friction can exceed 3 N in some trocars and that it depends on both the movement velocity and the movement direction of the utilized instrument. In addition, torque values of up to 0.7 Nm are generated in instruments as a result of interactions between the trocar and the abdominal wall while tilting the surgical instrument [4,38,43].

The internal friction in an instrument's mechanism considerably affects the amount of haptic feedback

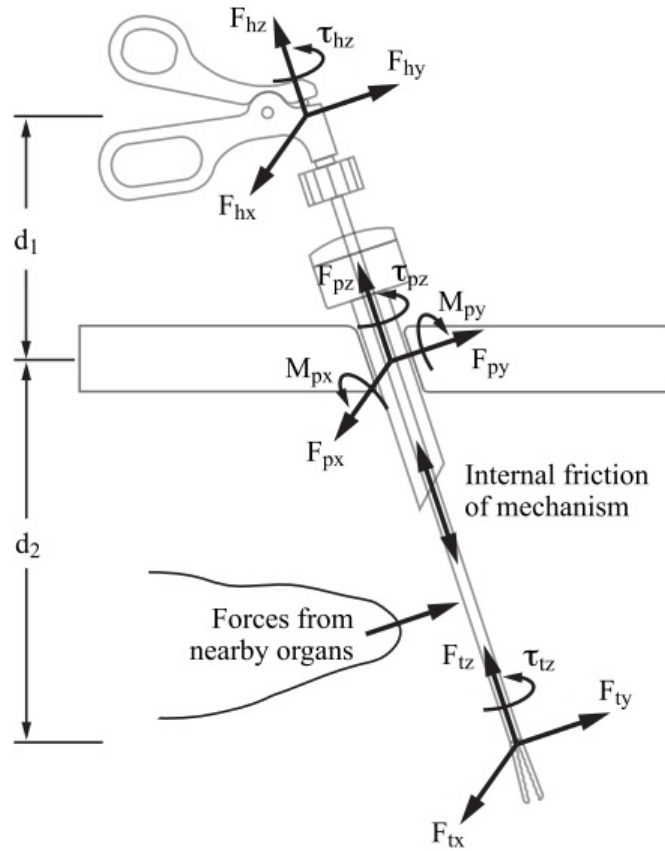


Figure 2.3: Forces acting on minimally invasive instruments (used with permission) [4].

experienced by users. According to [44–46], the average efficiency of force transfer for commercialized laparoscopic instruments is 33% while it can considerably be different for various instruments, as presented in Table 2.1. Therefore, an instrument with a low-friction actuation system, e.g. a roller link mechanism, can transfer more realistic haptic feedback to an operator’s hands [47]. Furthermore, in most surgical instruments, driving cables or rods are responsible for opening and closing the grasper by transferring actuation forces from the handle of the instrument to its jaws. Grasping forces not only cause tension in these cables/rods but also cause lateral forces at the jaw joint. These lateral forces are dependent on the location and surface properties (coefficient of friction) of the grasped objects. The axial portion of these undesired forces impairs any axial force measurement conducted on the instrument shaft. As a consequence of these two issues, decoupling the acquired axial forces on the instrument shaft from the exerted grasping forces on the instrument jaws is not possible.

Considering the effects of the aforementioned factors that affect force measurements, it is important to place force sensors at the most proper location on the instrument. To determine the best location, researchers have measured grasping forces on different locations on surgical dissectors. In [13, 48], the force sensor was located at the handle of the instrument in order to acquire grasping force data outside of the patient body; whereas [4, 49] incorporated force sensors on the instrument shaft to measure forces inside of the body. In addition, some studies focused on measuring grasping forces at the tool tip in order to achieve more accurate measurements [19, 33, 50–60]. In order to obtain desired force information, the pros and cons of placing force sensors on different locations should be studied. The advantages and drawbacks of measuring forces outside of a patient’s body include:

- Sterilization is not necessary.
- There is no size constraint.
- Measurements are affected by friction at the insertion point (trocar) and the internal friction of the mechanism.
- The created torque due to the trocar–abdominal wall interactions impair the accuracy of the acquired torque data on the shaft outside of the entry port.
- The obtained force information is not the exact indicator of the tool–tissue interaction forces or the grasping force.

On the other hand, force measurement on the instrument shaft after the entry port (inside a patient’s body) comes with its own pros and cons as listed here:

- Kinesthetic force information at the instrument tip is correctly measurable.
- The sensor must be sterilizable and cleanable.
- Since the size of the instrument is limited to the size of the trocar, the sensor should comply with the same size restrictions.

Table 2.1: Average mechanical efficiency (ME) of four commercialized laparoscopic instruments

Instrument	Wilmer <sup>®</sup>	5-mm reusable	10-mm reusable	5-mm disposable
ME	96%	33%	28%	8%



- Measurements are affected by the internal friction in the instrument mechanism.
- Adapting the sensor to a non-planar tool shape is possible.
- Applied forces on the tool tip affect the measured force information on the instrument shaft. Consequently, decoupling is required for all DOFs.
- Inertial and actuation forces generated by the actuation cables or rods impair sensor measurements.

Similarly, locating force sensors on the tip of the instrument has its own challenges and benefits, as follows:

- Both kinesthetic and tactile force information are obtainable.
- Mechanism internal friction or other disturbance forces do not affect the acquired information.
- The sensor size needs to be miniaturized with respect to the grasper dimension.
- Shape and geometry of the instrument should be considered in designing the sensor.
- More complicated fabrication process is needed for building the sensor.
- The sensor must be sterilizable and cleanable.

In order to obtain the most accurate and realistic data, the literature has suggested placement of force sensors as close as possible to the exertion point of actual forces. Based on this assumption, the most ideal location for force measurement in MIS is the tip of the instrument [56,61–63].

### **2.3.2 Essential force directions in MIS**

The requisite for force information in different DOFs depends on several factors including the surgical task, the type of the instrument, and personal preferences of users. Considering different mechanical designs for surgical instruments, further force/torque information might be required to decouple the measured forces. For instance, in an ideal case, the bending sensor should have been isolated from effects of torsion; whereas applying torque during a needle driving task affects bending measurements notably [20]. Therefore, it is important to have access to all of the required force data in order to decouple the obtained forces in different DOFs.

In general, providing force/torque information in 7-DOF is sufficient for most laparoscopic operations. 7-DOFs include information on three orthogonal forces, three orthogonal moments and actuation force at the grasper [20]. However, in some publications 6 or even less DOFs have been considered sufficient [4, 13, 32, 61]. Depending on the task, the required force information may vary. For instance, grasping information is required in gripping and cutting tissues. Axial force information is needed for preventing stitch breakage while tightening the knot or for palpation purposes. Torque and bending moments are needed when driving a needle for suturing purposes. Finally, all force and torque data could be used for skills assessment and training purposes. Thus, force and torque data in 5-DOF— three orthogonal forces, torsion and actuation force at the grasper— can satisfy force requirements of all of these tasks [4]. It is possible to theoretically calculate lateral forces from the obtained bending moments by taking into account the distance between the force sensor and the location of the exerted forces. The following four sections present the literature on the 5-DOF force and torque measurements.

### 2.3.2.1 Grasping force sensing in MIS

Measurement of grasping forces on any location rather than tool tip comes with a considerable amount of error due to the presence of disturbance variables such as inertia, internal friction, backlash and gravity. In contrast, the direct measurement of exerted forces at the tool tip reduces the influence of these error sources. Therefore, many researchers have integrated force sensors at the tip of surgical instruments in order to improve sensing accuracy. Hong *et al.*, designed a 2-DOF compliant forceps with circular flexure hinges capable of measuring pulling and grasping forces at the instrument tip. A half Wheatstone bridge, type II, was formed by locating two strain gauges on the top and bottom surfaces of the jaw hinges of the instrument for measuring the exerted forces. Bending strain generated at the hinges was measured using sensors mounted on the tool. Measured strain values were implemented in screw-based Jacobian theory to calculate the pulling and grasping forces. A Finite Element Analysis (FEA) method was employed to validate the proposed design concept. The conclusion was that locating the force sensor on the tool tip enabled more precise measurement of applied forces [64].

In [59, 65] piezoresistive force sensors were integrated into the jaws of an MIS instrument to measure the exerted forces. The overall appearance and functionality of the designed instruments are quite different compared to conventional laparoscopic tools, calling into question their practical usage. King *et al.* has

developed a multielement tactile feedback system, which can be mounted onto the grasping manipulators of the daVinci surgical robot. The designed system transfers grip force information from the robot end effector to a surgeon's hands. They showed that the developed system is capable of transferring static or dynamic force distribution applied at the grasper to the fingers of the operators [59]. Similarly, in a work by Vakili *et al.*, a paper-thin piezoresistive force sensor was integrated on one of grasper jaws at the instrument tip to minimize the risk of tissue trauma during dissecting tasks. The jaws of the grasper were designed in a parallel structure in order to facilitate gripping of tissues and distributing exerted forces equally all over the surface of grasper jaws [65].

A Polyvinylidene fluoride (PVDF)-based tactile sensor capable of measuring the magnitude of forces and their position on the grasper surface was designed and developed by Qasaimeh *et al.* [66]. The micro-fabricated sensor has a corrugated shape, which prevents slippage during grasping, handling, twisting, and lifting soft slippery tissues.

Capacitive sensors are used in some studies to develop multi-axis force-sensing forceps for MIS; however, their ability to withstand sterilization has not been presented. In [67], a 4-DOF force sensor was designed and fabricated. By utilizing capacitive transducers, the sensor was able to measure 3 DOFs pulling forces and 1 DOF grasping force at the instrument tip. The fabricated sensor was mounted on the Raven II surgical platform for test experiments. The obtained results show that the RMS errors are around 0.1 N. Moreover, the sensor has shown good repeatability and low hysteresis throughout the experiments. In a similar work by Lee *et al.*, a new film-like capacitive-type sensor was used to measure 2-DOFs shear forces and a single DOF normal force on the jaws of the forceps. The prototyped sensor is adoptable based on the shape and functionality of the utilized surgical grasper. It is concluded that a more delicate fabrication process will improve the sensitivity of the sensor and the accuracy of the acquired data [68].

Due to their small size and high sensitivity, optical fibre-based sensors have recently been investigated for measuring grasping forces on the tip of surgical instruments. As presented in [53], a soft material tactile array was designed and 3D printed for a surgical grasper. A multi-core optic fibre cable was located at the end of the flexible material to capture light intensity changes caused by the exerted forces onto the soft material channel and to send it back to an optical interrogator. The deformable silicone channel was designed based on the Bernoulli pipe structure to increase the sensitivity of the system through diameter differences at the input and output of the channel. In order to simplify the manufacturing complex, they

have employed rapid fabrication methods such as 3D printing and soft material casting. Although the sensor is adaptable to different MIS instruments, the force measurement range of the sensor is limited to 0 to 1.622 N. In a similar work by Callaghan *et al.*, FBG sensors were mounted on the upper surface of laparoscopic scissor blades to measure friction and cutting forces between scissor blades. The optical sensor is capable of measuring strain changes caused by applied forces on the grasper. In this work, it is assumed that all the exerted loads to the sensorized blades are either lateral loads or direct loads. Based on this assumption, basic equations of beam theory were implemented to decouple these forces theoretically. Moreover, the author studied the effect of exerting forces with an offset with respect to the neutral axis of the blades. It is indicated that there is no distinguishable error in assuming concentric (not eccentric) loads on blades. As a result, implementation of the basic beam theory, with respect to the assumption that all forces are applied at the neutral axis of the blades, is reasonable. The average resolution of the designed sensor is 0.5 N over a 30 N load range. In addition, an evaluation platform was designed and developed for sensor characterization purposes [55]. The strain gauge-based test-bed was utilized to validate measured force information by the FBG sensor and to provide real-time force feedback. Obtained force information from the test-bed were compared to a theoretical analysis for decoupling recorded forces. Subsequently, it is demonstrated that there is a close correlation between forces measured directly by the FBG and forces acquired from a load cell on the test-bed [54–57]. In [51,52], an MRI-compatible optical fibre-based tactile sensor was developed and fabricated for minimally invasive robotic surgery. The sensor is capable of measuring both static and dynamic loads and it consists of a moving part. The moving part of the sensor is a beam shape structure that behaves with respect to the Euler/Bernoulli beam theory. The sensor measures deflection of this beam in three points along the jaw. In order to provide this unique measurement characteristic along the beam, three optical fibres with single FBGs were embedded inside the surgical jaw. One side of the optical fibres was fixed to the support material, while the other side was connected to a laser light source. Eventually, a prototype of the sensor was manufactured to prove the feasibility of the concept to provide force feedback for MIS graspers. Both the theoretical model of the sensor and its FEA were studied to validate acquired force information. Results of the study illustrate that the sensor shows linear behavior in the range of 0 – 4 N. Moreover, the delicate design of the sensor makes implementation of this concept in miniature surgical graspers possible through a microfabrication processes. Furthermore, the size and the material of the sensor beam can be altered based on the use of the sensor in different surgical instruments. Besides, the resolution

of the sensor in characterizing discrete force distribution can be tuned based on the required information for different tasks.

### 2.3.2.2 Axial force sensing in MIS

Fundamentally, force sensors rely on measuring micro deflections in components created by applied loads. Hence, the ability of sensors to measure these deformations not only depends on their sensitivity, but also on the flexibility and deformability of the structure onto which they are integrated. For instance, in a work by Trejos *et al.*, strain gauges were integrated into the shaft of a surgical instrument to measure strain generated in the shaft by axial forces [22]. Since the obtained results in the axial direction for the first prototype of this sensor were unsatisfactory, they developed a novel structural element for the second generation of the device which deforms when exposed to external axial loads. Moreover, two holes were drilled through the instrument shaft in order to locally increase the generated axial strain. Strain gauge-based force sensors were located on the structural element to measure strain values created by axial forces. To maximize the signal to noise ratio, strain gauges were connected in a Type III full-bridge configuration. It is mentioned that opening and closing the grasping actuator generates tension in the inner shaft, which disturbs the axial measurements. Consequently, it was not possible to decouple the axial force sensor and the grasping sensor. As expected, the study showed that there is a trade-off between the rigidity of the flexible structure and its ability to adequately deflect for measuring axial forces. Therefore, it is important to keep the balance between these two terms in order to achieve the best outcome.

In the study presented in [69], a 3-axis distal force sensor was developed for tissue palpation in MIS. The system is capable of measuring all three orthogonal forces acting on the tip of the instrument. In this design, strain gauges were located on a flexible tripod design to differentiate strain values generated by external loads in different directions. Subsequently, optimization methods were implemented to obtain the best balance between maximizing the sensitivity of the flexible structure and its stiffness. The flexible tripod structure consisted of lower and upper platforms connected through three cross beams. Both applied axial and radial forces cause deformation in the tripod structure. However, it is assumed that the generated axial deformation dominated the structural motions and therefore the influence of radial forces was neglected. In addition, this paper discussed three main types of flexible structures including: the tubular structure, the cross beam structure and the Stewart platform. The tubular structure did not provide high sensitivity in

the axial direction. On the other hand, the cross beam structure offered good sensitivity and high stiffness. However, it required a complex fabrication process of its hollow section. Similarly, the Stewart platform also required a complex manufacturing process. Nevertheless, it had many advantages to offer such as high sensitivity, high stiffness, scalability and adaptability. The developed tripod in this work was a modification of the cross beam structure, which is able to provide axial force information in a range of  $\pm 3.0$  N and radial force data in a range of  $\pm 1.5$  N.

In [70], a 3 axis FBG-based force sensor was developed to measure lateral and axial forces in MIS. A tubular structure was chosen for the flexible part of the sensor to provide sufficient room for the axial sensor placement in the center of the instrument shaft. This configuration maximizes the decoupling of axial and transverse forces by isolating the central sensor from the disturbing strain caused by the transverse forces. Additionally, three FBG sensors were symmetrically attached on the instrument shaft to measure transverse forces exerted on the tool tip. Moreover, He *et al.* studied and analyzed three flexure structures that are able to increase sensor sensitivity for the axial force measurement. Structures with V-shape struts, multilayer parallel slots, and spring-shaped designs all showed promising results in terms of increasing axial force sensitivity. However, safety concerns related to the structural failure, as well as fabrication complexity, need to be considered in different applications and designs. Furthermore, the effects of different materials (with different stiffness) in increasing the sensitivity of the axial force sensor was studied. The superelastic Nitinol (with 41 GPa Young's module) was chosen as the most appropriate material among other candidates, such as stainless steel and titanium. Nitinol is a metal alloy of nickel and titanium that offers an acceptable amount of elasticity in addition to its precise cutting manufacturability through micromachining. In this work, temperature compensation of FBG sensors was considered and FEA methods were implemented to study the safety of the design concepts within their working load range. Furthermore, an automated calibration and evaluation system was developed for the sensor validation and repeatability testing. In an other similar work, a spring shape-based structure was used by Yang *et al.* for the design of a miniature force-sensing catheter [71]. The force-deformation transferring component showed promising results in providing force information in the range of 0.2 – 1.0 N. In order to protect the internal structure of the sensor, a protective layer was bonded over the force-deformation transferring component. Nonetheless, potential safety concerns related to structure failure caused by excessive force exertion on the instrument has not been considered [71].

In [13, 31, 72–77] the feasibility of increasing axial sensitivity by creating a flexure segment in the instrument shaft was studied and demonstrated. However, the disruptive influence of grasping forces on the axial measurement has not been considered in any of these studies.

Peirs *et al.*, has designed and prototyped a sensorized needle driver that measures strain in the axial and radial directions. The proposed sensor has force measurement ranges of 0 – 2.5 N and 0 – 1.7 N for axial and radial directions, respectively. The instrument has been equipped with optical fibres capable of providing 0.01 N resolution. The three sensors were mounted on the instrument shaft at 120° from each other. Thanks to this arrangement, all three fibres experience an identical amount of strain caused by axial forces; whereas, radial forces and bending moments generate unidentical strain values over these three FBG sensors. Titanium alloy was chosen for manufacturing the sensor due to its many advantages such as: good corrosion and shock resistance, biocompatibility, sterilizability, high fatigue resistance, high stiffness, and low Young's module (for increasing sensor sensitivity) [32].

### 2.3.2.3 Lateral forces and bending moment sensing in MIS

Applying lateral forces at the tip of an instrument creates bending moments in its shaft. Generated bending stress on the cross section of the instrument is proportional to the acting forces on the tool tip in the transverse plane (perpendicular to the tool shaft) and the distance from the tip to where the stress is being measured, Equation 2.1 [78].

$$\sigma = \frac{y}{R}\sigma_{max} = \frac{My}{I} = \frac{FLy}{I} \quad (2.1)$$

where  $y$  is the distance from the surface to the neutral axis,  $R$  is the bending radius,  $I$  is the moment of inertia of the shaft cross section,  $M$  is the moment at the tip,  $L$  is the distance of the strain measurement location from the tip and  $F$  is the applied transverse forces on the tool tip. These bending moments create strain on force sensors. In order to calculate the strain measured by force sensors, the previous formula can be modified based on Hooke's elasticity law [78]:

$$\varepsilon = \frac{\sigma}{E} = \frac{FLy}{IE} \quad (2.2)$$

in which  $E$  is the modulus of elasticity of the material of the shaft. Different force sensors provide various outcomes as a result of bending strain acting on them. For instance, FBG optical sensors display wavelength

shift when experiencing strain over their grating segments. Strain values acting on the instrument shaft have three main components: The strain caused by bending and lateral forces, the strain caused by applied torques at the tip and the strain caused because of the temperature gradient. Therefore, decoupling methods should be implemented for isolating effects of the other perturbing sources, as it is in Equation 2.3 [70]:

$$\Delta\lambda = K_\varepsilon\varepsilon + K_t\Delta t + G\varphi \quad (2.3)$$

where  $K_\varepsilon$  is the bulk modulus for the generated strain ( $\varepsilon$ ),  $K_t$  is the bulk modulus for temperature variation ( $\Delta t$ ),  $G$  is the shear modulus and  $\varphi$  is the angle of twist from its equilibrium position. Based on this theory, several researchers have integrated force sensors along the instrument shaft to measure bending and lateral forces. For example, He *et al.* designed, fabricated and calibrated a 2-DOF force sensing micro-forceps for vitreoretinal surgery. In this work, three FBG sensors were placed into the distal portion of the tool shaft with a symmetric arrangement of  $120^\circ$  around the shaft. This sensor is capable of providing 0.25 mN of force resolution in its lateral directions. In a similar work, they modified the design and developed a 3-DOF instrument with the same lateral measurement concept. Although the effect of torsion was not considered in decoupling measurements, temperature compensation was computed using following equation [27, 70]:

$$\Delta\lambda_i = \Delta\lambda_i - k\frac{1}{3}\sum_{i=1}^3\Delta\lambda_i \quad (2.4)$$

where  $\Delta\lambda_i$  is the wavelength shift induced by the temperature change in every FBG and  $k$  is the slope of the linear dependence between the temperature gradient and the wavelength change. In other similar studies, FBG sensors were symmetrically mounted around surgical instrument shafts to sense the transverse loads [13,26,28–30]. A similar concept was implemented using strain gauge sensors in [8] by mounting two sets of strain gauge sensors in a half bridge Type II configuration on opposite sides of a surgical dissector shaft. The undesired effects of axial forces on transverse force measurements were neglected thanks to the unique configuration of strain gauges in this design [4].



### 2.3.2.4 Torsion sensing in MIS

Providing torque information is very important for conducting specific MIS tasks such as needle driving. Various studies have developed specific force feedback systems to address this issue. One example of this is the Stewart Platform, which has been used in [23,24,61] to acquire torque information. The sensor consists of two plates connected by six links (legs). Considering its unique arrangement, the sensor is capable of providing 6-DOF force/torque information including torsion. Advantages of this design include the miniature size of the sensor (scalability) and the adaptable properties of the sensor for different instruments. On the other hand, problems with this design are sensor fabrication complexity, nonlinear behavior of the structure in specific loading cycles and temperature fluctuation impact on sensor measurements (need for temperature compensation).

In theory, the amount of created torque in a shaft can be calculated by using the Equation 2.5 in which  $J$  is the polar moment of inertia of the cross-section of the shaft,  $r$  is the shaft radius,  $T$  is the applied torque and  $\tau$  is shear stress [78].

$$\tau = \frac{T.r}{J} \quad (2.5)$$

The generated shear stress produces strain in measuring elements at  $45^\circ$  angles with respect to the tool shaft. As a result, torsion sensing elements have been mounted on the instrument shaft at  $\pm 45^\circ$  in [79–81].

In [82], two symmetrical planes at  $\pm 45^\circ$  angles have been machined on the instrument shaft. Two parallel FBGs were bonded on these engraved planes to detect torsional deflections. The sensing system provided high torsion sensitivity and low temperature sensitivity. In this work, FEA has implemented to verify feasibility, rationality and safety of the shaft design. In a similar work by Tian *et al.*, the feasibility of measuring torsion by installing force sensors on the tool shaft in a helical arrangement was proven. In addition, the optimized helical angle for the sensor was determined to be  $45^\circ$ , at which the highest sensitivity and the lowest percentage of errors were obtained [83]. Simultaneous torsion and force measurement was possible by twisting FBG sensors in a helical pattern. Moreover, different configurations can be implemented due to the possibility of integrating various gratings in one optical fibre. Furthermore, helically wrapped FBG sensors are capable of providing both the amplitude and direction of the exerted torsion on the instrument [84]. In [85], a helical FBG-based torsion sensor was developed. The effect of the direction in which the FBG is twisted was assessed with respect to the functionality of the optical sensor, and

it was demonstrated that clockwise or counterclockwise twisting patterns can create completely different optical responses. In a similar work, Ryu *et al.* implemented helical configured FBG sensors on an instrument shaft to measure shape and curvature changes [86]. FBG-based optical sensors were embedded in small-diameter tools at 120° symmetric angles. In this study, the created strain in each of FBG sensors in this work, considering effects of applied moments and temperature, were calculated using the following equations:

$$\begin{aligned}\varepsilon_1 &= \eta \cdot \{\varepsilon_{max} \cdot \sin(\alpha) + \varepsilon_a\} + \varepsilon_t \\ \varepsilon_2 &= \eta \cdot \{\varepsilon_{max} \cdot \sin(\alpha + 120^\circ) + \varepsilon_a\} + \varepsilon_t \\ \varepsilon_3 &= \eta \cdot \{\varepsilon_{max} \cdot \sin(\alpha + 240^\circ) + \varepsilon_a\} + \varepsilon_t\end{aligned}\tag{2.6}$$

where  $\eta$ ,  $\varepsilon_a$ ,  $\varepsilon_{max}$ ,  $\alpha$  and  $\varepsilon_t$  are strain transfer ratio from the surface to the fibres, the axial strain caused by the applied moments, the maximum bending strain in the tube, the angle of rotation and the thermal strain, respectively. Likewise, in a paper by Xu *et al.*, a high precision and high resolution sensing technology capable of measuring both torque and lateral forces in a continuum tube was studied. FBG optical fibres were engraved in Nitinol tubes in a helical pattern. The importance of considering the bending radius of the utilized optical fibres in order to prevent fibre damage was explained in this work [87]. In addition, Equation 2.7 was used to calculate the required amount of pitch ( $h$ ) for the design of a 3D helical path, by considering that the bending radius of the fibres ( $b$ ) should be larger than the specified minimum bending radius.

$$b = (r^2 + (h/2\pi)^2)/r\tag{2.7}$$

It is shown that the sensitivity of the sensor can be altered by changing the pitch amount of the helix.

## 2.4 Force Sensing Technologies in MIS

In the last few years, various force sensing technologies have been developed to provide haptic information for MIS. Fabrication constraints and the working environment of different sensors require different sensing technologies. The state of the art in different sensing systems and their application as well as their pros and cons are discussed in the following sections.

### 2.4.1 Strain gauges

Strain Gauges (SG) are the most common force sensing technology available. They work by measuring mechanical strain generated by applied forces. Integrating SGs in special structures or specific configurations is necessary for multi-axis measurements. Strain gauges have been successfully implemented in medical applications thanks to their low cost, adequate sensitivity, proper sensing range and small size [21, 24, 88–90]. Moreover, these sensors have been widely used in various applications for a long time and therefore they are known as the most well established product in the force sensing field. For instance, the ATI multi-axis force/torque sensor system is a commercially available sensor that uses silicon strain gauges to sense forces. Considering ATI's capability for measuring all six components of force and torque, it has been used in several medical applications and sensorizing laparoscopic instruments [91, 92]. However, the sensor's bulky size compared to a surgical instrument limits its application in specific circumstances. For example, it is not possible to locate the ATI sensor close to the tool tip where the actual forces are applied. Therefore, despite the high resolution (0.03 N) of actual ATI sensor, the acquired force measurements in the mentioned studies, come with a significant amount of error (30 % of the actual values) [91].

According to the literature, drawbacks of strain gauge sensors limit their application in MIS. These drawbacks include their high susceptibility to humidity, temperature changes and electromagnetic noise, which cause high hysteresis and drift in these sensors. Hence, Wheatstone bridge configurations of SG are used by researchers to address these limitations. Moreover, another considerable problem with these sensors is their non-linear response after being overloaded due to their inability to quickly recover [4, 19, 88–90, 93, 94].

### 2.4.2 Capacitive Sensors

The working principle of capacitive sensors is based on capacitive couplings to measure displacements caused by applied forces. Two conductive plates and a dielectric material between them are the main components of these types of sensors. The capacitance of these sensors can be calculated by Equation 2.8.

$$C = \frac{A\epsilon_0\epsilon_r}{d} \quad (2.8)$$

where  $C$  is the capacitance,  $A$  is the overlapping area of the two plates,  $\epsilon_0$  is the relative permittivity of free space,  $\epsilon_r$  is the relative permittivity of the dielectric material and  $d$  is the distance between the two plates. Capacitive sensors exhibit better stability and sensitivity compared to SG. In addition, limited hysteresis, temperature independency, good frequency response, high spatial resolution and a large dynamic sensing range are the advantages of these types of sensors. In contrary, these sensors are susceptible to noise and as a result they require complex signal processing techniques [4, 88, 90].

### 2.4.3 Piezoelectric Sensors

Piezoelectric sensors generate a voltage upon application of pressure or strain. The produced voltage is proportional to the exerted forces. The most commonly used piezomaterial in medical applications is Polyvinylidene Fluoride (PVDF), which has been used in some force sensors designs for medical applications [59, 66]. These sensors provide high-frequency responses and high bandwidth, high sensitivity, high dynamic range, low weight, compact size, and mechanical flexibility. On the other hand, piezoelectric sensors are very temperature dependent which leads to a drifting signal. Moreover, they require charge amplifier due to a charge leakage, and they do not provide reliable information in static applications [4, 88, 90, 95, 96].

### 2.4.4 Optical Fibre-based Sensors

Recent developments in the field of fibre optics have made this type of sensor an ideal haptic technology for medical systems. Optical fibres satisfy most of the requirements of a medical sensor due to their inherent advantages such as small size, sterilizability, local simplicity, high sensitivity, ElectroMagnetic (EM) noise immunity, biocompatibility, chemical inertness, non-toxicity, and MRI compatibility [13, 25, 97–99]. On the other hand, there are still challenges with optical fibres that need to be addressed [4, 25, 88, 90]. These challenges and problems are listed below:

- They cannot typically achieve small bending radii and consequently they show signal attenuation due to excessive bending or misalignment.
- An external readout unit is required to interpret the Fibre Optic Sensors (FOS) measurements, which is a disadvantage for medical devices in terms of portability.

- Currently, costs related to the optical interrogation units are remarkably high, which increases the final cost of the medical devices developed using this technology.
- The high sensitivity of FOS to various stimuli such as strain, temperature, and acceleration cause coupling problems in some applications. Therefore, complex design concepts are required to isolate the effects of strain from the others stimuli considering the initial intention of the measurements.

Considering all the pros and cons of the Fibre Optic Sensors (FOS), researchers have used the optical sensors in various force sensing applications [13, 25, 90, 97, 98, 100–102]. FOS are mainly categorized in two groups: intrinsic sensors and extrinsic sensors. The former type of the FOS has the sensing element by itself and therefore it internally manipulates the wavelength spectrum of the light in the fibre. The latter group however, merely conveys the observed light to the measurement unit at the end of the fibre. Intensity, frequency and other features of the sent light determine the extrinsic sensor's behavior. The potential advantage of the extrinsic sensor is the possibility of achieving smaller size sensors thanks to the ability to keep the acquisition unit away from the sensing location. In either method, the light signal reflected by the FOS is analyzed at the interrogation unit using four main methods:

- Comparing the reflected light intensity to a reference fibre,
- Analyzing the actual optical spectrum of the returned light,
- Determining wavelength properties by splitting the reflected light signal and remixing it out of phase, and
- Using swept-laser to determine the wavelength of the received light.

In recent decades, researchers have developed various optical force sensors for medical applications that detect the pressure and strain based on light intensity modulation [13, 25, 88, 97, 98, 103–110]. Nonetheless, FBG sensors have been the most common optical sensors to be used in MIS thanks to their distinct advantages over other FOS [97]. For instance, it is easily possible to accommodate several independent FBG sensors on a single FBG fibre due to the ease of multiplexing. Furthermore, the problem of light intensity fluctuation has been solved by using the absolute wavelength in these technologies [97]. A review of force sensing principles of FBG sensors is presented in the following section.

#### 2.4.4.1 FBG Working and Sensing Principle

Intense ultraviolet (UV) laser light is used in a spatially-varying pattern to illuminate the core of a suitable optical fibre in the process of generating Bragg gratings [111]. The created grating serves as a series of internal mirrors along a specific portion of the optical fibre. The FBG reflects a narrow spectrum of traveling light down the fibre as it passes through each grating section on the fibre [25]. The reflected wavelength by the Bragg grating depends on the optical properties of the fibre and the experienced thermal/strain perturbations caused by the grating. Equation 2.10 shows that the maximum reflectivity occurs at the so-called Bragg wavelength  $\lambda_B$ :

$$\lambda_B = 2n_{eff}\Lambda \quad (2.9)$$

where  $n_{eff}$  is the effective refractive index and  $\Lambda$  is the grating pitch. As is shown in Figure 2.4, the peak wavelength of the back-reflected light is shifted with respect to the experienced external perturbations [112, 113].

As a result, when an FBG sensor is subjected to mechanical load or thermal changes, a wavelength shift  $\Delta\lambda_B$  occurs in the reflected light [97, 114]. The generated wavelength shift in response to the applied mechanical strain ( $\varepsilon$ ) or temperature stimulus ( $t$ ) can be expressed as the following equation:

$$\Delta\lambda_B = 2 \left[ \Lambda \frac{\partial n_{eff}}{\partial \varepsilon} + n_{eff} \frac{\partial \Lambda}{\partial \varepsilon} \right] \Delta\varepsilon + 2 \left[ \Lambda \frac{\partial n_{eff}}{\partial t} + n_{eff} \frac{\partial \Lambda}{\partial t} \right] \Delta t \quad (2.10)$$

Considering the simultaneous influence of temperature and mechanical strain on the FBG output, researchers have tried to isolate one of the parameters in order to study its particular effect in the measurement. This method, thermal/strain equilibrium, is useful for determining the measurement properties of the sensor for each particular stimulus [25]. The equations below show potential responses of the sensor for thermal and strain stimuli:

$$\frac{1}{\lambda_B} \frac{\delta\lambda_B}{\delta t} = 6.67 \times 10^{-6} t^{-1} \quad (2.11)$$

$$\frac{1}{\lambda_B} \frac{\delta\lambda_B}{\delta \varepsilon} = 0.78 \times 10^{-6} \mu\varepsilon^{-1} \quad (2.12)$$

By interpreting the equilibrium equations, the strain and temperature sensitivity of FBG sensors are approx-

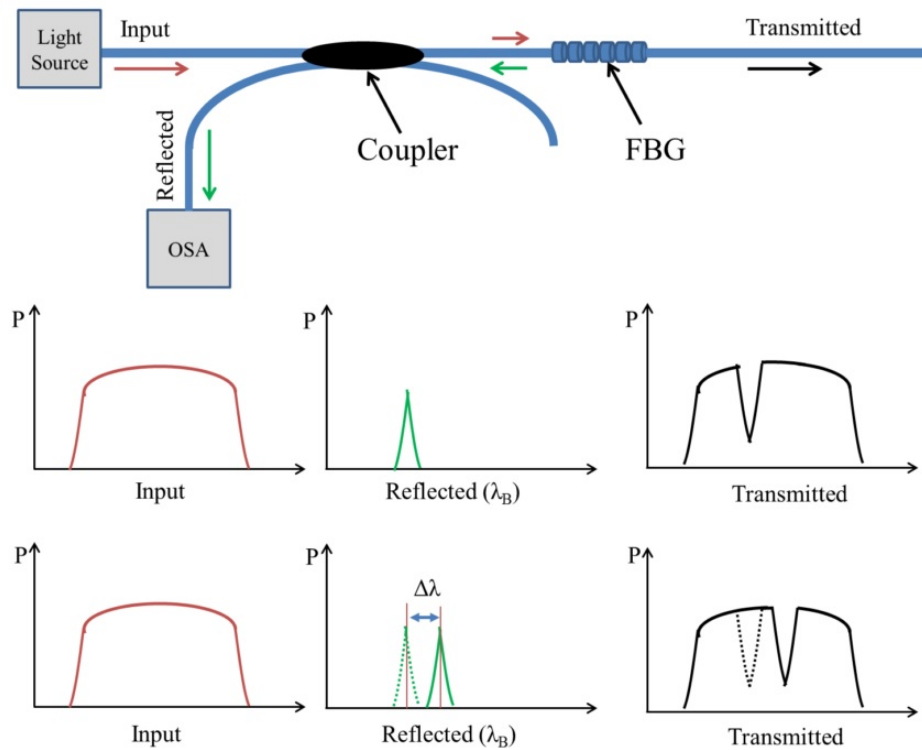


Figure 2.4: The red color line shows the transmitted light source through the FBG while the green color line illustrates the back-reflected portion of the light from the grating segment. Lower graphs show the wavelength shift provided by the FBG sensor (used with permission) [112].

imately  $1.2 \text{ pm}/\mu\text{E}$  and  $10 \text{ pm}/^\circ\text{C}$ , respectively [25, 115]. Although the effects of the temperature change can be neglected for imprecise dynamic loads, for medical usage of FBG, especially in *in vivo* applications, the effects of temperature difference inside and outside of a patient's body must be taken into account [89].

#### 2.4.4.2 FBG Temperature Compensation Methods

Although FBG sensors have several advantages over other sensing systems, their high thermal sensitivity is a significant disadvantage for *in vivo* MIS applications. In a real surgery, a force sensor is subject to severe temperature variations after it enters a patient's body compared to the ambient temperature of Operation Room (OR). Therefore, temperature compensation methods are required to neutralize the temperature impact on FBG measurements. In a work by Mo *et al.* [116], three main temperature compensation methods are explained, as follows:

1. The first temperature compensation approach is to set a reference temperature sensor. By isolating

the temperature reference sensor from any applied mechanical strain or other perturbations in the design, it is possible to calculate the influence of temperature variation. In so doing, the amount of wavelength shift caused by temperature fluctuations can be subtracted from the final measurements of the sensor.

2. The other compensation approach is to design a mechanically self-compensated structure for the sensing system. An example of this type of structure is a system consisting of different materials with different thermal coefficients. In [117], different materials with different thermal expansion coefficients were used to shape an air cavity around the optical force sensor. This design is able to reduce the influence of temperature variation by preventing the temperature flow transfer to the FBG.
3. A third way of doing temperature compensation is by miniaturizing the sensing structure. For instance, miniaturizing the air cavity length of a Fabry–Perot Interference (FPI) sensor can reduce the temperature cross-sensitivity of this optical force sensor [118].

The second approach, a mechanically self-compensated structure, requires a relatively large structural space. Consequently, this method is not the most favorable solution for MIS applications considering the existing space and size restrictions in MIS instruments. On the other hand, the third compensation method requires complex fabrication methods. Manufacturing complexity is undesired for device development [116]. As a result, the first approach for temperature compensation, setting a reference sensor, has been used most commonly in medical applications [27, 54, 60, 70, 97, 113, 116, 119].

In order to address the thermal sensitivity issue of FBG sensors, researchers have developed new types of optical fibres that are less sensitive to temperature variations. Photonic Crystal Fibres (PCF) have been presented as a promising alternative for FBG sensors. Due to their novel structure, PCFs provide approximately 10 times lower temperature sensitivity and 2 times more strain sensitivity compared to FBG fibres. In addition, they tend to be more bending insensitive, which can be a pivotal parameter of precise designs. However, further developments in terms of sensor fabrication simplicity, sterilization and sensor measurement reliability are required for real-world use of these sensors [120–124].



### 2.4.4.3 Optical Interrogation System

In order to interpret light properties of FOS reflections, a monitoring and analyzing unit, i.e. an interrogation system, is needed. Various interrogation systems have been developed for different FOS. Most of these systems have components in common. The main components of every interrogator are the isolator, the circulator, the splitter, the main light source, and the analyzing unit. An isolator serves as a directional internal filter to guide the reflected lights to a specific direction. The circulator isolates the strain-affected light from the transmitted light. Single fibre optical sensors have emerged thanks to the presence of this component, which allows a single optical fibre to convey both transmissive and reflective lights simultaneously. The splitter divides the received signal at the acquisition point based on the interrogator requirements and the main light source is the most essential and fundamental part of an optical system. In addition, the observed wavelength shift is recorded by the analyzing unit. This system interprets the properties of the reflected light and provides a proportional conversion of it in an electrical signal form [25, 111]. As a result, interrogation systems are required in order to provide readable and user-friendly data measured by the FBG sensors.

After investigating different force sensing technologies and their technical specifications, the manufacturing methods for fabricating the sensorized instrument by these force sensing technologies, must be taken into consideration.

### 2.4.4.4 Manufacturing Methods of Sensing System

Sensor sterilizability and fibre placement restrictions limit manufacturing methods available for building sensorized instruments. According to [125], embedding sensors into the instrument is the best way to maintain the original shape of the instrument and its functionality, while satisfying sterilization requirements. In addition, embedding force sensors inside of the tool tip makes direct force measurement possible [56, 125].

There are three main sensor embedding techniques in MIS: Shape Deposition Manufacturing (SDM), sputtering and electroplating. Based on the sensor type and the instrument material, each of these methods could be the most appropriate fabrication method. Nevertheless, SDM is the most common method for medical applications [56, 57, 126, 127]. Through an SDM technique force sensing elements get embedded into stainless steel or polymer-based structures in layer. This method protects the force sensors from

external damages caused by exerted forces or excessive temperature exposure [56, 115].

## 2.5 Different Feedback Methods

There are three main classifications for feedback modalities including visual, auditory, and haptic [56].

Visual feedback has been employed in various studies to provide force information to operators [13, 16, 128]. For instance, in [16] a Graphical User Interface (GUI) was designed and developed to process, record and present obtained force data in real-time through a computer software. The user-friendly software was developed in C++ through the Qt GUI library. A simple calibration feature was included as part of this computer interface, which allows users calibrate the sensorized instrument in a simple manner.

Several studies have investigated the effectiveness of auditory feedback in users' performance [56, 129, 130], and have determined that the usefulness of the auditory feedback is very much person dependent. In other words, it appears to be a personal preference among subjects to conduct surgery with or without auditory feedback. The main reason for this variability is the disruptiveness of direct auditory feedback for some users. Moreover, some surgeons have mentioned that the auditory feedback is confusing, considering the already noisy environment of operation rooms [56, 129, 130].

Improving users haptic' perception in MIS is the ultimate goal of a force measurement system. Considering the intuitive nature of haptic feedback, provided information in this method is more understandable and comprehensible for subjects [18]. As a result, several attempts have been made to provide haptic feedback through different methods such as vibrational actuators, Virtual Fixtures (VF), and motor actuated handles [18, 39, 130, 131, 131, 132]. Designing an instrument handle in an ergonomic way is a fundamental parameter to consider when designing a haptic interface [133]. Ergonomic handles are adaptable to various hand sizes to provide precise manipulation moves and to improve the sense of touch by contacting more sensitive areas of users' hands [133]. Indeed, several work have studied the effects of ergonomic handles in improving the efficiency and performance of operators [131–138].

Virtual Fixtures (VF) are type of haptic feedback that prevent users from applying excessive amount of forces or entering undesired regions during surgery by creating resistance using motors and actuators. As mentioned in [56, 139], accurate and reliable force measurements are vital for providing an acceptable VF force feedback for MIS applications. Implementing actuators into the surgical instruments to provide

VF-Type haptic feedback, has drawn attention towards the necessity of developing mechatronic and robotic systems for medical and surgical applications.

## 2.6 Mechatronics and Robotics in MIS

Recently, technologists have developed various hand-held mechatronic instruments in order to add extra DOFs to conventional surgical instruments [92, 140–143]. In these studies, instruments' end-effectors are controlled using integrated buttons, dials, or joysticks on their handles [143, 144]. Although, the developed instruments were more dexterous and intuitive, most subjects preferred to use classic laparoscopic instruments due to their simplicity and light weight [92, 143].

Robotic systems have been developed to address operational issues related to conventional and mechatronic instruments. Developed systems have been able to address dexterity and user comfort issues of traditional instruments. However, operational error is still probable due to the absolute lack of direct contact between the surgeon's hands and the patient's body. Additionally, the longer set up time requirements, considerable space requirements in the OR, and extensive purchase and maintenance costs of robotic systems are among their main disadvantages [3, 5, 7, 92, 143, 145, 146].

In order to authorize the safety and reliability of the developed surgical instruments and robotic systems before commercializing them, strict regulations exist to control and approve the efficiency of the developed systems for real-world applications. Therefore, the developed instruments are expected to satisfy the quality and safety requirements, which affects the design process of medical systems. As a result, the next chapter is devoted to review the existing medical device regulations in North America.

## 2.7 FDA and Health Canada Medical Device Regulation

The FDA (Food and Drug Administration) approval process classifies medical devices into three main categories based on the risk level associated with the device. These classifications include: Class I, Class II, and Class III for the lowest to highest risk associated devices, respectively. In order to commercialize medical devices, they must be approved by the FDA beforehand [147]. Furthermore, according to the FDA regulation process, since August 26th of 2011, any medical device which is Not Substantially Equivalent (NSE) to any identifiable predicate device is automatically classified as a Class III device. However, there

is a special process, De Novo, for reclassifying these types of devices. This provision which is referred as the re-evaluation of automatic Class III designation provision, De Novo, is intended to apply to low-risk products that have been classified as Class III because they lack substantial equivalency to any commercially distributed device [148]. The De Novo process has been around since the implementation of the FDA Modernization Act of 1997 (FDAMA). The FDAMA was intended to improve the efficiency of bringing low-risk medical devices to the market by allowing the reclassification of devices that were classified as Class III due to the lack of a suitable predicate. The FDA process for substantial equivalency determination is elaborated in the flow chart illustrated in Figure 2.5 [149].

Under this provision, within 30 days of receiving an NSE determination, the manufacturer may request that a risk-based classification determination to be made for the device in order to reclassify the product from Class III into Class I or Class II. The FDA will review the device classification proposal and either recommend special controls to create a new Class I or II device classification or determine that the product is a Class III device. If the FDA determines that the level of risk associated with the use of the device is appropriate for a Class II or Class I designation, the product can be cleared as a 510(k) regulation category in which the FDA will issue a new classification regulation and product code. A device placed into Class I or Class II, can then be commercially distributed following the procedure demonstrated in Figure 2.6 and the FDA must publish a notice in the Federal Register for reclassifying the device type. However, if the device is not approved through De Novo, then it must go through the standard Premarket Approval (PMA) process for Class III devices or completed Product Development Protocol (PDP) before being commercially distributed [147, 148].

As part of a reclassification request, a petitioner should provide the results of Non-clinical/Bench studies and tests in order to prove the applicability of the provision in that specific circumstance [148]:

- Biocompatibility and material test
- Performance testing bench test
- Simulated use testing
- Shelf life/sterility test
- Electromagnetic compatibility and electrical safety test

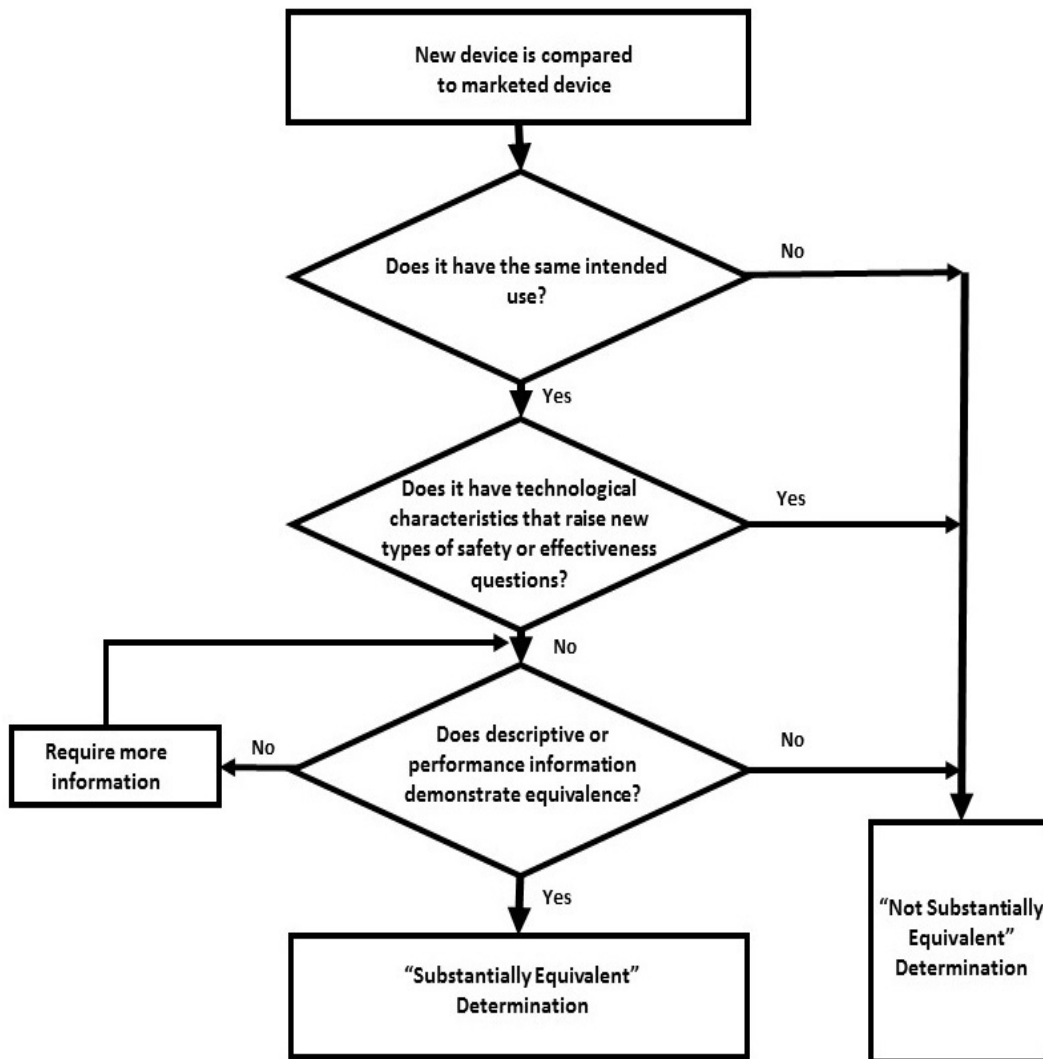


Figure 2.5: The substantial equivalence process flow chart [149]

This process has been precisely followed for a novel developed surgical instrument as presented in [11, 150, 151].

Health Canada medical device regulation classifies the medical devices based on the risk level associated with them. Similar to the FDA, devices with higher classification are subject to more stringent regulatory oversights. Health Canada categorizes medical devices in four classes: Class I, Class II, Class III, and Class IV.

According to Health Canada regulations, MIS used surgical tools are defined as "surgically invasive

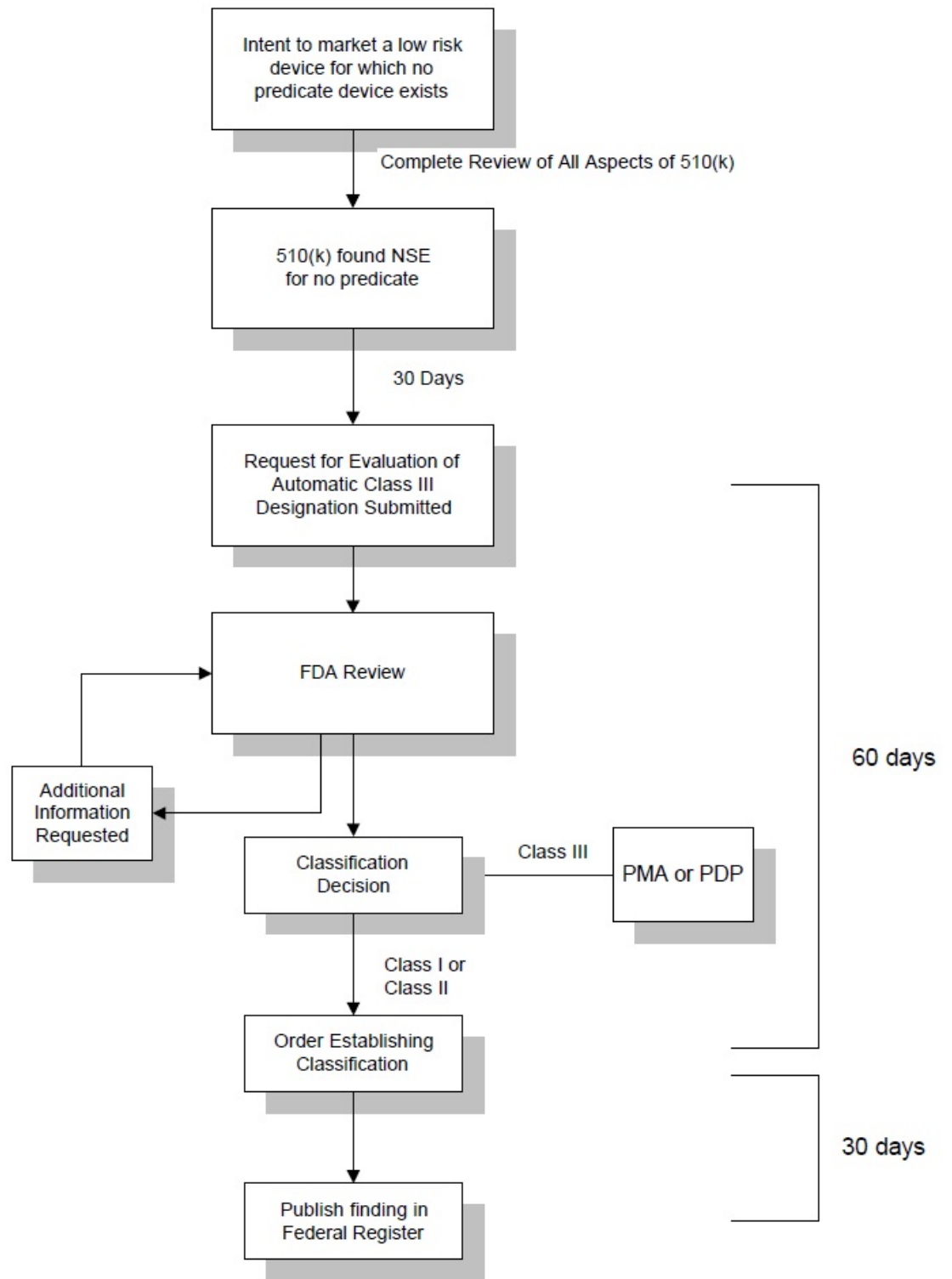


Figure 2.6: Evaluation of automatic Class III designation process [147, 148]

device” or ”surgical or dental instrument”. These two groups include devices that are intended to enter the human body through artificial openings. Devices in these categories are allowed to be used in surgical tasks without any connection to an active device. Considering Health Canada risk-based regulatory system, pre-market, post-market and quality management system requirements apply to all Class III and Class IV devices. Moreover, product licensing is mandatory for these two groups and the certification that the device is designed and manufactured according to ISO 13485 should be provided.

After reviewing the technical requirements and governmental regulations for developing surgical instruments, a summary of the design specifications for a sensorized laparoscopic instrument development is presented in the following section.

## 2.8 Force Sensor Design Specifications

A number of critical design requirements must be considered when designing force sensing systems for *in vivo* use of MIS instruments. A list of the most important requirements is provided as follows:

- **Performance:**

Laparoscopic instruments are used in MIS surgical tasks. Therefore, the designed devices should be able to transfer applied forces sufficiently from the handle of the instrument to its jaws while conducting MIS tasks such as tissue dissection or needle driving.

- **Force Feedback:**

Grasping force, axial force and torque are essential actuation directions in many MIS tasks. Force information in these DOFs could help surgeons in conducting various MIS tasks including: tissue manipulation, needle slippage prevention, precise palpation for tumor localization, adequate torque application for needle drive and suture breakage prevention while tightening knots. As a result, providing 3 DOFs of force information is necessary for improving user performance. However, in order to isolate and decouple these force signals from other disruptive forces existing in the instrument’s working environment, the sensorized device should be able to measure force and torque information at least in 5 DOFs including: grasping force, lateral forces ( $x$  and  $y$ ), axial force ( $z$ ), torque. Also to compensate for the effect of temperature on the force data, a reference sensor for temperature

compensation should be integrated into the device [4].

- **Range and Resolution:**

Generally, a force range of  $\pm 10$  N with a resolution of 0.2 N is required for axial force measurements in MIS [4]. Nevertheless, pulling stitches by a needle driver for tightening knots creates axial forces in a range of 2 – 5 N with resolution of 0.1 N [129, 152]. It was determined by Trejos *et al.* that grasping forces over 20 N are applied by some subjects during instrument assessment [4]. However, typically the expected force range for holding a needle using a needle–driver does not exceed 10 N [3, 129]. The range of measured lateral forces on the tool tip has found to be between -10 N and +10 N [25]. Developed torque sensors should be able measure torsional forces up to 100 Nmm during needle driving tasks [3, 129]. Considering human hand actuation frequency and human haptic perception capability, a force sensor with a sampling rate under 100 Hz and low hysteresis and linear behavior is desired [3, 70, 75].

- **Ergonomic:**

Although an instrument is intended to adequately perform surgical tasks, providing the following features is equally important: ease of handling the driver, sufficient grip for the grasper in order to hold the needle, ease of locking/unlocking the driver, and less hand fatigue. Furthermore, the handle should be strong enough to tolerate actuated forces, since applied grasping forces to the tool handle can exceed 75 N in some cases [133]. Palm pistol shape grippers are widely accepted among different surgeons due to their strong and comfortable design as well as their ease of use.

- **Environmental:**

Since a surgical instrument is intended to be used in *in vivo* applications, it should be biocompatible and sterilizable, in order to avoid any reaction with the human body. Furthermore, for autoclave sterilization and cleaning purposes, the device should be high temperature resistant and chemically-inert [4, 25]. In an autoclave, the most common sterilization system in most hospitals, surgical instruments are exposed to high temperature steam, reaching 105 – 135° C, at a high pressure of around 207 KPa and 100% humidity for 30 minutes [20].



- **Customer:**

Surgeons are the main customers of medical devices. Therefore, overall similarity of the developed devices to traditional instruments is notably important. In addition, light-weight devices with comfortable usage are more favorable. Finally, the low cost of an instrument is one of the most effective parameters in commercializing a medical device [4].

- **Material:**

The most important requirement for the material is that it must be biocompatible. The second expected feature of the material is its ductility. From a safety point of view, in terms of design failure, the instrument should first start yielding before any breakage occurrence. Tool fracture leading to small pieces spreading inside a patient's body can have catastrophic consequences.

MRI compatibility and EM inertness would make it feasible to use the instrument in other medical environments or for future application of the sensor in robotic-imaging fields [4, 25]. Stainless steel, titanium, and Nitinol are widely used in medical applications due to their biocompatibility and ductility [70].

- **Geometric features:**

The Outer Diameter (OD) of the developed laparoscopic instrument must be smaller than the size of the trocar being used in the procedure. Although in most of cases 10mm trocars are used as body entry ports, specific surgeries require 5mm trocars [4]. In general, the size and weight of a designed instrument are better to be the same as a commercially available instrument of its own type. The average weight of hand-held laparoscopic instruments is 70 grams, while the working length of needle drivers is 30 – 45 cm [133]. Moreover, no sharp corners should exist on a surgical tool to avoid accidental tissue cutting [25].

- **Manufacturing:**

Building parts in several pieces and assembling them afterward is a helpful step in simplifying the design process. By doing so, it is possible to fabricate instrument parts with either conventional methods (machining, milling and CNC (Computer Numerical Control) cutting) or with newer methods such as 3D printing and rapid prototyping.

- **User Interface:**

The developed user interface should be user-friendly in order to allow users to monitor real-time force feedback.

## 2.9 Research Motivation and Objectives

Significant advancements in measuring axial and grasping forces in MIS laparoscopic instruments have been reported in the literature; however, the reliability of measured forces is arguable in most of the presented work. Measuring axial force at any location except at the instruments tip comes with a considerable amount of error caused by friction and disturbing forces of other DOFs. Grasping forces exerted on the instrument jaw influence the measured axial forces on the instrument shaft. Moreover, driving cables or rods are responsible for opening and closing the grasper in most instruments by transferring force from the tool handle to its jaws. Applying grasping forces not only causes tension in these cables or rods but also causes lateral forces at the joint support of jaws. These lateral forces are dependent on the location and surface properties (such as coefficient of friction) of the grasped objects. The axial portion of these undesired forces impairs the axial force measurement on the shaft. Likewise, the friction present in the tool joints and internal mechanism frictions cause measurement inaccuracy. All together, these factors make it very difficult to decouple the measured axial force on the instrument shaft from the grasping force. Although Rosen *et al.* developed a model of the internal mechanism of the grasper in order to cancel this effect through computer software processes, the obtained results are not accurate enough for medical applications [91].

Based on our experience with sensing technologies, calibration of FBG-based sensors lasts longer than other similar sensors. In addition, FBG sensors satisfy sterilizability requirements. High sensitivity and accuracy of FBG sensors make them a good choice for medical applications. As a result, a device with FBG sensors is more practical for *in vivo* applications.

In summary, measuring forces at the tip of surgical instruments has led to provide more reliable force information for MIS. However, to the best of our knowledge, a sterilizable technology with high measurement accuracy and resolution is still missing. Therefore, the goal of this work was to develop a sterilizable 5-DOF laparoscopic needle driver capable of measuring applied grasping and axial forces on the tool tip and two orthogonal moments and torsion over the instrument shaft. The sensorized instrument is intended

to be able to measure torsion and bending moments caused by transverse forces. Since measuring axial and grasping forces on the tool tip was the novel part of this work and it has not been tested in any work, partial prototypes of this design were developed and built to demonstrate the feasibility of this novel concept, as described in the following chapters. Subsequently, this concept was implemented into a complete 5-DOF needle-driver design.

## Chapter 3

# First Generation of Sensor Prototype

### 3.1 Introduction

In order to study the feasibility of measuring grasping and axial forces on the tool tip, a prototype of the sensorized grasper has been designed and built. The developed prototype is a laparoscopic needle-driver-type grasper that is capable of measuring forces in 2-DOF. Sterilizability requirements were considered for choosing the prototype material and that of the force sensors. This chapter describes the design, development and assessment of the first prototype. This chapter is based on reference [153].

### 3.2 Design Specifications

Table 3.1 presents the design specification list for the first prototype. The developed prototype has a similar size and appearance to a commercial instrument and it fits inside of a 5-mm trocar. 12 mm of working length is considered over the grasper jaw for grasping a needle during suturing and knot tying tasks. Since the instrument comes in contact with body organs, it needs to be made from biocompatible materials. The chosen material must be nontoxic, corrosion-resistant, and neutral in the human body in order to not react with body in any way. For sterilization and cleaning purposes, the chosen material should be able to stand steam sterilization in an autoclave. These conditions include high pressure of up to 200 KPa, 100% humidity, and high temperature (105 – 135° C) for 30 minutes [20]. As it is shown in Figure 3.1, CES software was used to evaluate different available materials for the sensor fabrication [154]. Hence, stainless

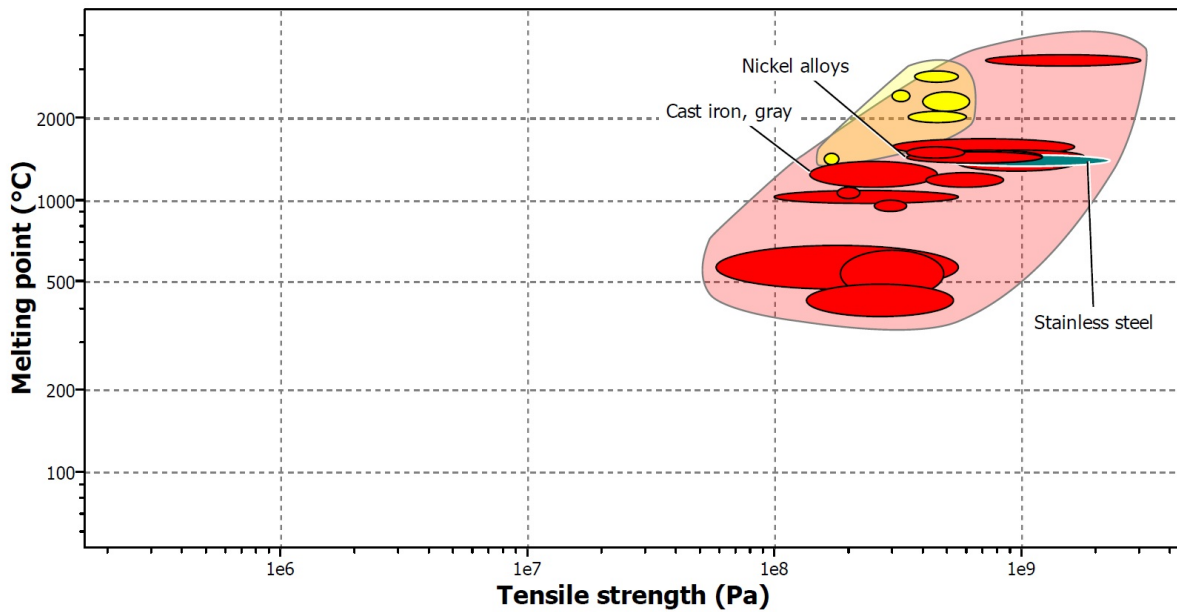


Figure 3.1: CES material selection bubble charts; the axis are displayed on a logarithmic scale. The bubble chart is the classical Ashby selection chart. The bubble that represents each material is the ellipse that circumscribes those values when plotted on the X and Y axes. Melting point (sterilizability) vs. Tensile strength (mechanical behavior of various materials).

steel (SAE 316) was chosen for the sensor fabrication considering its general mechanical properties, density, biocompatibility and sterilizability. Considering existing size restrictions at the tool tip, FBG optical sensors were chosen due to their small size. In addition, FBG sensors are capable of withstanding high temperature and high pressure conditions during sterilization cycles in an autoclave. Furthermore, their high sensitivity makes them a good fit for measuring forces in MIS tasks.

After determining the design specifications, a model of the sensorized instrument was designed, as presented in the following section.

### 3.3 Mechanical Design of the Partial Prototype

The CAD model of the 2-DOF novel grasper was designed and developed using SolidWorks, as shown in Figure 3.2. In this 2-DOF sensorized grasper, grasping and axial forces are measured at their exertion point on the tool tip. The elongation caused by the exerted axial forces over the jaw is measured by the optical sensing system as an indicator of the experienced axial forces while pulling objects. A flexure segment

Table 3.1: Summary of design specifications

Parameter	Value	FBG	SG
Dimension	5 mm	✓	×
Grasper type	Laparoscopic needle-driver	✓	✓
Jaw working length	5–20 mm	✓	×
Force sensor type	FBG (Optical sensor)	✓	×
Performance DOF	6-DOF and grasping	✓	✓
Force sensing DOF	2-DOF (Axial-Grasping)	✓	✓
Temperature compensation	No	✓	✓
Axial force range	2–5 N	✓	✓
Axial force resolution	0.1 N	✓	×
Grasping force range	0–10 N	✓	✓
Grasping force resolution	0.2 N	✓	×
Force sampling	<100 Hz	✓	✓
Maximum gripping force at handle	75 N	×	✓
Handle type	Not applicable for this prototype	×	×
Working temperature	37°C	✓	✓
Maximum temperature	135°C (Autoclave)	✓	✓
Torque range	Not applicable	✓	✓
Biocompatibility	Yes	✓	✓
Sterilizability	Yes	✓	×
Sealed (Waterproof)	Yes	✓	×
Material	Stainless steel - Titanium - Tungsten Carbide	✓	✓
Disposable	No	×	✓
Manufacturing method	Rapid prototyping - Machining	✓	✓

was considered in the grasper design in order to increase the sensitivity of the axial sensor. Therefore, each grasper jaw consists of a deformable part and a fixed part, as shown in Figure 3.2. Since the deformable part has to elongate only in the axial direction, a guide channel underneath the sliding part (deformable part) was designed in order to constrain its movement in 1-DOF.

In order to reduce the friction between the sliding and stationary parts, 6 titanium balls (high-strength Grade 5 titanium), 0.8 mm in diameter were placed in the guide channel in order to minimize the contact surface. As a result, the deformable part smoothly slides over the balls during an axial force application, as shown in Figure 3.3. In addition, both the upper jaw and the lower jaw of the grasper have similar structures in order to provide a symmetric displacement when pulling objects. As shown in Figure 3.3, the

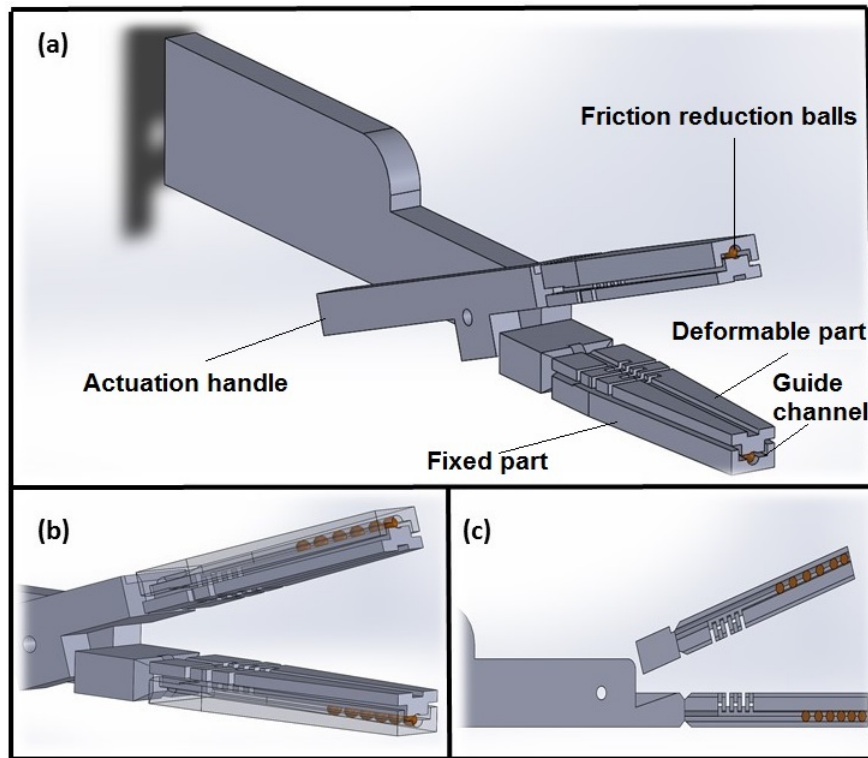


Figure 3.2: a) CAD model of the sensorized grasper; b) Placement of titanium balls in the guide channel to reduce friction; c) Cross-sectional side view of the grasper showing the flexure segment and the friction reduction balls (used with permission) [153].

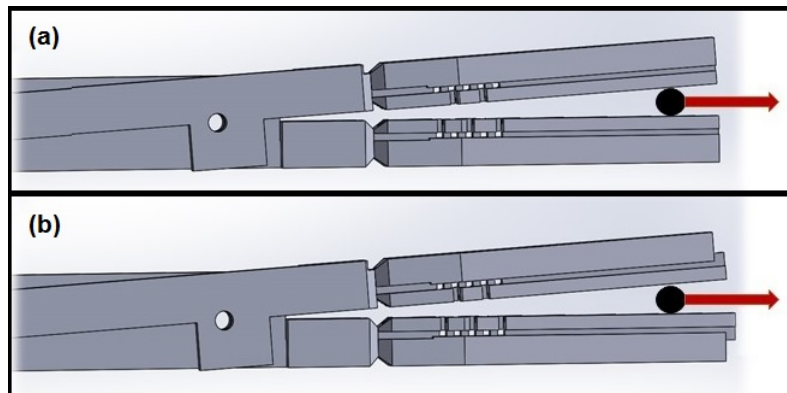


Figure 3.3: An applied axial force causes the deformable part to slide over the fixed part while pulling an object— drawing not to scale— (used with permission) [153].

synchronized deflection of both jaws increases sensing accuracy by preventing slippage between the pulled object and the jaw.

A  $0.8 \times 0.3$  mm channel was designed over the grasper jaw for embedding optical sensors. Two optical

fibre-based force sensors were placed in this channel for measuring axial and direct grasping forces. Since the axial force sensor is placed on the tool tip, neither the joint friction nor the axial force generated by driving cables or rods, affect its measurements. Hence, more reliable axial force measurements can be achieved. Furthermore, in order to isolate the axial sensor from the effects of exerted bending or torsion (decoupling axial from torsion/bending), the sensor was located on the crossing point of the neutral axes of the grasper (the geometric centroid of the instrument).

Finally, since the lower jaw of a needle–driver does not move with respect to the instrument shaft, it was possible to route the fibres from this jaw without bending them excessively. The FBG channel was continued at the end of the jaw to provide an outlet for fibre passage. In order to avoid fibre damage, the channel used for the fibres was designed considering the fibres' bending radius of 17 mm [87, 155].

### 3.4 Finite Element Simulation

An FEA was performed in ANSYS in order to examine the practicality of the design in providing an adequate amount of strain over the 3 mm grating of the axial force sensor. As shown in Figure 3.4, the first FEA was performed in a 2D-ANSYS. However, the 2D-ANSYS was incapable of modeling several parts of the grasper and existing boundary conditions between them. Therefore, a 3D model of the design, considering different materials for optical fibres and the grasper jaw, was developed and analyzed in the ANSYS Workbench environment, as demonstrated in Figure 3.5. In this model, stainless steel and polyethylene have been chosen as the grasper and optical fibre materials with Young's moduli of  $2 \text{ E}+11$  and  $1.1 \text{ E}+9$  GPa, respectively.

As shown in Figure 3.5, a maximum displacement of  $29.7 \mu\text{m}$  (which equals  $1650 \mu\epsilon$  considering the 18mm jaw length) was obtained for the highest expected load during the suturing task (5 N). As a result, adequate axial force sensing ability was expected from the placement of the sensor on this flexure structure considering the physical properties of FBG sensors, their strain limit of up to  $5000 \mu\epsilon$  and their strain sensitivity of  $1.2 \text{ pm}/\mu\epsilon$ .



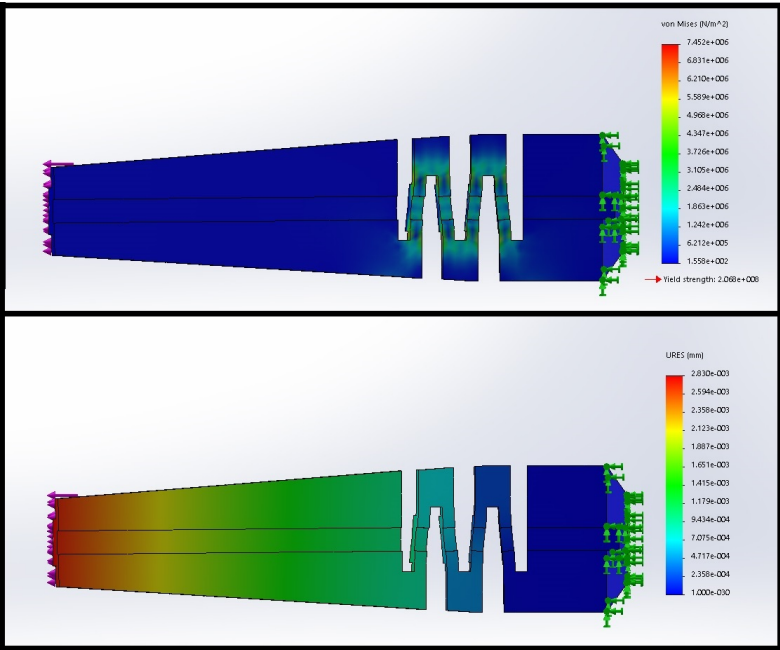


Figure 3.4: FEA in 2D-ANSYS.

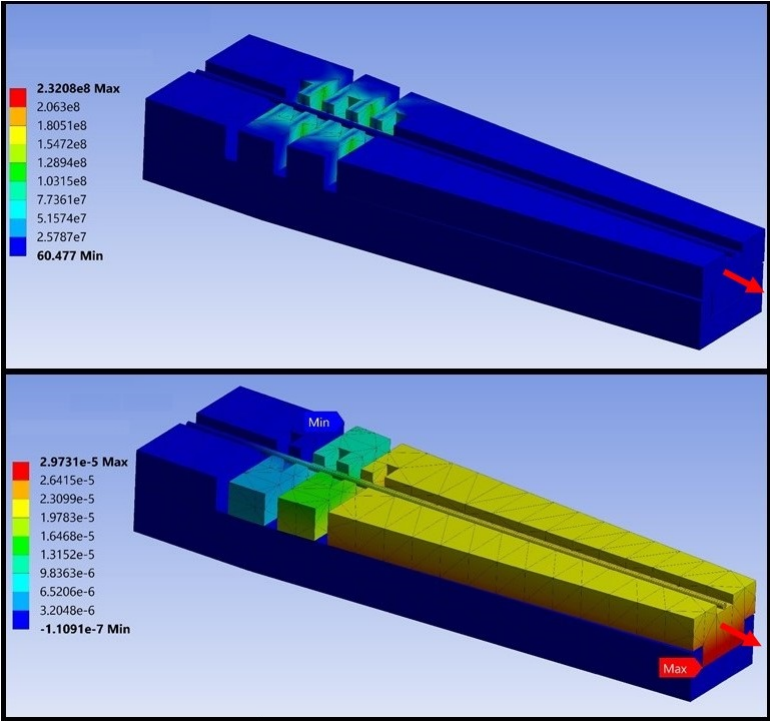


Figure 3.5: FEA for the generated strain and stress by 5N axial force over the axial FBG in 3D-ANSYS.

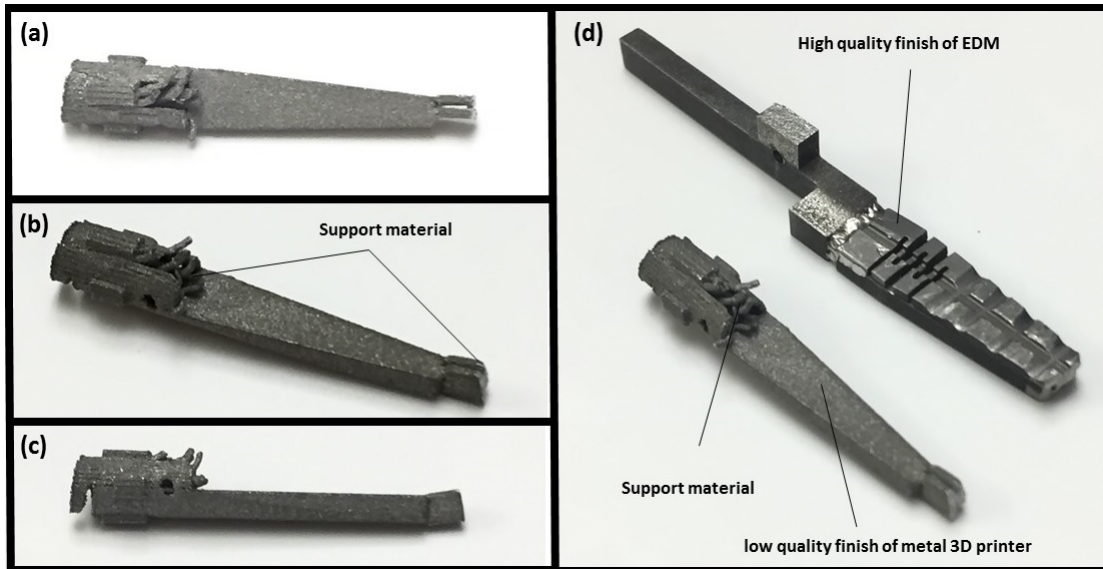


Figure 3.6: a) Top view of the SLM printed part showing low finish quality; b) The problem related to support material and difficult post-processing; c) Side view showing the low quality hole for dowel pin joint; d) Low quality finish of the SLM part compared to the high quality finish in EDM machining.

### 3.5 Sensor Fabrication and Prototyping

After finalizing the design, possible fabrication methods were considered to build the grasper. As shown in Figure 3.6, a prototype using a Selective Laser Melting (SLM) machine (SLM 500, SLM Solutions Group AG, 23556 Lubeck, Germany) was built. Although, building complex parts by SLM was simple, the surface finish of the fabricated parts (roughness value of  $20 \text{ Ra } (\mu\text{m})$ ) was not satisfying compared to the high quality finish of traditional machining methods (roughness value of  $4 \text{ Ra } (\mu\text{m})$ ), as shown in Figure 3.6 (d). In addition, cleaning the support material out of parts during post-processing required a lot of effort and time. Figure 3.6 (b) shows the remainder of the support material after initial post-processing. Therefore, a wire-EDM (Electrical Discharge Machine) was used to manufacture the grasper components, as shown in Figure 3.7. As a result, an iterative design process followed regarding the machining constraints and requirements. In order to simplify the manufacturing process, the parts were designed and manufactured in several simple pieces, as shown in Figure 3.8. Subsequently, a Computer Numerical Control (CNC) micromachine was used to drill the 1 mm holes of the grasper joint. Finally, the micro-welding method (using autoclavable 316 L filler rod) was used to attach the fabricated pieces, as shown in Figure 3.9.

In order to address safety concerns when using welded parts in a medical application, the strength of the

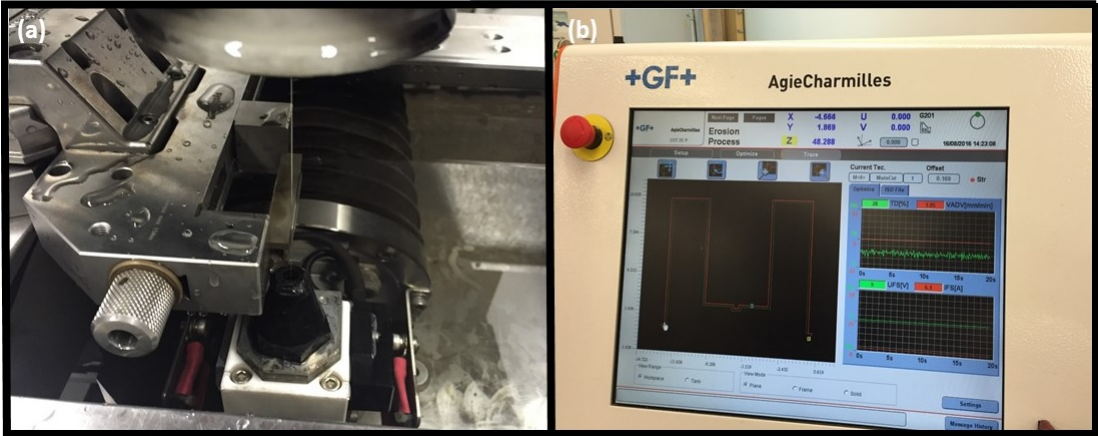


Figure 3.7: EDM machining

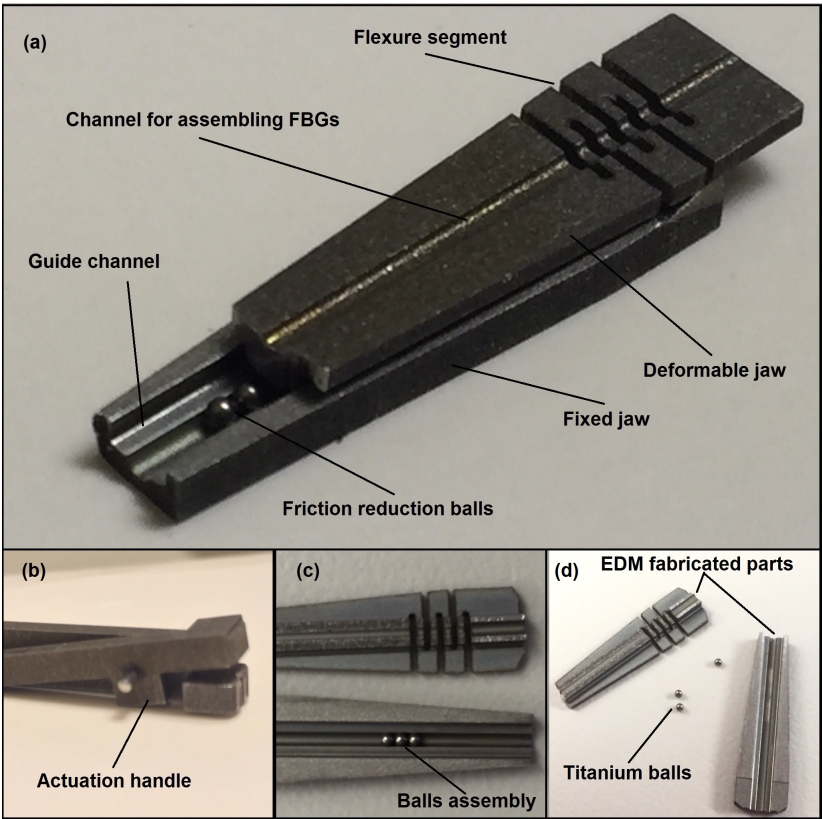


Figure 3.8: a) Assembly of EDM fabricated pieces; b) Actuation handle; c) Ball placement in the guide channel; d) Grasper pieces before welding (used with permission) [153].

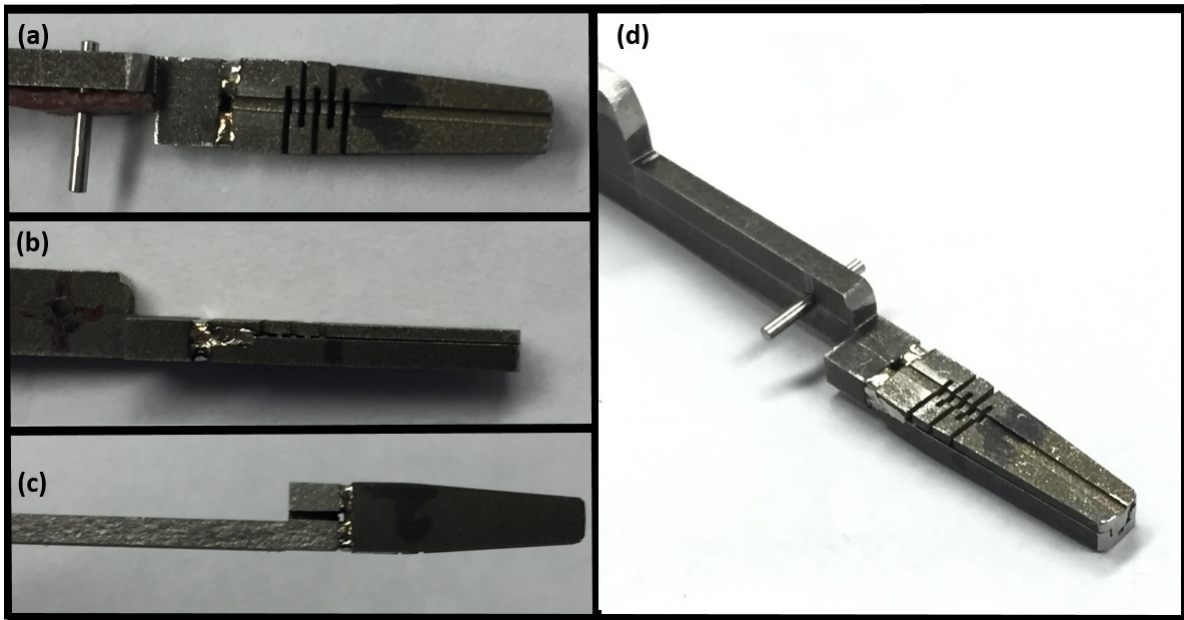


Figure 3.9: a) Top view of the welded grasper; b) Side view of the welded grasper; c) Bottom view of the welded grasper; d) Lower jaw of the needle-driver grasper after welding several pieces of the jaw.

micro-weld was tested by holding one of the jaws in a cantilever position and applying known loads to its tip, as shown in Figure 3.10 (c). Although a peak force of 10 N would satisfy the strength requirements for the grasper application, the weld was able to withstand 50 N without breaking, which was 5 times greater than the necessary amount. Therefore, considering the safety factor of 4 for medical applications, the weld adequately satisfies the safety requirements. It worth mentioning that the friction reduction balls were placed in the guide channel prior to welding and the FBG sensors were embedded in the device afterwards.

Two FBGs (os1100, Micron Optics Inc., Atlanta, GA, USA) were placed into the machined channel over the lower jaw for force measurement. The jaw was sensorized with 8- and 3-mm grating FBG optical fibres for grasping and axial force measurements during tasks such as object manipulation and stitch pulling. As shown in Figure 3.10 (d), the 3-mm axial FBG was glued over the deformable segment of the jaw considering the effects of the flexure structure in increasing the axial sensitivity of the sensor. Furthermore, the grasping FBG was mounted over the jaw proximally after the flexure segment for pure grasping force measurement. As demonstrated in Figure 3.10 (b), superglue (Krazy Glue, Elmer's products Canada) was used to attach both grasping and axial sensors to the jaw.

Once the sensors were mounted over the instrument, a data acquisition method was required to record



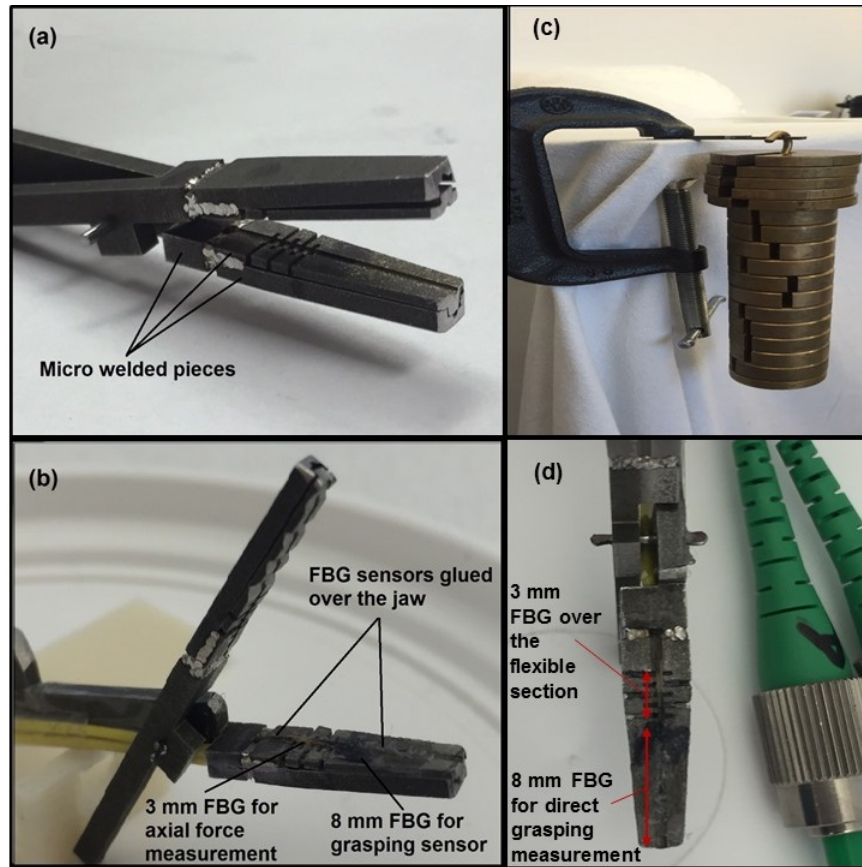


Figure 3.10: a) Assembled and welded parts; b) Sensorized jaw; c) Weld strength test at 17 N load; d) Installation of FBG fibres on the grasper (used with permission) [153].

force information provided by FBG sensors.

### 3.6 Data Acquisition

An optical interrogator (SM130, Micron Optics Inc., Atlanta, GA, USA) was used for FBG data acquisition. The reflected light intensity of each wavelength from the FBGs were acquired by the interrogator. The interrogator is capable of collecting data with a sampling rate of 100 Hz. In order to provide visual feedback for users, the acquired data were presented to the users through a custom-made computer interface.

Figure 3.11 illustrates the developed user-friendly graphical interface for acquiring information from the interrogator and displaying it to the users. Through this software, users are allowed to query data from the FBG sensors, calibrate the sensors and monitor the real-time processed data in graphical charts. The real-time graphs display raw and processed/calibrated force data. In addition, all this information can be

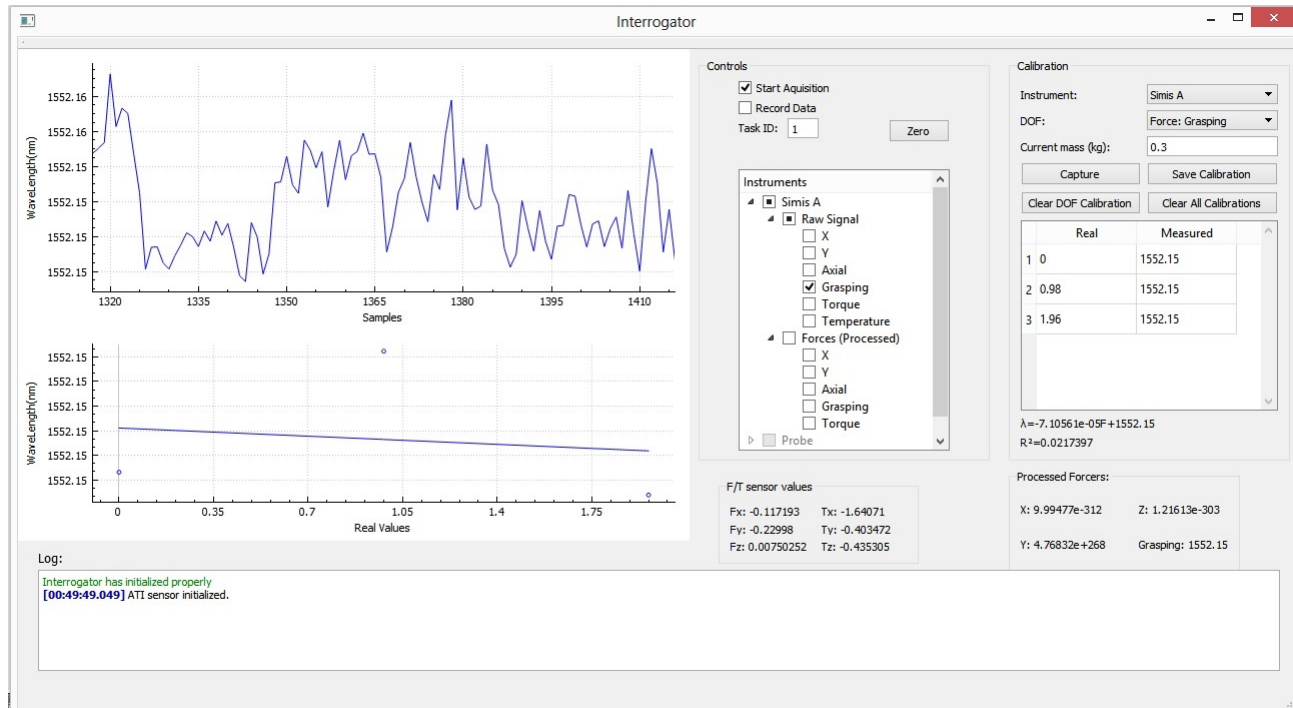


Figure 3.11: Custom-made user interface: The top graph presents the real-time acquired force data from FBG sensors and the processed data. The bottom graph shows the linear regression slope used for sensor calibration. Force and torque values received from F/T ATI sensor are provided for users in a quantitative method. The user-interface is able to present acquired and processed force and torque data, as well as data received from temperature compensation FBG.

stored for post-processing and further analysis purposes. Simultaneously, the force information from a commercial force/torque (F/T) sensor (ATI Nano-17, ATI Industrial Automation, Apex, NC, USA) can be obtained and recorded for sensor calibration and performance validation. Real-time force values obtained from the F/T sensor were also displayed to users, as shown in Figure 3.11. The bottom graph of Figure 3.11 shows the calibration diagram. Details of the calibration process are presented in the following section.

## 3.7 Calibration

### 3.7.1 Calibration Setup

An ATI F/T sensor was used to calibrate the grasping and the axial force sensors. Through simultaneous data measurement between the two sensors, a relationship was established between the acquired wavelength information from the FBGs and the collected force information from the F/T sensor. Thus, a wavelength

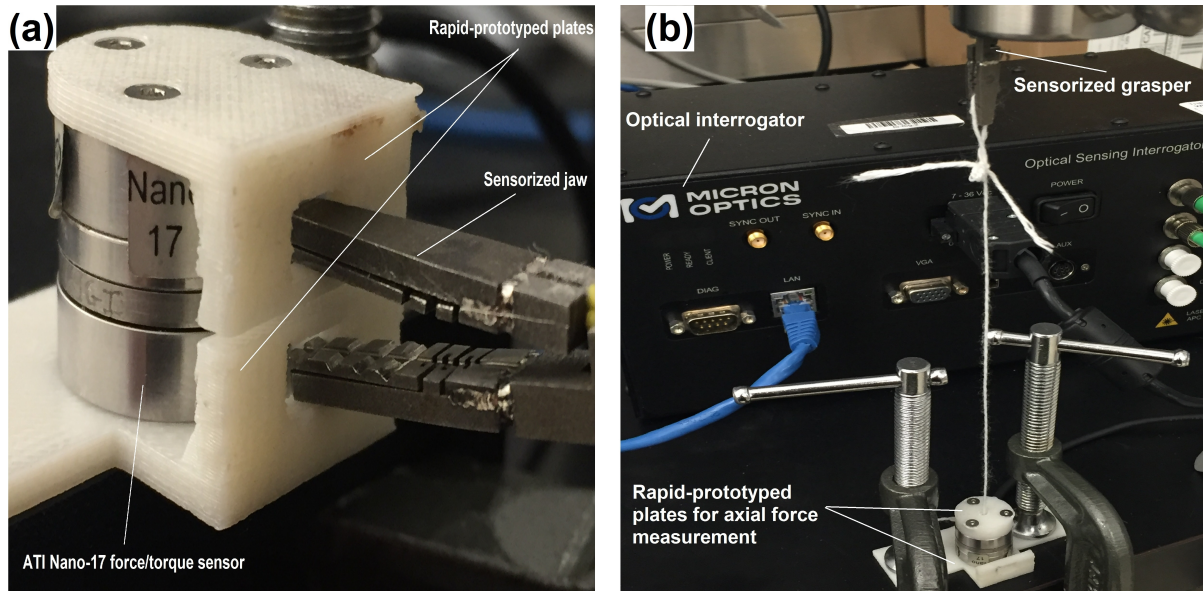


Figure 3.12: a) Setup for calibrating the grasping force sensor; b) Setup for calibrating the axial force sensor (used with permission) [153].

shift in the FBGs signal could be related to the applied forces on the F/T sensor. For this purpose, calibration plates were designed and attached to both sides of the F/T sensor in order to transfer the exerted grasping and axial forces from the grasper to the F/T sensor. Rapid prototyping methods were used to fabricate these parts using a 3D-printer. As shown in Figure 3.12 (a), for calibrating the grasping sensor, the grasper jaws grasped plastic calibration plates in a perpendicular direction with respect to the pivotal axis of the F/T sensor. As a result, the applied grasping forces generated a torque in the ATI F/T sensor at a 14-mm distance.

To calibrate the axial sensor, a rope was attached to a calibration plate and mounted on top of the F/T sensor, as shown in Figure 3.12 (b). By pulling on this rope, axial forces were generated on both the F/T sensor and the grasper. In order to achieve the best possible results, the grasper was aligned with the axial direction of the F/T sensor in order to avoid the effects of angular force exertion.

### 3.7.2 Calibration Method

To calibrate the grasping sensor, the grasper jaws squeezed the calibration plates and applied a steadily increasing amount of force until the F/T sensor reached 10 N. Similarly, the axial calibration plate was pulled upward by the rope in a steady manner until the F/T sensor indicated the application of 5 N of force.

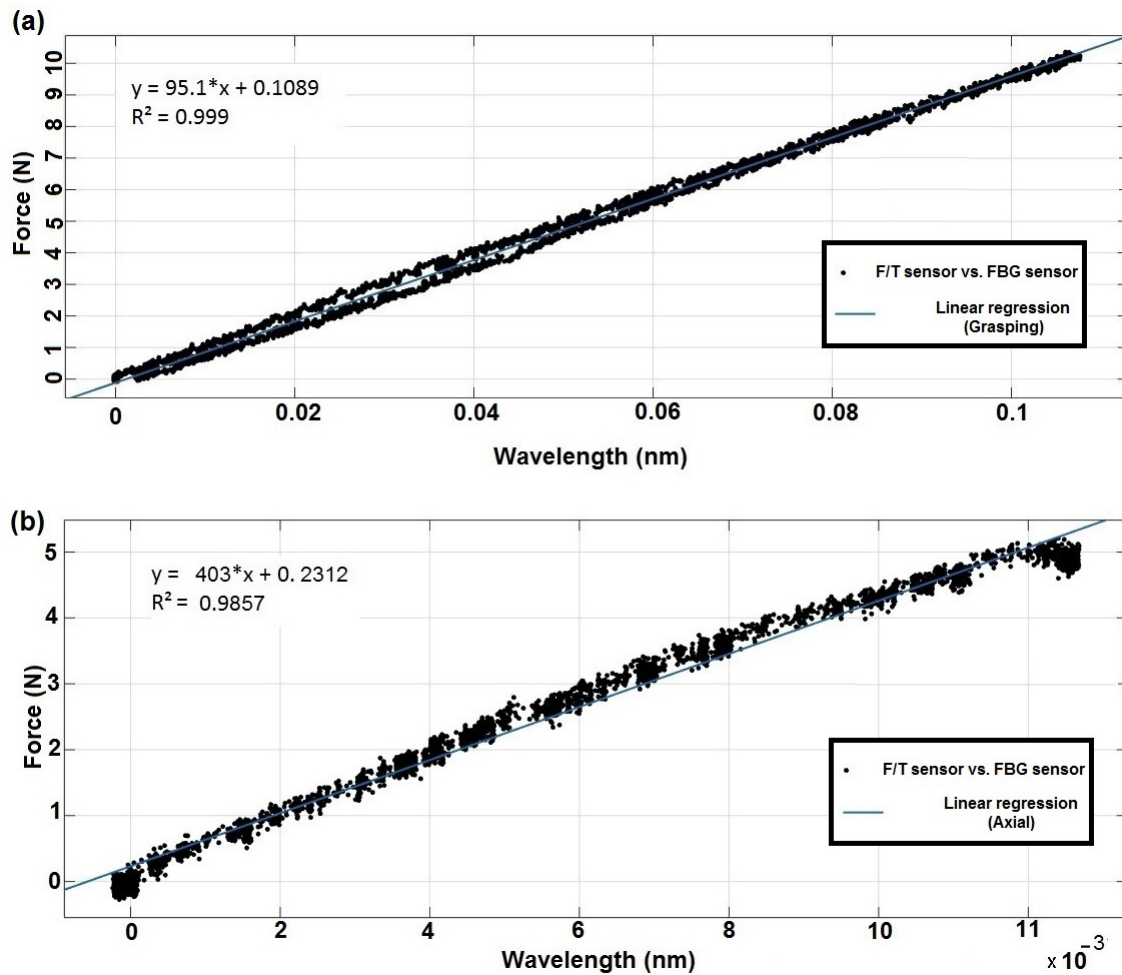


Figure 3.13: Relationship between the FBG wavelength and the F/T sensor values: a) Grasping force sensor calibration b) Axial sensor calibration (used with permission) [153].

In all of the experiments, the bias in sensor measurements was removed before starting the calibration or data acquisition.

Force data from the F/T sensor and the sensorized grasper were simultaneously acquired and recorded using the developed graphical user interface. These data were used to calculate a linear regression in order to determine a relationship between the wavelength of the FBGs and the force values of the ATI F/T sensor. The linear regression equation was calculated using the *cftool* toolbox in MATLAB. Figure 3.13 shows the calibration diagrams and the fitted lines for the axial and grasping calibration. The regression equation and its coefficient of determination value are shown on the top left corner of these diagrams.



### 3.8 Sensor Performance Assessment

To assess the performance of the grasper after calibration, the same method used for calibration was repeated three additional times. For this assessment, real-time force values from the F/T sensor and the calibrated FBG signals were recorded. The recorded data were analyzed in order to determine the following measurements:

- Accuracy: the accuracy was calculated as the root-mean-square (RMS) of the difference between the measured force of the FBG and the F/T sensor.
- Hysteresis: the hysteresis was determined as the difference between the RMS error for the loading and unloading phases of the grasping sensor.
- Repeatability: To study the repeatability of the sensors, the standard deviation of the three RMS errors for each trial was calculated.
- Drift: to calculate signal drift, FBG force values were recorded under no load. Two sets of force values, recorded for 10 seconds, 10 minutes apart were used.
- Noise: the noise was calculated as the difference between the lowest and the highest force value observed in a 10 second data set.

### 3.9 Results and Discussion

Figure 3.14 shows the results of the processed force data from the sensorized grasper compared to the actual force values obtained from the F/T sensor. The presented graph distinctly shows the ability of the FBG sensors to accurately follow the F/T sensor in one assessment cycle. Assessment results for all three validation cycles are presented in Table 3.2. Accuracies of 0.19 N and 0.26 N were achieved for the grasping and axial sensors, respectively. An RMS error of 0.19 N for the grasping sensor in a working range of 0 – 10 N satisfies the grasping force requirements for suturing and knot tying tasks. Similarly, the results of the axial sensor are accurate enough for measuring axial forces in MIS in the range of 2 – 5 N [2].

The amounts of noise and drift present in the developed FBG-based sensors are acceptable for medical applications performed via a needle-driver [2]. This indicate that the use of FBG sensors can result in

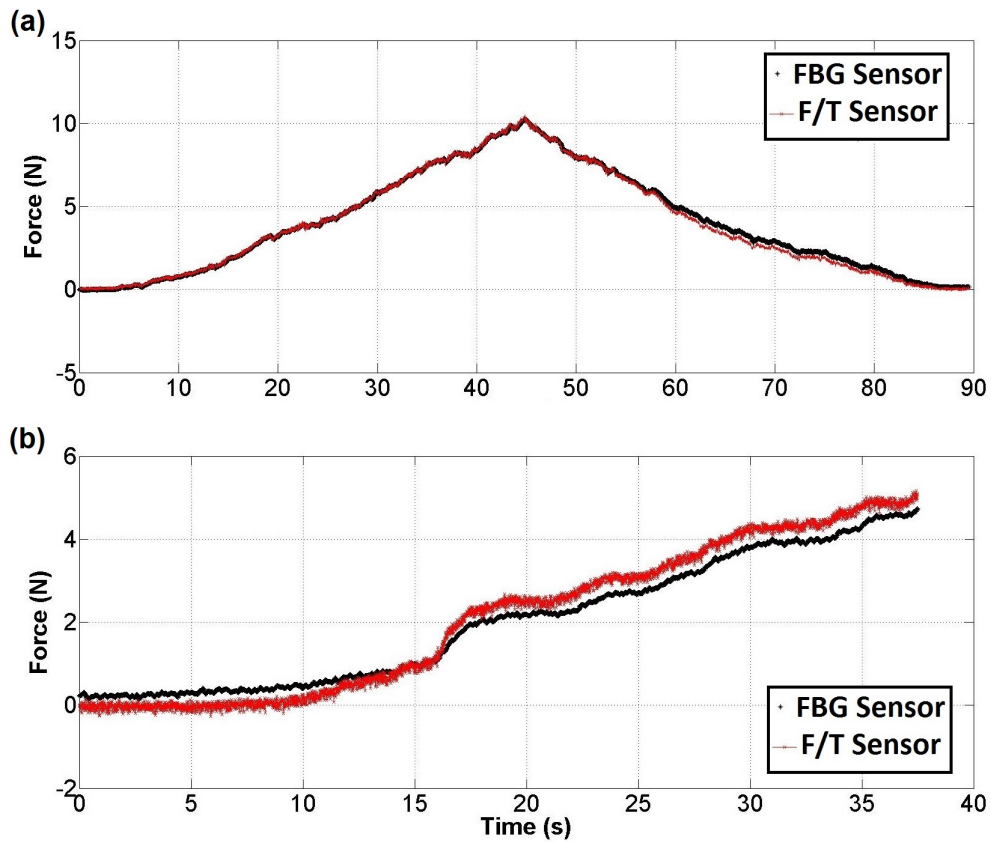


Figure 3.14: Comparison of the force data obtained from the ATI force sensor and the FBG grasping sensor (*top*) and from the ATI force sensor and the FBG axial sensor (*bottom*) (used with permission) [153]

reliable and repeatable force sensing results during long operations. As presented in Table 3.2, the amounts of noise in sensors (0.056 N for the grasping sensor and 0.049 N for the axial sensor) are better than the provided range (0.1 – 0.3 N) in the literature [2]; however, the amount of drift is not within the exact expected range reported in Table 3.1. To our knowledge, this is due to the intrinsic characteristics of the utilized interrogator.

For this generation of the sensor, the hysteresis for the axial direction was not calculated, as we were only interested in the loading phase. Nonetheless, a hysteresis of 0.11 N was observed for the grasping sensor over three trials. We consider this to be an acceptable value for the hysteresis behavior of the grasping sensor.

Table 3.2: Performance of the first generation of the sensorized grasper [153].

	Grasping (N)	Axial (N)
RMS Error	0.19	0.26
Repeatability	0.21	0.35
RMS Hysteresis	0.11	—
Drift	1.48	1.85
Noise	0.056	0.049

### 3.9.1 Conclusion

In conclusion, although the novel idea of measuring grasping and axial forces at their exertion point on the tool tip was feasible and effective, some problems with the first generation of the developed sensor were identified. If addressed, it would serve to significantly improve sensor efficiency. The problems related to the first generation of the sensor are listed as follows:

1. Grasping an object causes the jaws of the grasper to microscopically bend outward. However, its influence on force measurements was neglected in the design of the sensing system. This fact considerably impaired the functioning of both grasping and axial sensors. In other words, the grasping sensor produces different results for similar forces exerted at different locations on the grasper jaw. Hence, the results of the grasping sensor were repeatable only when forces were exerted on the same location on the jaw, which is not a realistic assumption for the actual use of the instrument. Similarly, the axial sensor was coupled with bending in the jaw. Locating the axial sensor on the neutral axis of the grasper isolated it from the effects of overall bending of the tool but further design modifications are required to minimize the undesired effect of outward bending of the sensorized jaw on the axial and grasping sensors.
2. Even though only the loading phase of the axial force sensor is needed in knot tying and suturing tasks, sensor hysteresis must be evaluated in order to expand the sensor application to other surgical tasks, such as palpating, in which both loading and unloading phases are required [58].
3. The melting point of the chosen superglue was  $62^{\circ}$  C, which is not suitable for autoclave sterilization.
4. The F/T sensor does not have sufficient resolution for the torque measurement required when calibrating the grasping force. Hence, a new calibration setup for the grasping sensor based on the force

direction of the F/T sensor is required.

5. The elastic behaviour of the rope used for axial sensor calibration changed with use. This problem led to the poor repeatability of the obtained force information in the axial direction after a couple of experimental cycles. As a result, a more reliable calibration and validation setup for the axial sensor is required.

To address these issues, a second generation of the grasper prototype was designed and developed, as presented in the following chapter.

## **Chapter 4**

# **Second Generation of Sensor Prototype**

### **4.1 Introduction**

The first generation of the sensorized grasper was adequately capable of measuring axial and grasping forces at their exertion point. The practicality of the idea of integrating force sensors on the tool tip was proven. However, a few limitations restricted its use in real-world applications. Therefore, the second generation of the sensor was designed, developed and evaluated in order to address these limitations that is described in this chapter. This chapter is based on reference [156].

### **4.2 Design Solutions**

#### **4.2.1 Introduction**

The main imperfection with the first generation of the sensor was its inability to repeat similar outputs for identical forces applied on different locations over the jaw. This problem was caused because of the outward bending of the jaw at a microscopic scale during grasping. As a result, the main goal of the new grasper design was to mechanically strengthen the grasper in order to decrease the amount of bending while grasping objects; however the trade-off between rigidity of the sensing structure and sensitivity of the axial force sensor should be considered. Therefore, in order to decrease the effect of undesired outward bending of the jaw, different alloys of stainless steel and various biocompatible materials such as titanium and Nitinol (with Young's modulus of 105 GPa and 75 GPa, respectively) were considered as alternatives to

stainless steel. An ANSYS FEA was conducted to study the efficiency of these alternatives. None of these materials presented less bending compared to stainless steel despite the fact that they have higher yield strength. It was because of their lower elastic modulus (Young's modulus of 203 GPa) than stainless steel. As a result, similar to the former sensor, surgical and implantable stainless steel (SAE 316) was chosen for the second generation of the grasper due to its high strength and corrosion resistance.

The next solution for reducing the outward bending of jaws was to improve the overall design of the grasper. CAD model of a new type of sensorized grasper for measuring the axial and grasping forces at their exertion point on the tool tip was developed [156]. Later, an iterative design process based on FEA was followed to maximize rigidity of the new grasper model and its ability to provide adequate strain for the axial force sensor. Figure 4.1 shows the CAD model of the new design. As shown in Figure 4.1, in a similar manner to the first prototype, each grasper jaw consists of a deformable (stretchable) element and a fixed segment. The deformable part was created by weakening the proximal end of the jaw. The elongation of this flexure segment is limited to 1 DOF and it is meant to increase the axial sensitivity while pulling. As is shown in Figure 4.2, the upper and lower jaws were designed in a symmetric manner in order to provide synchronised sliding and prevent slippage between jaws and the pulled object. As shown in Figure 4.1, friction reduction balls are not considered for the second prototype of the sensor. Based on our experience with the first generation of the sensor, the impact of friction balls is negligible in sensor measurements since the deflections in the grasper were in the micro range. As a result, no friction reduction balls were included in the second design.

The latter generation of the grasper is designed considering basic principles of bending stress in beams. In this regard, the following equations are presented from the literature [78]:

$$\sigma = \frac{M \cdot C}{I} \quad (4.1)$$

$$\varepsilon = \frac{\sigma}{E} = \frac{M \cdot C}{I \cdot E} \quad (4.2)$$

where  $\sigma$  is the bending stress caused by the grasping force,  $M$  is the bending generated by grasping objects,  $\varepsilon$  is the axial strain caused by the bending stress,  $E$  is the Young's modulus of the chosen material,  $C$  is the distance between the sensor location and the neutral axis of the cross section and  $I$  is the second moment

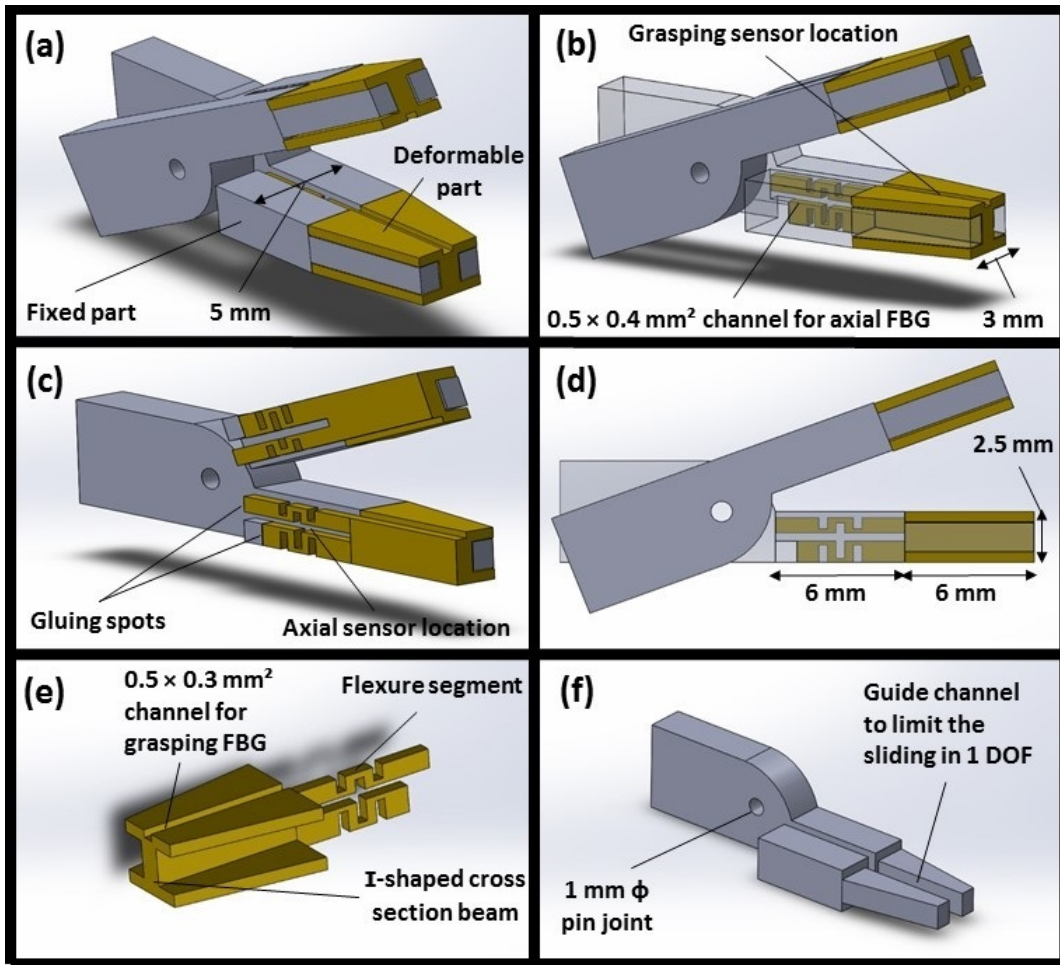


Figure 4.1: a) CAD model of the second generation of the grasper; b) Grasping and axial sensor locations; c) Section view of the grasper structure; d) Accordion shape deformable structure; e) Moving piece of the grasper; f) Fixed piece of the grasper (used with permission) [156].

of area of the bending cross section of the jaw.

As illustrated in Figure 4.3, the cross section of the deformable part of the new grasper jaw is designed in an I-shape in order to increase grasper rigidity; whereas the cross section of the first sensor was T-shaped. Figure 4.3 shows that the second moment of area of an I-shaped cross section ( $5.39 \text{ mm}^4$ ) is greater than the second moment of area of a T-shaped cross section ( $3.69 \text{ mm}^4$ ). As a result, based on Equation 4.1, the I-shaped cross section results in less bending stress and it will decrease the undesired influence of bending over the FBG sensors. In addition, Equation 4.2 shows that placing the axial force sensor as close as possible to the crossing point of the neutral axes of the cross section of the jaw ( $C \rightarrow 0$ ), theoretically decreases the bending strain generated on the axial force sensor during grasping. Moreover, the disturbance

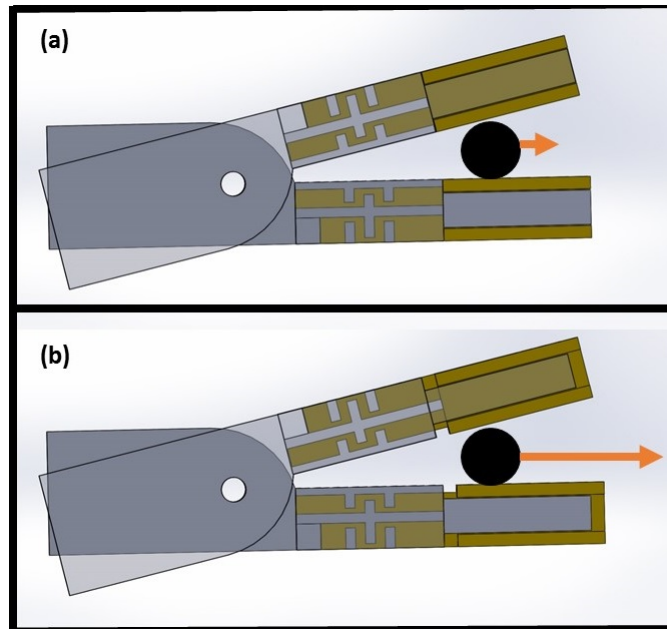


Figure 4.2: Synchronous sliding of the top and bottom graspers: a) no load condition, b) an applied axial force causes the moving parts to slide over the fixed parts while pulling an object— drawing not to scale— (used with permission) [156].

effects of the driving cables or rods and the effect of joint friction on the axial force sensor was eliminated by placing the axial sensor at the tool tip.

As shown in Figure 4.1 (b), a  $0.5 \text{ mm} \times 0.4 \text{ mm}$  crevice was designed for the axial force sensor embedment at the flexure segment located at the proximal end of the jaw. However, it is noteworthy that the neutral axis of the jaw is not the same as the neutral axis of the grasper (the grasper includes both upper and lower jaws). Consequently, placement of the axial sensor on the neutral axis of the jaw will merely isolate it from undesired effects of outward bending of that jaw caused by grasping objects; whereas, since the axial sensor is not located on the neutral axis of the grasper, overall bending of the instrument caused by exertion of transverse forces on the tip will impact the axial sensor measurements. Nonetheless, it is possible to calculate the generated strain due to transverse forces and compensate the axial force outcome for the effect of instrument overall bending. The equations for calculating the bending strain caused by transverse forces are studied in [26, 28].

As shown in Figure 4.1 (e), similar to the previous sensor, a  $0.5 \text{ mm} \times 0.3 \text{ mm}$  channel was designed over the surface of the grasper in order to embed an FBG fibre to measure grasping forces at their exertion point.



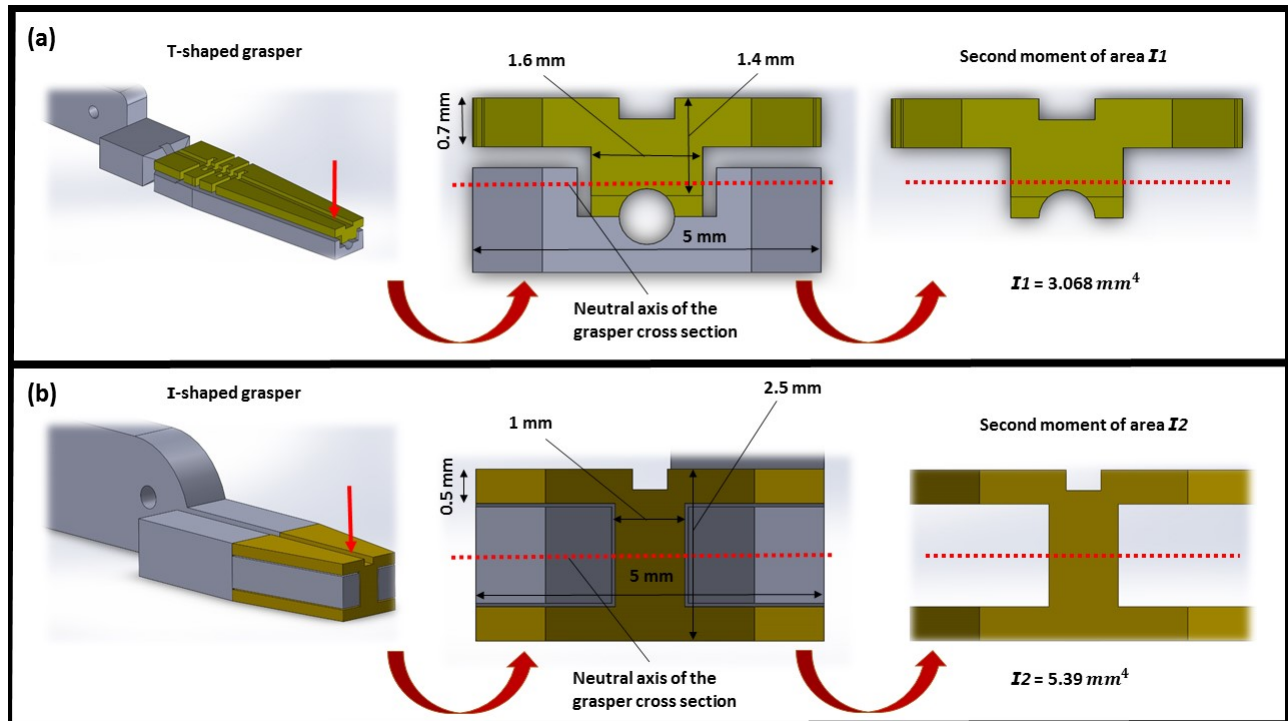


Figure 4.3: An I-shaped grasper provides a greater second moment of area in comparison to a T-shaped one, which decreases the undesired effects of the outward bending of the jaw. The placement of the axial sensor on the neutral axis of the grasper cross section isolates it from measuring the generated strain due to bending of the jaw (used with permission) [156].

With the basic geometry of the jaw determined, an FEA was performed to determine the dimensions of the flexure segment and the I-shaped cross section. In addition, different configurations and shapes of the flexure segment were analyzed. The goal of this analysis was to achieve the highest axial sensitivity by weakening the flexure segment and the lowest outward bending of the jaw by maximizing the second moment of area of the jaw's cross section. In order to prevent any safety concerns due to mechanical failure of the device, a safety factor of 10 was considered in all FEA steps. More details of this analysis are given in the following section.

#### 4.2.2 Finite Element Analysis

A finite element analysis was performed using ANSYS Workbench to validate the results of the theoretical calculations in Equation 4.2 and Figure 4.3 for both I- and T-shaped jaws. The capability of ANSYS Workbench in 3D modeling as well as defining boundary conditions between various parts resulted in an

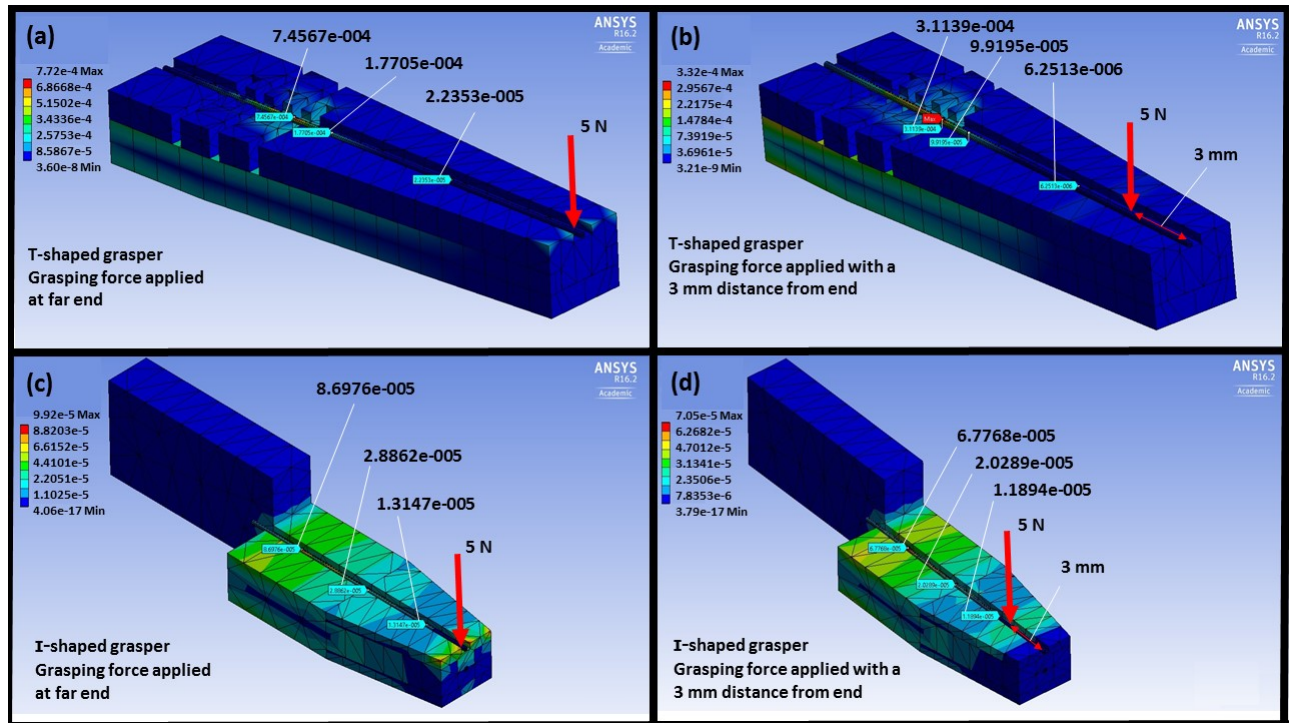


Figure 4.4: Strain generated by applying a 5 N force at: a) the far end of T-shaped jaw; b) a 3-mm distance from end of the T-shaped jaw; c) the far end of I-shaped jaw; and d) a 3-mm distance from the end of I-shaped jaw (used with permission) [156].

accurate and reliable analysis outcome. In this analysis, stainless steel and polyethylene have been chosen as the grasper and optical fibre materials with Young's moduli of  $2 \times 10^{11}$  and  $1.1 \times 10^9$  GPa, respectively. The possibility of choosing different materials in ANSYS Workbench is an important tool for making realistic assumptions in FEA modeling.

As illustrated in Figure 4.4, the bending strains generated by applying a 5 N force at the end of both I-shaped and T-shaped graspers are of the order of  $10^{-4}$  and  $10^{-5}$ , respectively. Therefore, as expected from Equation 4.2, an I-shaped design reduces the influence of bending on the grasping force sensor due to its greater second moment of area. In addition, FEA simulations show the effectiveness of the I-shaped grasper in providing consistent strain on the grasping FBG for a 5 N force applied on different locations, as is shown in Figures 4.4 (c) and (d). Conversely, applying a similar force at the end and middle of the T-shaped grasper generates strain values that are 10 times higher, as illustrated in Figures 4.4 (a) and (b). Therefore, it is concluded that the I-shape design can efficiently eliminate the undesired influence of the grasping force location on both the axial and grasping measurements.

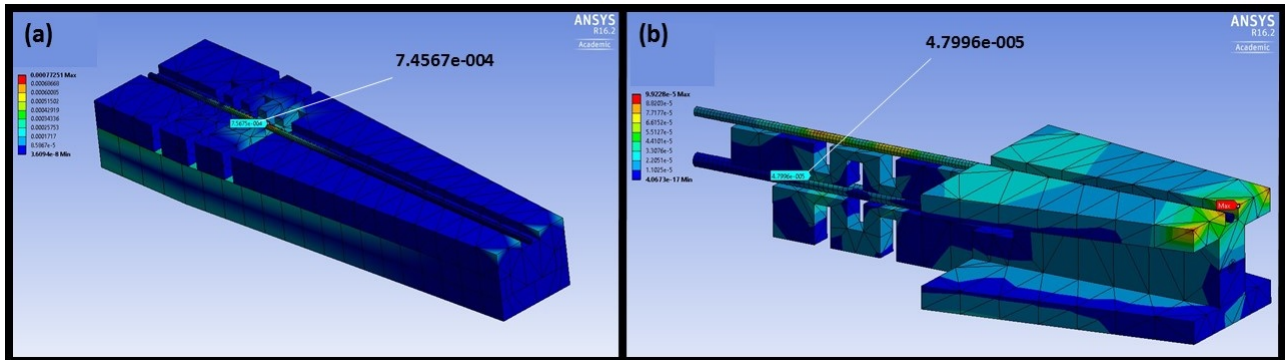


Figure 4.5: Strain generated over the axial FBGs by an applied grasping force of 10 N on the jaw: a) T-shaped jaw; b) I-shaped jaw (used with permission) [156].

The influence of grasper's outward bending on the axial FBGs in two different designs is simulated by applying a 10 N grasping force on the jaw, as shown in Figure 4.5. Comparing Figures 4.5 (a) and (b), shows that placing the axial FBG sensor on the neutral axis of the jaw in the second design reduces the effect of outward bending of the jaw on the axial sensor by 15 times.

Finally, to provide adequate deflection during pulling objects, finite element models of three flexure structure designs were analyzed in order to determine the best dimensions and shape, as shown in Figures 4.6. The stress concentration on the flexure segment of the three designs are shown in Figures 4.6 (b), (d) and (f). The second and third designs with 0.64 MPa and 0.94 MPa amount of stress respectively, provide remarkably lower stress concentration in comparison to the first design with 21 MPa. Therefore, considering the yield strength of stainless steel (210 MPa), the safety factor for the first design is 10 times less than for the other two. Thus, the first design was not chosen due to safety concerns although it was able to provide three times greater strain value over the axial FBG, as shown in Figure 4.6 (a). On the other hand, symmetric deformation of the second design (Figure 4.6 (c)) and its better axial deflection as well as its capability to provide more space for gluing the axial FBG on the flexure segment make it a favorable choice compared to the third design (Figure 4.6 (e)). As a result, the accordion shape structure (Figures 4.6 (c) and (d)) was chosen for the flexure segment of the proximal end of the jaw due to its ability for providing the maximum amount of axial strain while satisfying the rigidity and safety requirements.

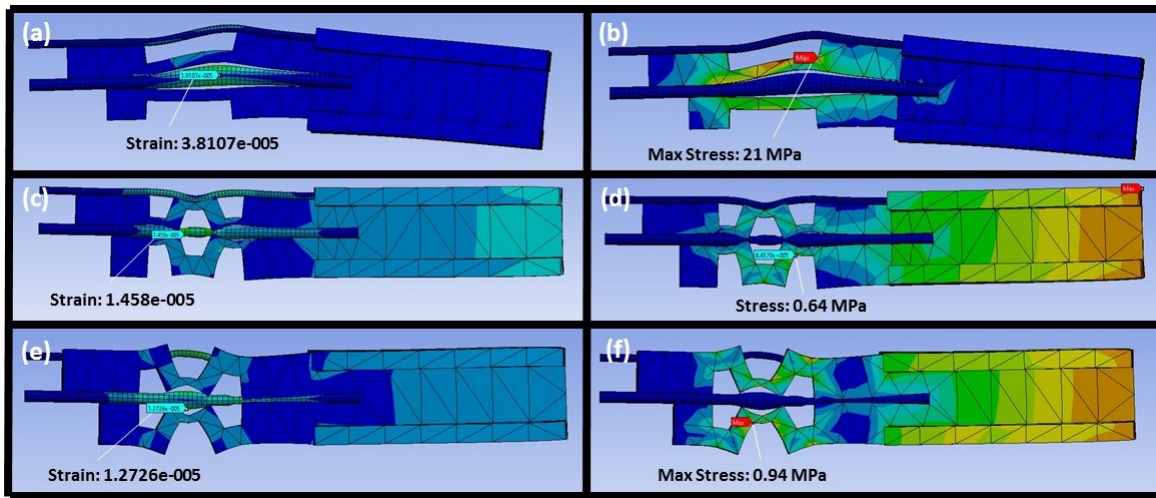


Figure 4.6: The FEA results for strain and stress caused by 4 N axial force on three different designs: a) Strain of 1<sup>st</sup> design, b) stress of 1<sup>st</sup> design, c) strain of 2<sup>nd</sup> design, d) stress of 2<sup>nd</sup> design, e) strain of 3<sup>rd</sup> design, f) stress of 3<sup>rd</sup> design (used with permission) [156].

### 4.3 Sensor Fabrication and Prototyping

Similar to the first prototype, the grasper was fabricated in several pieces using a wire EDM machine due to its high-quality finish. Fabricating the grasper jaw in several small pieces simplifies the manufacturing process as well as the sensor integration. High quality finish of EDM machining plays a vital role in increasing the accuracy of axial force measurements in absence of friction reduction balls. Since the flexible piece is meant to slide over the fixed jaw during tasks involving pulling, reducing the amount of friction between these pieces is essential. Holes with a 1 mm diameter were drilled on grasper jaws for the dowel pin joint.

As illustrated in Figure 4.7 (a), only the lower jaw of the grasper was sensorized considering the simplicity of routing out optical fibres from the jaw without bending them excessively. As a result, two FBGs (os1100, Micron Optics Inc., Atlanta, GA, USA) were integrated into the grasper lower jaw for force measurement. For direct measurement of grasping forces at their exertion point, a 5-mm grating FBG optical fibre was mounted over the working length of the grasper. Similarly, a 3-mm grating FBG was placed in the crevice in the deformable structure for measuring axial forces during pulling tasks. Superglue (Krazy Glue, Elmer's Products Canada) was used to attach the FBG fibres over the jaw regardless of its low melting point (62° C) compared to the high temperature autoclave sterilization process. However, the superglue



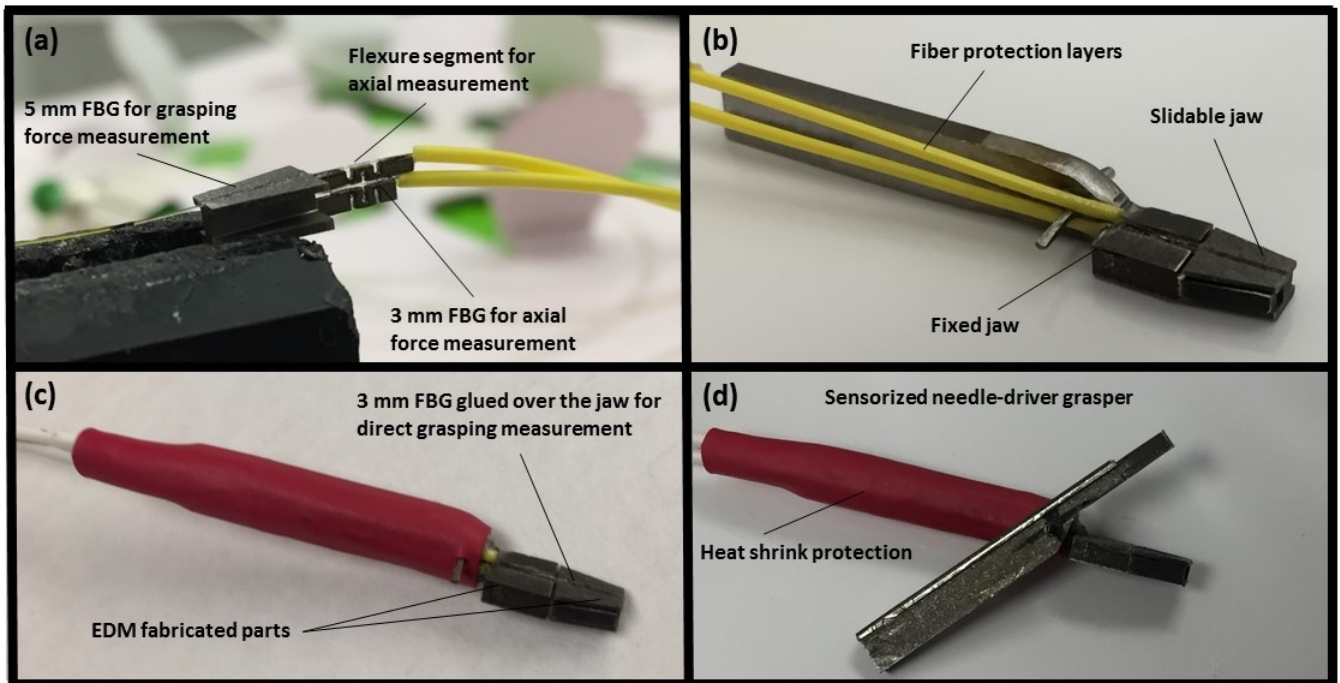


Figure 4.7: a) Installation of FBG fibres on the moving jaw; b) fixed jaw assembly; c) sensorized jaw assembly and heat shrink protected optical fibres; d) assembled sensorized grasper (used with permission) [156].

layer was covered with a Loctite medical grade coating (Loctite M-11FL, Henkel AG & Company, KGaA, Dusseldorf, Germany) for the sake of protecting fibres during high temperature autoclave sterilization. Figure 4.8, shows the autoclave sterilization test for examining the practicality of Loctite coating to protect the optical fibres against severe autoclave conditions. Once both FBG sensors were adequately installed in the moving piece of the lower jaw, it was then slid into the fixed jaw through the guide channel, as shown in Figure 4.7 (b). Subsequently, autoclavable Loctite M-21HP adhesive was used to glue the end part of the movable piece to the immobile jaw. Attachment of these pieces using Loctite adhesive was preferred over micro-welding them due to capability of autoclavable adhesive in providing sufficient amount of strength. After following the cure process of the Loctite glue, FBG fibres, from the grasper until the interrogator, were covered using fibre protections (Glass Fibre Reinforced Plastic (GFRP) wire form protections, FBGS Technologies GmbH, Jena, Germany) and heat shrink layers to prevent any potential external damages, as depicted in Figure 4.7 (c) and (d). Finally, a 1-mm dowel pin was used to connect two jaws of the grasper at the joint. Subsequently, the same data acquisition method, the Micron optical interrogator and user interface developed at CSTAR for the first generation of the sensor, was used for sensor performance evaluation

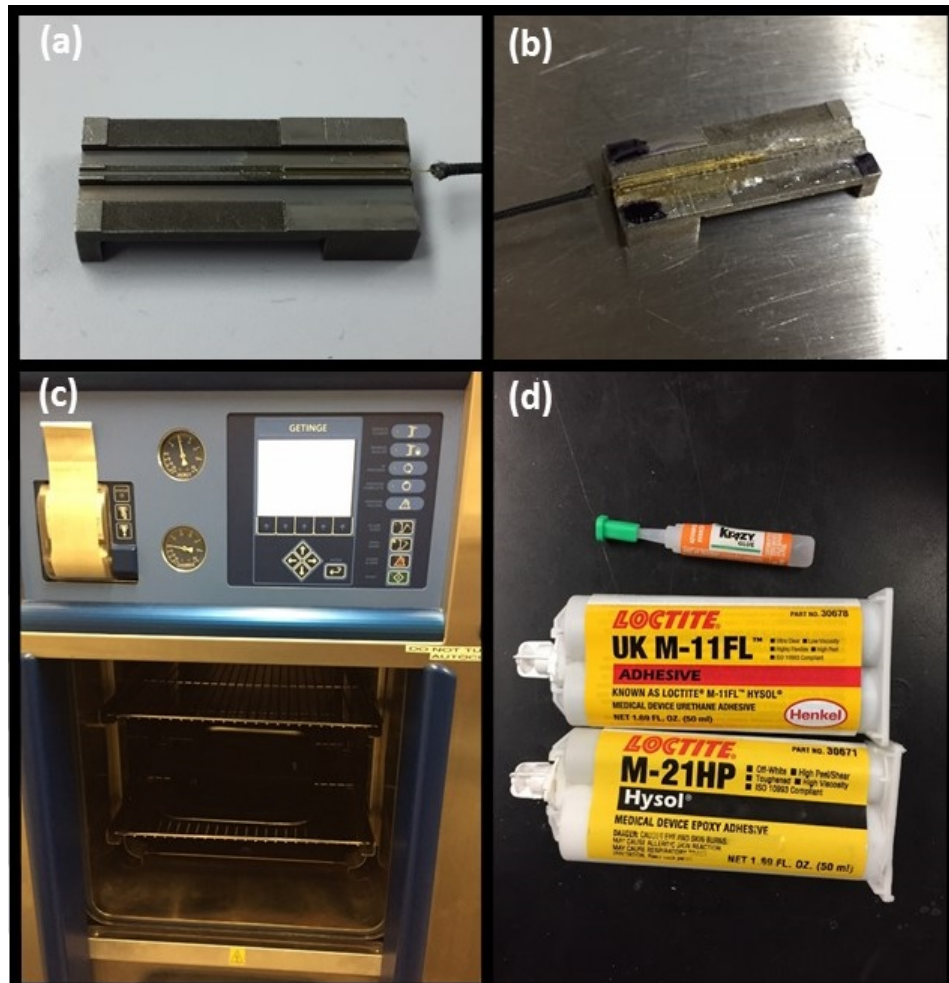


Figure 4.8: a) before test; b) after test; c) Autoclave; d) Adhesives and superglue.

and for calibrating the second generation of the sensorized grasper.

## 4.4 Calibration Setup Solutions

### 4.4.1 Introduction

Similar to the previous calibration setups, the F/T sensor was used for calibrating the axial and grasping sensors. The outcomes of both the F/T sensor and the FBG sensors were recorded simultaneously using the user interface developed at CSTAR. The measurement bias of both sensors was removed and the linear regression method was used to establish a relationship between force data of the F/T sensor and wavelength information from the FBG sensors. As shown in Figure 4.9, the calibration lines were fitted for both the

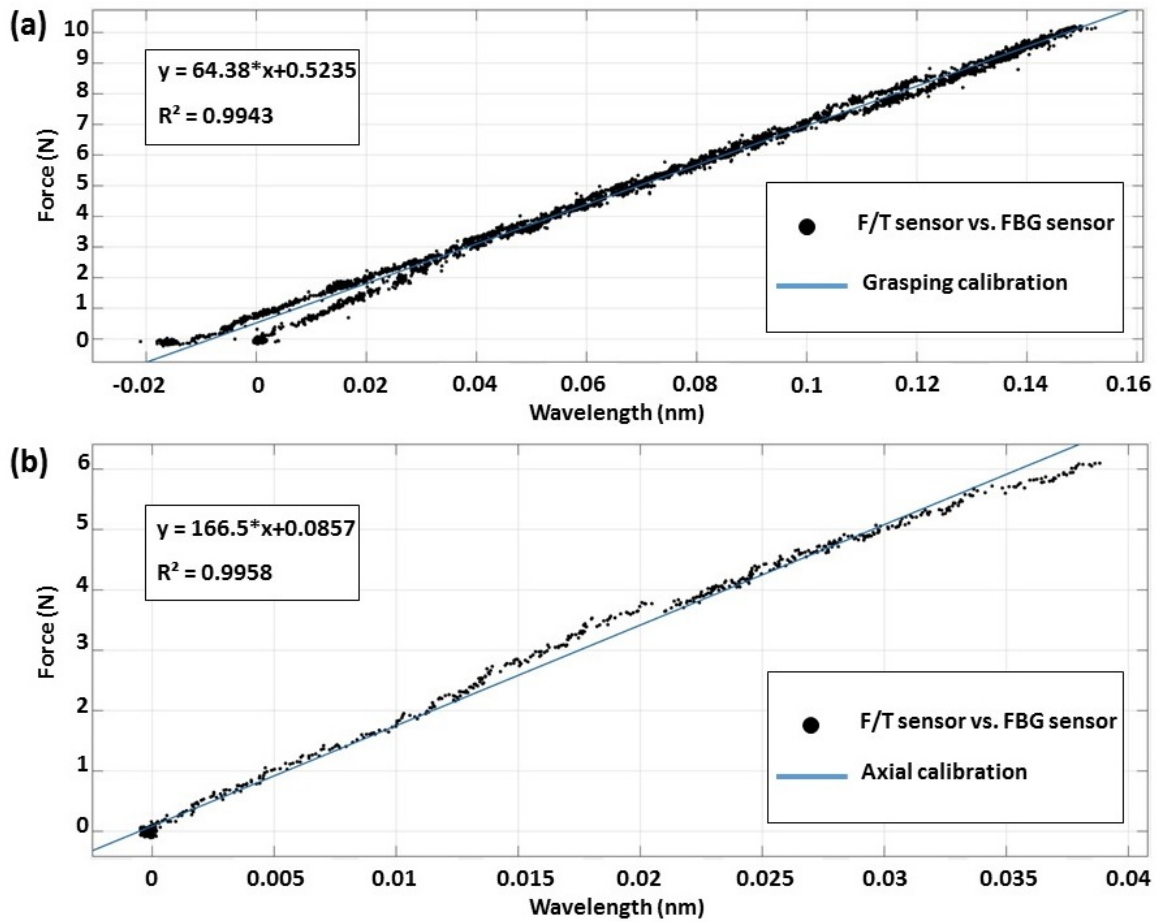


Figure 4.9: Linear regression fitted line for: a) Grasping force sensor calibration; b) Axial sensor calibration (used with permission) [156].

grasping and axial sensor data based on the calculated coefficients of the linear regression expression. Subsequently, the stored processed/calibrated data from the grasper were compared to the actual force values obtained by the F/T sensor in order to verify the sensor functionality. Issues encountered with the previous calibration setups were addressed by designing new grasping and axial calibration setups, as shown in Figure 4.10. 3D printed coupling plates were attached to both sides of the F/T sensor to connect it to the grasper.

#### 4.4.2 Grasping Setup

According to the technical specifications of the ATI F/T sensor, the resolution of force information recorded in the axial direction is higher than the resolution of the obtained torque data. Therefore, a new calibration

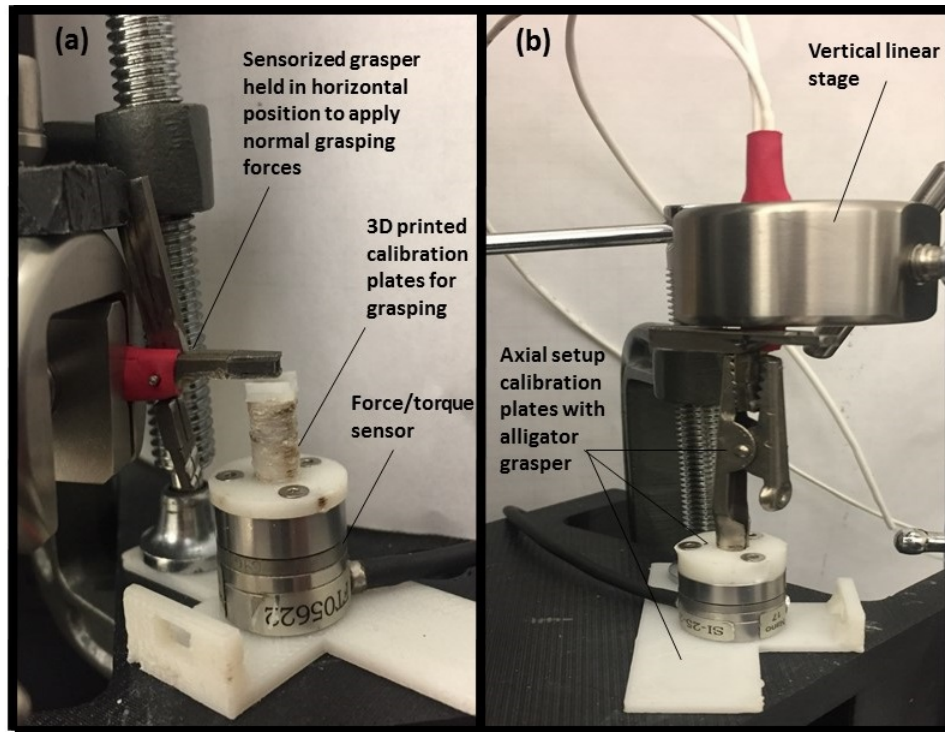


Figure 4.10: a) Grasping calibration setup and b) axial sensor calibration (used with permission) [156].

setup for the grasping sensor was designed using the axial direction of the F/T sensor. The new calibration setup was designed considering the fact that only the lower jaw of the grasper is sensorized and required to be calibrated. As illustrated in Figure 4.10 (a), the lower jaw of the grasper was placed on the F/T sensor in order to apply pressure in a perpendicular direction. A linear stage (M4965-06-L, Parker Hannifin Corporation, Daedal Division, Irwin, PA, USA) was used to hold the sensorized jaw of the grasper perpendicular to the axis of the F/T sensor. Consistent force up to 10 N was applied on the F/T sensor by the sensorized jaw. As illustrated in Figure 4.11, by moving the linear stage forward and backward, the influence of exerting grasping forces on different locations over the 6-mm working length of the grasper was evaluated.

#### 4.4.3 Axial Setup

In order to increase the accuracy and repeatability of acquired force data from the axial calibration setup, the string used in the previous setup was replaced by a rigid alligator grasper. Figure 4.10 (b), shows the new axial setup in which the sensorized grasper was held by an alligator grasper attached to the F/T sensor. In order to apply forces only in the axial direction of the grasper, the linear stage was positioned in a vertical



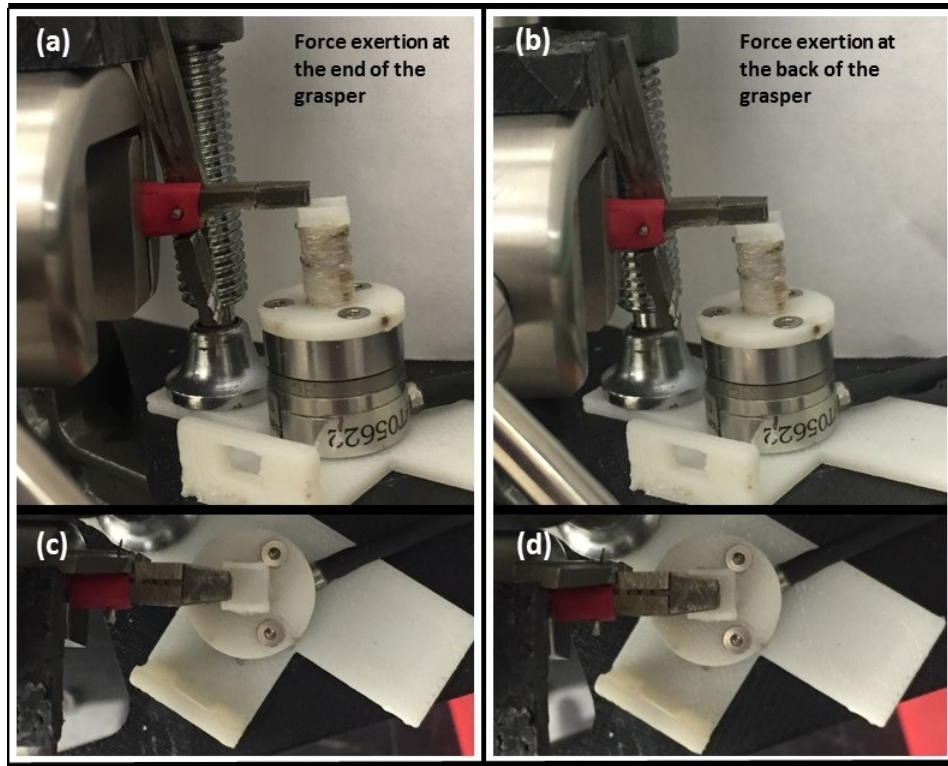


Figure 4.11: Setup for exerting forces on different locations on the grasper jaw: a) side view and c) top view of the end of the grasper; b) side view and d) top view of the back of the grasper (used with permission) [156].

direction. Since the axial sensor was intentionally designed for measuring forces during pulling tasks, the grasper was pulled upward by the linear stage until a 5 N axial force was measured by the F/T sensor.

After calibrating the sensor, experiments were conducted to evaluate the performance of the grasping and axial sensors. Similar to the first sensor assessment, each experiment was repeated three times in order to assess the following performance measures of the sensing system: accuracy, hysteresis, repeatability, noise and drift.

## 4.5 Results and Discussion

Figure 4.12 shows the efficiency of the axial and grasping FBG sensors in accurately tracking the F/T sensor output for one of the trials. Table 4.1 presents the results of the sensor experimental evaluation for the second sensor. All of obtained results satisfy the required force specifications for MIS tasks in working ranges of 0–10 N and 0–6 N for the grasping and axial sensors, respectively. As presented in the first

column of Table 4.1, Grasping 1 refers to the accuracy of the grasping sensor at the same location used during calibration, which shows an RMS error of 0.23 N. Grasping 2 refers to the accuracy when grasping forces were exerted 6 mm away from the calibration point, where the maximum amount of error due to outward bending of the jaw is expected. This location showed an accuracy of 0.31 N. These results show the ability of the sensor to minimize the influence of the force location on the grasping measurements. The total RMS error in grasping was 0.27 N. Although this error is greater than the 0.19 N accuracy of the first prototype, these results are independent of the location of applied forces.

The local repeatability of the sensor is similar to that of the first prototype (0.26 N compared to 0.21 N); whereas the total repeatability of the sensor is significantly improved, 0.37 N regardless of the exertion point of grasping forces, which makes the second sensor more reliable compared to the first prototype. Results acquired from the second prototype are more reliable and repeatable and therefore the second design is more practical for medical applications. In addition, the behavior of the grasping sensor was noticeably improved in terms of hysteresis compared to the previous design.

The axial sensor was characterized during pulling tasks (the loading phase) in order to simulate suturing and knot tying tasks. Similar to the first prototype, the axial sensor was able to provide accurate and reliable force information in terms of accuracy and repeatability. Moreover, the second sensor can be used to provide force information in other tasks such as tissue palpation as a result of its low hysteresis (0.33 N).

Although the amount of noise and drift present in the developed sensing system are acceptable for MIS applications, no significant improvements have been achieved compared to the first prototype, since the same interrogation unit and type of optical sensors were used for both designs.

Regarding the autoclave sterilization process, the medical grade Loctite glue comprehensively protected FBG fibres against severe autoclave conditions and kept the sensors in their desired place during and after sterilization. However, melting of the super glue underneath the adhesive affected the calibration of the system. Therefore, in order to reuse the sensors after sterilization, the calibration process should be repeated.

#### 4.5.1 Conclusion

In conclusion, the second generation of the sensorized grasper was able to address the discussed accuracy and reliability issues of the previous sensor. The influence of the force location on the grasping sensor

Table 4.1: Results of the performance evaluation of the second generation of the sensorized grasper.

	<b>Grasping 1 (N)</b>	<b>Grasping 2 (N)</b>	<b>Grasping-Total (N)</b>	<b>Axial-Loading (N)</b>	<b>Axial-Total (N)</b>
RMS Error	$0.23 \pm 0.14$	$0.31 \pm 0.18$	$0.27 \pm 0.16$	$0.30 \pm 0.23$	$0.50 \pm 0.34$
Repeatability	$0.26 \pm 0.14$	$0.40 \pm 0.18$	$0.37 \pm 0.16$	$0.38 \pm 0.23$	$0.73 \pm 0.34$
RMS Hysteresis	0.02	0.06	0.04	—	0.33
Drift	1.2	1.2	1.2	0.42	0.42
Noise	0.048	0.048	0.048	0.072	0.072

measurements was minimized and the grasping force information with high accuracy was acquired. The axial force sensor was successfully isolated from the influence of the grasping forces by placing its FBG on the neutral axis of the jaw. In addition, the axial sensor satisfied the hysteresis requirements for various MIS tasks such as palpating. As a result, the second prototype of the sensorized grasper has increased repeatability, while conserving the accuracy characteristics of the first prototype. More accurate and reliable setups were designed for calibrating the axial and grasping sensors. Higher resolution results for calibrating the grasping sensor were obtained by using the axial direction of the F/T sensor. Replacing the string with an alligator grasper in the axial calibration setup resulted in more accurate and repeatable outcomes.

Coating superglue with medical adhesives prevented fibres from severe heat damages during the autoclave cycle. However, a more reliable medical glue (EP42HT-2Med, Master Bond Inc., Hackensack, New Jersey, USA) is recommended to connect various grasper pieces and to mount fibres over the instrument in order to guarantee the reusability of the instrument after multiple autoclaving cycles.

As the next step, the developed prototype for the axial and grasping force measurement will be incorporated into a complete laparoscopic needle driver. The instrument will measure force data in 5 DOF including the grasping and axial directions. In addition, an extra FBG sensor will be mounted on the device for temperature compensation purposes for *in vivo* applications.

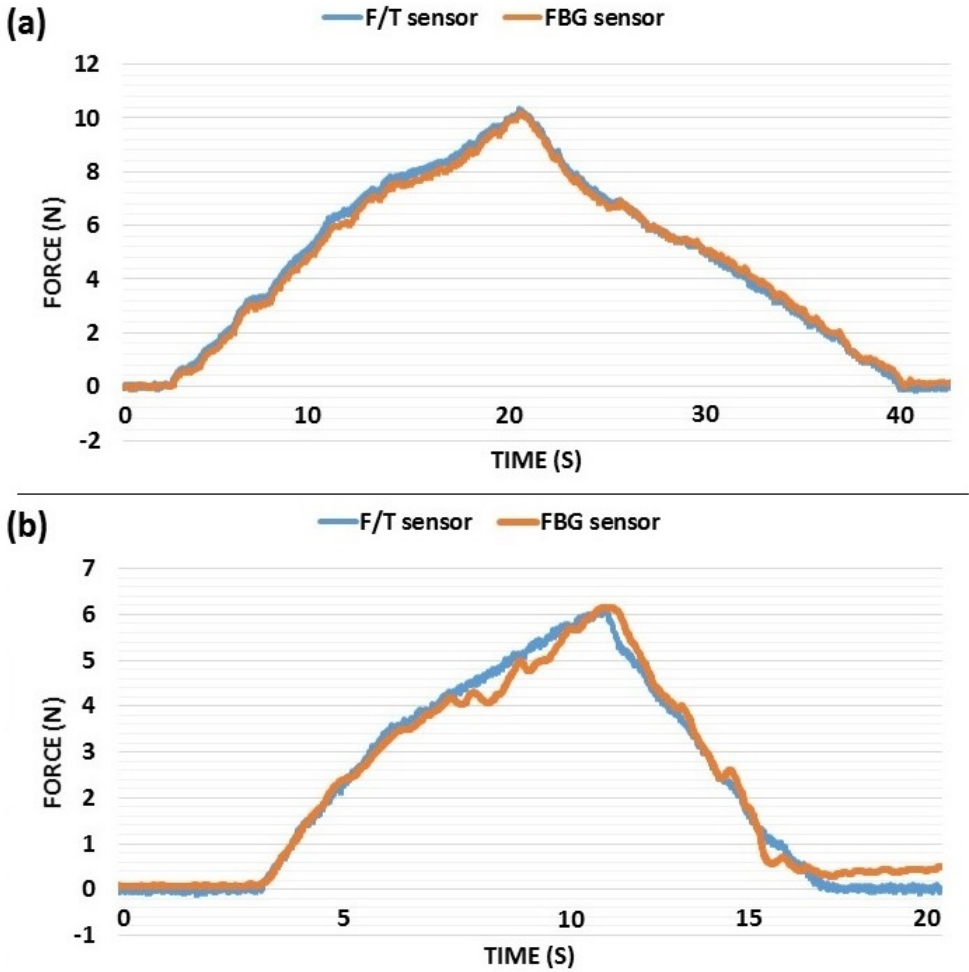


Figure 4.12: Comparison of the results from the FBGs and the F/T sensors in: (a) grasping and (b) axial (used with permission) [156].

## **Chapter 5**

# **Integration of the Novel Force Sensing Design into the Full Instrument Prototype**

### **5.1 Introduction**

The previous prototypes of the sensorized needle-driver showed the practicality of measuring the grasping and axial forces on the tool tip [153, 156]. Drawbacks of the first prototype were adequately addressed in the second prototype. Promising force results in terms of reliability and accuracy were presented by the second sensor [156]. However, force measurement only in 2-DOF (grasping and axial) was not satisfactory for the real-world application of the sensorized instrument. As a result, the concept of direct grasping and axial force measurement at the tool tip was integrated into the full instrument prototype design. The designed prototype for FBG-based force-sensing laparoscopic needle-driver is able to measure force and torque data in 5-DOF including grasping, axial, torsion and two lateral forces. In addition, an extra FBG for temperature compensation method is considered in sensor design.

### **5.2 Design Specifications**

A laparoscopic needle-driver with similar appearance, size and weight to commercial instruments was designed. The modeled instrument is intended to fit in a 5-mm trocar and to conduct suturing and knot tying tasks. The appearance of the designed instrument is similar to a commercial needle-driver and it provides

users with easy access to internal body features thanks to its 440 mm length. 12 mm of working length was considered over its jaws for holding a needle or pulling a stitch during surgical operations. In a similar manner to previous prototypes, autoclavable stainless steel (SAE316) was chosen for the instrument material due to its biocompatibility and sterilizability. Considering the promising outcomes of the previous sensor prototypes, 5 FBG sensors were used to measure force and torque in 5-DOFs including axial, grasping (actuation), lateral forces in two directions and torsion. Moreover, 1 FBG sensor was used as a temperature reference in order to compensate for the effect of temperature fluctuations on 5-DOF force measurements. Range and resolution of FBG sensors in each of the DOFs was presented in Table 3.1. The sterilizability and high sensitivity of FBG sensors make them the most appropriate technology for this application.

### 5.3 Mechanical Design of the Partial Prototype

As illustrated in Figure 5.1, the CAD model of a sensorized needle-driver grasper was developed using SolidWorks. In this 5-DOF sensorized instrument, grasping and axial forces are measured at their exertion point on the tool tip similar to the second prototype. As shown in Figure 5.2, two FBG sensors were considered to be embedded inside the grasper jaw. A  $0.5 \times 0.3$  mm channel was considered over the 12-mm working length of the jaw for grasping FBG embedment (Figure 5.3); whereas, the axial FBG was placed inside a  $0.5 \times 0.4$  mm crevice to measure the resulting axial strain over the flexible segment of the jaw, as shown in Figures 5.2 (b) and (c). A  $6 \times 3$  mm gap was designed at the end of the jaw in order to route the two optical fibres from the jaw towards the instrument back, as shown in Figure 5.2 (a). The fibres were meant to be guided towards the interrogator through a  $1 \times 0.5$  mm channel on the instrument's outer shaft, as it shown in Figure 5.4 (b). Moreover, three FBG optical fibres were placed over the instrument shaft to measure exerted lateral forces, in  $x$  and  $y$  directions, and torsion, with respect to Equation 2.6. For this purpose, 3 channels with  $0.8 \times 0.3$  mm dimensions were designed in a symmetric  $120^\circ$  arrangement over the instrument outer shaft for embedding the FBG fibres (Figure 5.4 (a)). As demonstrated in Figure 5.4 (a), the instrument has a hollow shaft with an inner diameter (ID) of 3 mm and an outer diameter (OD) of 5 mm. The inner actuation shaft with 2.8 mm diameters is responsible for opening and closing the jaw with a slider–crank mechanism. The inner actuation shaft fits inside the hollow shaft and is connected to the grasper upper jaw using a connection link, as shown in Figure 5.2 (e). 1 mm diameter dowel pins were

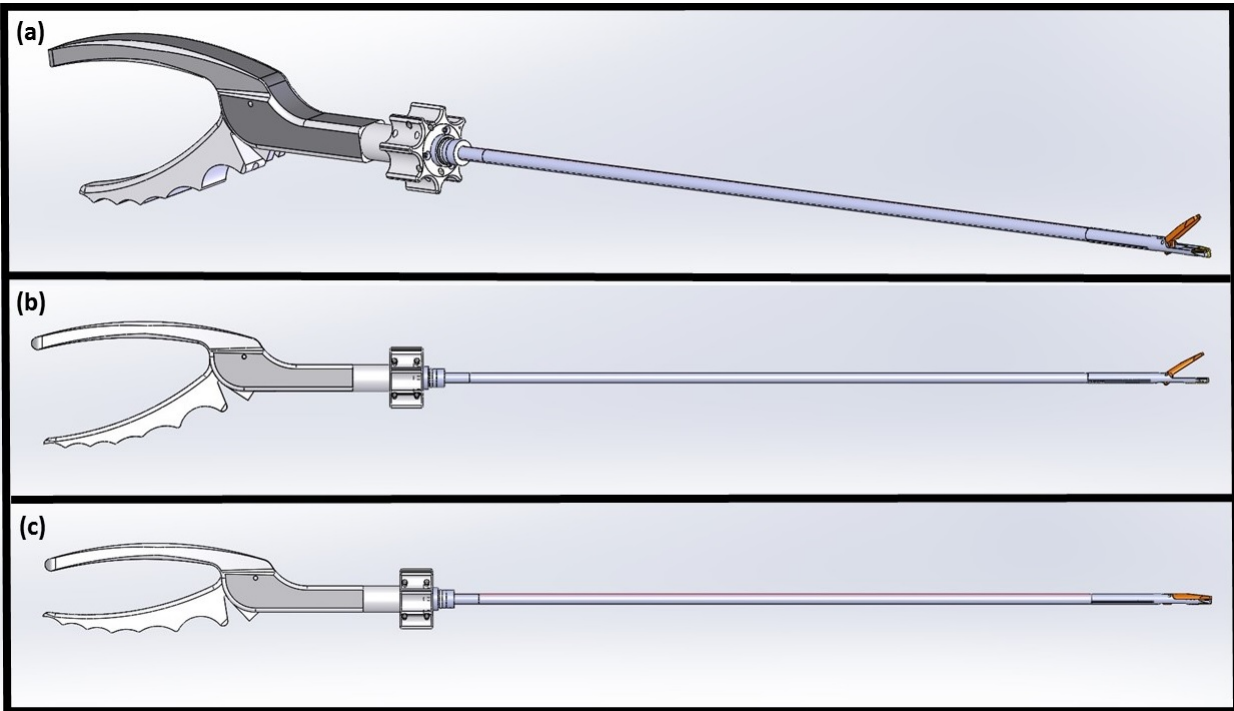


Figure 5.1: a) CAD model of the sensorized laparoscopic needle-driver; b) Side view of the instrument with an open jaw; c) Side view of the instrument with a closed jaw.

considered to attach the upper jaw to the connection link as well as to the instrument's fixed frame.

Similar to the second prototype of the sensor, the moving part of the lower jaw was designed in an I-shaped in order to reduce the undesired effect of the outward bending of the jaw during grasping. Similar to previous concepts, the moving part was expected to elongate during pulling tasks in order to increase the sensitivity of axial measurements. The grasping sensor was integrated on the grasper jaw for direct measurement of grasping forces.

In order to eliminate the effects of temperature fluctuations from other sensors measurements, an FBG sensor was placed in the same fibre that the axial FBG was placed, as shown in Figure 5.2 (b). This sensor was designed to be located in the fibre's outlet gap at the end of the jaw in a floating manner (as illustrated in Figure 5.2 (b)) in order to measure purely temperature effects and to be isolated from effects of forces/torques applied to the instrument. Placement of the temperature compensation sensor as close as possible to the tool tip increases the accuracy of temperature variance by taking into consideration the heat transfer flow from the tool tip towards the end part of the instrument.

The bending moments generated by exerted lateral forces in the  $x$  and  $y$  directions and the torsion gen-

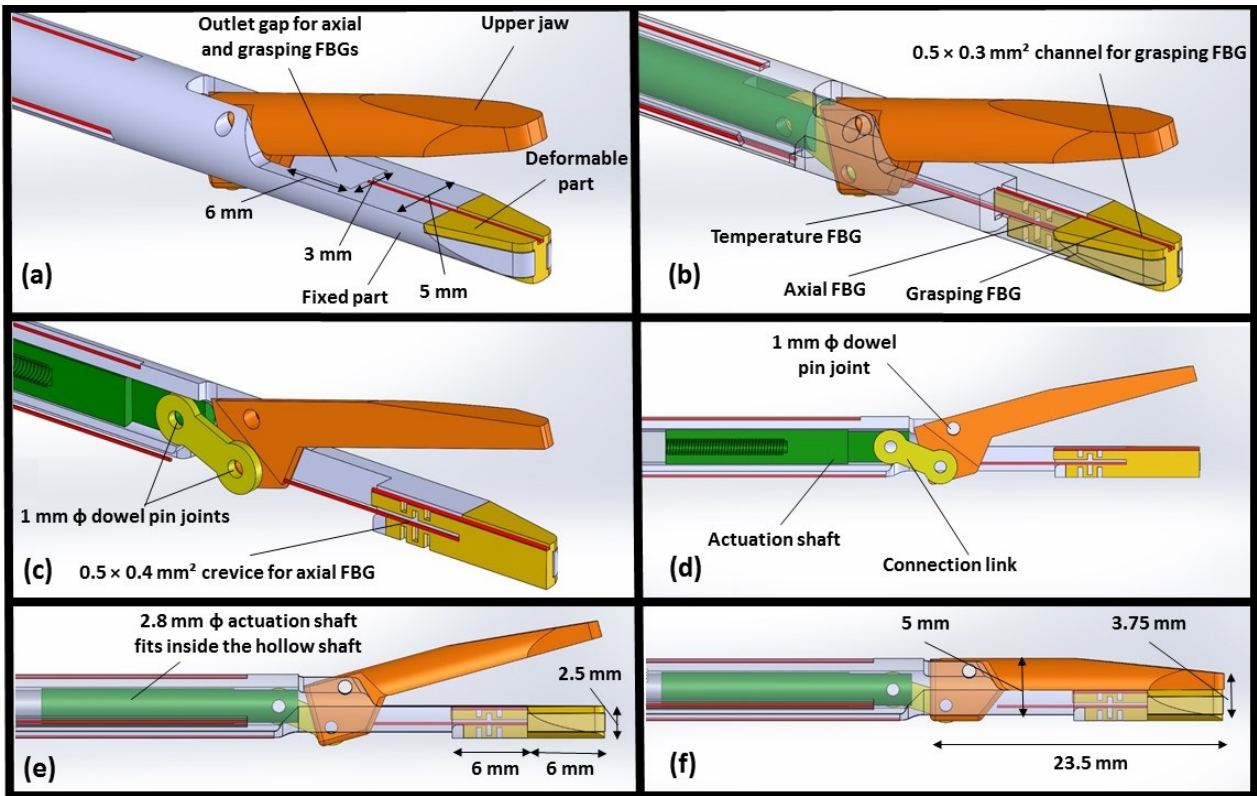


Figure 5.2: Mechanism and working principles of the final sensorized instrument

erated by the instrument are measured by three FBG sensors mounted on the instrument shaft. According to Equation 2.3, the overall strain measured by these FBG sensors is created due to the effects of the torsion, bending and temperature. However, it is possible to theoretically calculate the amount of torsion strain alone by implementing Equation 2.4 and subtracting the effects of temperature fluctuations. Subsequently, Equation 2.6 can be used to compute the bending moments in the  $x$  and  $y$  directions.

## 5.4 Sensor Fabrication and Prototyping

The sensorized instrument was intentionally designed in several pieces in order to make its fabrication through traditional machining methods possible. However, a metal 3D printer such as that in the Additive Design in Surgical Solutions (ADEISS) Centre at Western University could also be used for manufacturing the grasper in one piece. This machine has laser spot size of 70 microns and layer size of 40 microns and it is able to print parts with 0.2 mm resolution. Therefore, medical 3D printing could be an alternative method to traditional machining.



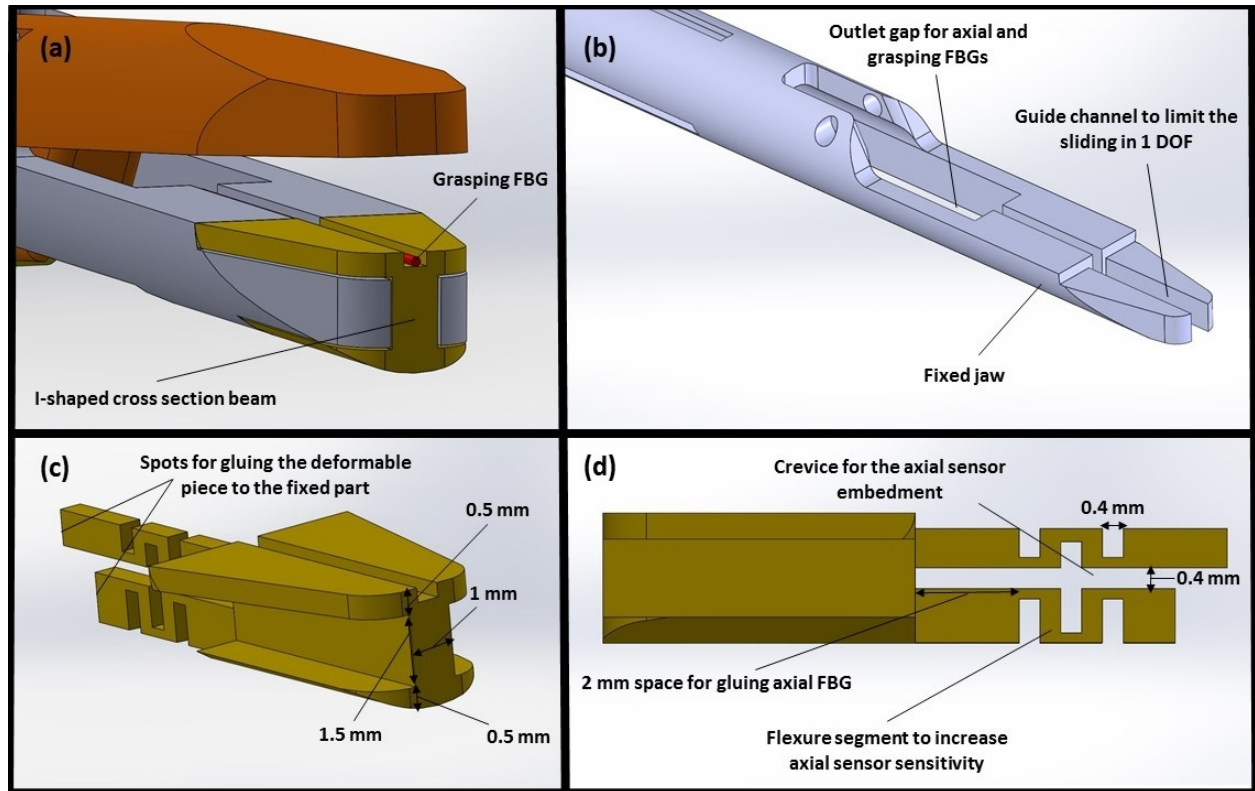


Figure 5.3: a) Sensorized needle-driver with an I-shaped grasper; b) Fixed part of the needle-driver lower jaw; c) Moving part of the needle-driver lower jaw; d) Accordion shaped deformable structure.

## 5.5 Results and Discussion

In conclusion, a CAD model of a sterilizable sensorized needle-driver with 5-DOF force/torque measurements was developed. The novel design for measuring grasping and axial forces directly at their exertion point on the tool tip was implemented in the instrument design. Moreover, the design proposed measuring the bending moments created by lateral forces in two directions as well as torsion measurements. An FBG sensor for temperature compensation was used for this prototype design.

As future work, the complete development of the final instrument for force and torque measurements in MIS is proposed. Further test experiments need to be conducted in order to evaluate the performance of the sensorized instrument in providing accurate force information. *In vitro* and *ex vivo* experiments should be conducted in order to assess the feasibility of the system in providing reliable and repeatable data before its actual test in *in vivo* applications.

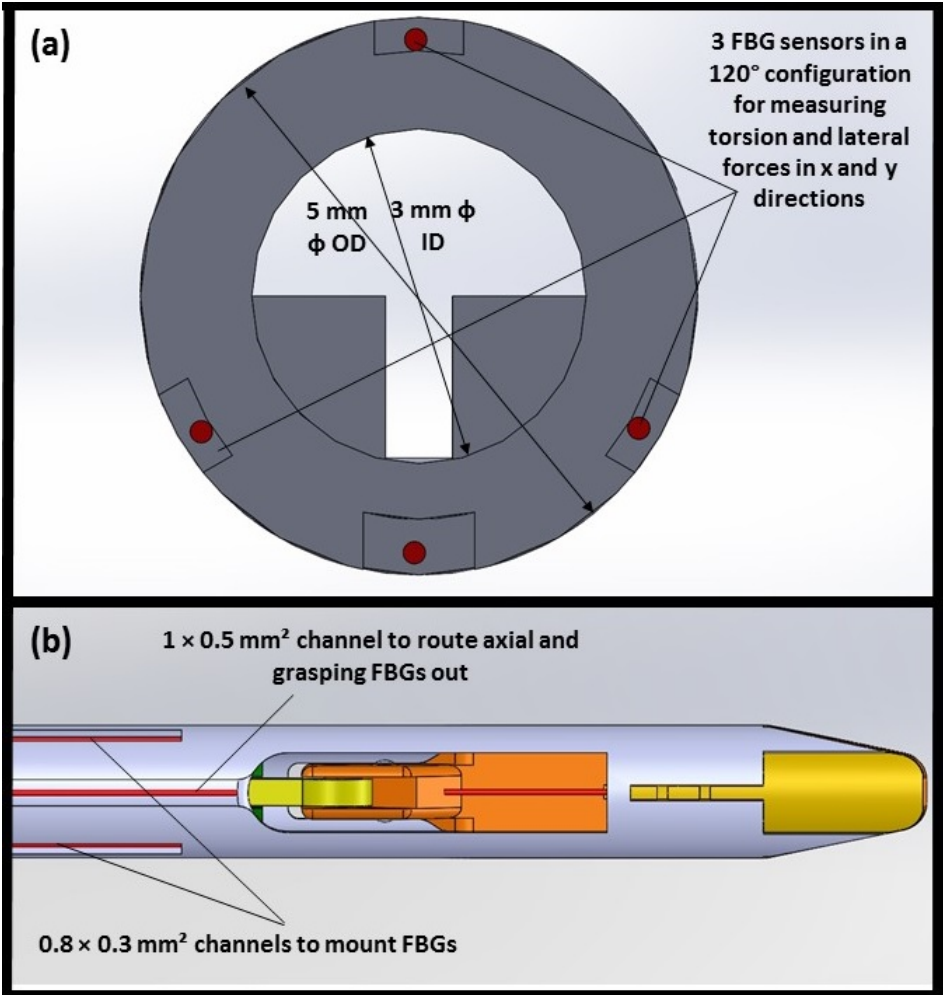


Figure 5.4: a) 3 FBG sensors at 120° arrangements for measuring applied torque and bending on the instrument b) Bottom view of the instrument showing designed channels to route axial and grasping FBGs towards the instrument back

## Chapter 6

# Conclusion and Future Work

### 6.1 Introduction

The work presented in this thesis was aimed at addressing the lack of appropriate force sensing in MIS by describing the development of a sensorized laparoscopic instrument. A comprehensive literature review was performed to show the absence of an instrument with reliable force sensing that can provide realistic force feedback for MIS. There are currently no commercially available laparoscopic instruments that can provide haptic information on tool–tissue interactions. Moreover, developed force sensing instruments in current state-of-the-art measure exerted forces far from their exertion point at the instrument shaft or handle [13, 20]. As a result, the accuracy of acquired force data in these work is questionable. Therefore, a sterilizable technology with high measurement accuracy and resolution is still missing. Therefore, the objective of this work was to fill this gap by designing a 5-DOF sterilizable instrument that is able to measure the forces acting on the tool tip.

Since measuring axial and grasping forces on a laparoscopic tool tip was the novel part of this work and has not been achieved to date to a high degree of accuracy and reliability, the first generation of the sensor prototype was designed and built to demonstrate the feasibility of the novel concept. The first prototype provided acceptable results for measuring applied forces at their exertion point on the tool tip. However, a few limitations (degraded sensor repeatability due to outward bending of the jaw) restricted its use in real-world applications. Therefore, the second generation of the sensor was developed to address these limitations.

The second generation of the sensorized grasper was able to address the limitations of the previous design. The influence of the force location on the grasping sensor measurements was minimized and grasping force information with high accuracy was acquired. The second prototype of the sensorized grasper also has increased repeatability, while still achieving the accuracy characteristics of the first prototype.

Prototypes of the sensorized grasper successfully provided reliable axial and grasping forces proving the practicality of direct force sensing. Therefore, a final model of the instrument was developed by implementing the novel concept of measuring grasping and axial forces on the tool tip. The final instrument provided force and torque information in 5 DOFs including: grasping, axial, lateral forces in two directions and torsion. Moreover, a reference temperature compensation method was implemented to eliminate effects of temperature fluctuations on sensor measurements.

## 6.2 Contributions

The work presented in this thesis will pave the way towards the development of smart surgical tools with haptic capability. The force sensing system developed in this work can be of benefit in MIS applications where the presence of force information is necessary or can provide greater safety or efficiency. The specific contributions of this thesis are as follows:

- Two sets of grasper prototype were designed and developed to measure applied grasping and axial forces at their exertion point on the tool tip. The developed sensing systems demonstrated the implementation of technology for direct and accurate force measurements in MIS. The force measurements showed high accuracy and resolution and low hysteresis, noise and drift characteristics. To the best of our knowledge, this was the first time that FBG sensors were used to measure tool–tissue interaction forces on a laparoscopic instrument tip with the lowest possible coupling. Based on the novel concept of direct force measurements, a sterilizable force sensing laparoscopic needle-driver was modelled and designed. The final prototype was intended to provide force/torque data in 5 DOFs with a temperature compensation capability. The low cost of the sensor development process that involves an EDM fabrication method and FBG sensors makes it possible to consider commercialization of the final design following *in vivo* testing of the instrument.
- Accurate and reliable sensor calibration setups were designed for calibrating the axial and grasping

sensors. Higher resolution results for calibrating the grasping sensor were obtained by using the force/torque ATI sensor.

### 6.3 Future Work

Although the feasibility of embedding force sensors in surgical graspers was shown, several points of improvement were identified that could increase the quality of force measurements. These are presented as follows:

- The final model of the sensorized needle-driver with 5-DOF force/torque measurements should be built for *in vivo* applications. To guarantee the reusability of the instrument after multiple autoclaving cycles, a more reliable medical glue (EP42HT-2Med, Master Bond Inc., Hackensack, New Jersey, USA) should be used. The instrument should be tested several times before and after the autoclave process in order to assess the reliability of the glue.
- Manufacturing grasper parts using rapid prototyping methods should be considered in order to reduce the time for the fabrication process. The finish of the built parts using a metal 3D printer in the Additive Design in Surgical Solutions (ADEISS) Centre at Western University should be examined as an alternative for traditional machining.
- Implementation of the novel direct force sensing concept to other types of surgical graspers (in addition to a needle-driver with a fixed lower jaw) should be investigated. A similar force sensing concept can be considered for surgical robotic applications. The da Vinci laparoscopic instruments can be sensorized using FBG sensors in order to measure axial and grasping force information on the instrument tip.
- *In vitro*, *ex vivo* and *in vivo* experiments should be designed to evaluate the practicality of the developed instrument in providing sufficient force/torque information for MIS. A graphical user-interface can be used to provide force information to the users in a reliable and consistent manner.
- Development of a reliable method for laparoscopic instruments that can provide realistic force information of tool–tissue interaction forces that can be used to provide greater realism in MIS virtual reality simulators and can be used for skills assessment purposes.

# Bibliography

- [1] T. Robinson and G. Stiegmann, “Minimally invasive surgery,” *International Journal of Endoscopy*, vol. 36, no. 01, pp. 48–51, 2004.
- [2] A. Trejos, R. Patel, and M. Naish, “Force sensing and its application in minimally invasive surgery and therapy: a survey,” *Journal of Mechanical Engineering Science*, vol. 224, no. 7, pp. 1435–1454, 2010.
- [3] M. C. Cavusoglu, W. Williams, F. Tendick, and S. S. Sastry, “Robotics for telesurgery: second generation Berkeley/UCSF laparoscopic telesurgical workstation and looking towards the future applications,” *International Journal of Industrial Robot*, vol. 30, no. 1, pp. 22–29, 2003.
- [4] A. L. Trejos, “A Sensorized Instrument for Minimally Invasive Surgery for the Measurement of Forces during Training and Surgery : Development and Applications,” *University of Western Ontario*, London, Canada, 2012.
- [5] H. G. Kenngott, B. P. Muller-Stich, M. a. Reiter, J. Rassweiler, and C. N. Gutt, “Robotic suturing: technique and benefit in advanced laparoscopic surgery,” *Journal of the Society for Minimally Invasive Therapy*, vol. 17, no. 3, pp. 160–7, 2008.
- [6] M. MacFarlane, J. Rosen, B. Hannaford, C. Pellegrini, and M. Sinanan, “Force-feedback grasper helps restore sense of touch in minimally invasive surgery,” *Journal of Gastrointestinal Surgery*, vol. 3, no. 3, pp. 278–285, 1999.

- 
- [7] H. Kang and J. T. Wen, "Autonomous suturing using minimally invasive surgical robots," *IEEE International Conf. on Control Applications*, Anchorage, Alaska, USA, Sep. 25-27, 2000, pp. 742–747.
- [8] A. L. Trejos, A. C. Lyle, A. Escoto, M. D. Naish, and R. V. Patel, "Force/position-based modular system for minimally invasive surgery," *IEEE Conf. on Robotics and Automation (ICRA)*, Anchorage, AK, USA, May 3-7, 2010, pp. 3660–3665.
- [9] O. Van der Meijden and M. Schijven, "The value of haptic feedback in conventional and robot-assisted minimal invasive surgery and virtual reality training: a current review," *Journal of Surgical Endoscopy*, vol. 23, no. 6, pp. 1180–1190, 2009.
- [10] W. J. Bishop, *The Early History of Surgery*. USA, Barnes & Noble Publishing, 1995.
- [11] G. David, L. Boni, S. Rausei, E. Cassinotti, G. Dionigi, F. Rovera, S. Spampatti, E. M. Colombo, and R. Dionigi, "Use of 3 mm percutaneous instruments with 5 mm end effectors during different laparoscopic procedures," *International Journal of Surgery*, vol. 11, no. 6, pp. S61–S63, 2013.
- [12] S. J. Spaner and G. L. Warnock, "A brief history of endoscopy, laparoscopy, and laparoscopic surgery," *Journal of Laparoendoscopic & Advanced Surgical Techniques*, vol. 7, no. 6, pp. 369–373, 1997.
- [13] D. S. Yurkewich, A. Escoto, A. L. Trejos, M.-E. LeBel, R. V. Patel, and M. D. Naish, "Low-cost force-sensing arthroscopic tool using threaded fiber bragg grating sensors," in *International Conference on Biomedical Robotics and Biomechanics*, Sao Paulo, Brazil, Aug. 12-15, 2014, pp. 28–33.
- [14] A. Talasaz, A. L. Trejos, and R. V. Patel, "Effect of force feedback on performance of robotics-assisted suturing," in *International Conference on Biomedical Robotics and Biomechanics (BioRob)*, Rome, Italy, June 24-27, 2012, pp. 823–828.
- [15] A. L. Trejos, J. Jayender, M. Perri, M. D. Naish, R. V. Patel, and R. Malthaner, "Robot-assisted tactile sensing for minimally invasive tumor localization," *The International Journal of Robotics Research*, vol. 28, no. 9, pp. 1118–1133, 2009.

- [16] A. L. Trejos, R. V. Patel, R. A. Malthaner, and C. M. Schlachta, "Development of force-based metrics for skills assessment in minimally invasive surgery," *Surgical Endoscopy and Other Interventional Techniques*, vol. 28, no. 7, pp. 2106–2119, 2014.
- [17] E. P. Westebring-van der Putten, J. J. van den Dobbelsteen, R. H. Goossens, J. J. Jakimowicz, and J. Dankelman, "The effect of augmented feedback on grasp force in laparoscopic grasp control," *IEEE Transactions on Haptics*, vol. 3, no. 4, pp. 280–291, 2010.
- [18] E. Westebring-Van Der Putten, R. Goossens, J. Jakimowicz, and J. Dankelman, "Haptics in minimally invasive surgery—a review," *Minimally Invasive Therapy & Allied Technologies*, vol. 17, no. 1, pp. 3–16, 2008.
- [19] P. Puangmali, K. Althoefer, L. D. Seneviratne, D. Murphy, and P. Dasgupta, "State-of-the-art in force and tactile sensing for minimally invasive surgery," *IEEE Sensors Journal*, vol. 8, no. 4, pp. 371–380, 2008.
- [20] A. L. Trejos, A. Escoto, D. Hughes, M. D. Naish, and R. V. Patel, "A sterilizable force-sensing instrument for laparoscopic surgery," in *International Conference on Biomedical Robotics and Biomechatronics*, Sao Paulo, Brazil, Aug. 12-15, 2014, pp. 157–162.
- [21] A. L. Trejos, R. V. Patel, M. D. Naish, A. C. Lyle, and C. M. Schlachta, "A Sensorized Instrument for Skills Assessment and Training in Minimally Invasive Surgery," *Journal of Medical Devices*, vol. 3, no. 4, p. 041002, 2009.
- [22] A. L. Trejos, R. V. Patel, M. D. Naish, and C. M. Schlachta, "Design of a sensorized instrument for skills assessment and training in minimally invasive surgery," *International Conference on Biomedical Robotics and Biomechatronics (BioRob)*, Scottsdale, AZ, USA, Oct. 19-22, 2008, pp. 965–970.
- [23] U. Seibold, B. Kübler, and G. Hirzinger, "Prototype of instrument for minimally invasive surgery with 6-axis force sensing capability," *IEEE Conf. on Robotics and Automation (ICRA)*, Barcelona, Spain, April 18-22, 2005, pp. 496–501.



- [24] M. S. Muller, L. Hoffmann, T. Christopher Buck, and A. Walter Koch, "Fiber Bragg Grating-Based Force-Torque Sensor with Six Degrees of Freedom," *International Journal of Optomechatronics*, vol. 3, no. 3, pp. 201–214, 2009.
- [25] D. S. Yurkewich, "Force Sensing in Arthroscopic Instruments using Fiber Bragg Gratings," *University of Western Ontario*, London, Canada, 2015.
- [26] I. Kuru, B. Gonenc, M. Balicki, J. Handa, P. Gehlbach, R. H. Taylor, and I. Iordachita, "Force sensing micro-forceps for robot assisted retinal surgery," *International Conference on Biomedical Robotics and Biomechatronics (BioRob)*, San Diego, California, USA, Aug. 28-Sep. 1, 2012, pp. 1401–1404.
- [27] X. He, M. a. Balicki, J. U. Kang, P. L. Gehlbach, J. T. Handa, R. H. Taylor, and I. I. Iordachita, "Force sensing micro-forceps with integrated fiber Bragg grating for vitreoretinal surgery," *SPIE BiOS*, San Francisco, California, USA, January 30th, 2012, pp. 82180W–82180W.
- [28] B. Gonenc, J. Handa, P. Gehlbach, R. H. Taylor, and I. Iordachita, "Design of 3-DOF force sensing micro-forceps for robot assisted vitreoretinal surgery," *International Conference of the IEEE Engineering in Medicine and Biology Society*, Osaka, Japan, July 3-7, 2013, pp. 5686–5689.
- [29] I. Iordachita, Z. Sun, M. Balicki, J. U. Kang, S. J. Phee, J. Handa, P. Gehlbach, and R. Taylor, "A sub-millimetric, 0.25 mN resolution fully integrated fiber-optic force-sensing tool for retinal microsurgery," *International Journal of Computer Assisted Radiology and Surgery*, vol. 4, no. 4, pp. 383–390, 2009.
- [30] B. Mitchell, J. Koo, I. Iordachita, P. Kazanzides, A. Kapoor, J. Handa, G. Hager, and R. Taylor, "Development and application of a new steady-hand manipulator for retinal surgery," *IEEE Conf. on Robotics and Automation (ICRA)*, Roma, Italy, April 10-14, 2007, pp. 623–629.
- [31] P. Puangmali, H. Liu, L. D. Seneviratne, P. Dasgupta, and K. Althoefer, "Miniature 3-axis distal force sensor for minimally invasive surgical palpation," *IEEE/ASME Transactions on Mechatronics*, vol. 17, no. 4, pp. 646–656, 2012.

- [32] J. Peirs, J. Clijnen, D. Reynaerts, H. Van Brussel, P. Herijgers, B. Corteville, and S. Boone, "A micro optical force sensor for force feedback during minimally invasive robotic surgery," *Sensors and Actuators*, vol. 115, no. 2-3 SPEC. ISS., pp. 447–455, 2004.
- [33] D. H. Lee, U. Kim, H. Moon, J. C. Koo, W. J. Yoon, and H. R. Choi, "Preliminary design of multi-axial contact force sensor for minimally invasive robotic surgery grasper," *IEEE Conf. on Robotics and Automation (ICRA)*, Karlsruhe, Germany, May 6-10, 2013, pp. 1019–1024.
- [34] A. Talasaz and R. V. Patel, "Remote palpation to localize tumors in robot-assisted minimally invasive approach," in *IEEE Conf. on Robotics and Automation (ICRA)*, Saint Paul, MN, USA, May 14-18, 2012, pp. 3719–3724.
- [35] A. S. Naidu, R. V. Patel, and M. D. Naish, "Low-cost disposable tactile sensors for palpation in minimally invasive surgery," *IEEE/ASME Transactions on Mechatronics*, vol. 22, no. 1, pp. 127–137, 2017.
- [36] A. S. Naidu, A. Escoto, O. Fahmy, R. V. Patel, and M. D. Naish, "An autoclavable wireless palpation instrument for minimally invasive surgery," in *International Conference on Engineering in Medicine and Biology Society (EMBC)*, Orlando, FL, USA, Aug. 16-20, 2016, pp. 6489–6492.
- [37] O. S. Bholat, R. S. Haluck, W. B. Murray, P. J. Gorman, and T. M. Krummel, "Tactile feedback is present during minimally invasive surgery," *Journal of the American College of Surgeons*, vol. 189, no. 4, pp. 349–355, 1999.
- [38] G. Picod, A. C. Jambon, D. Vinatier, and P. Dubois, "What can the operator actually feel when performing a laparoscopy?" *Surgical Endoscopy and Other Interventional Techniques*, vol. 19, no. 1, pp. 95–100, 2005.
- [39] N. Enayati, E. De Momi, and G. Ferrigno, "Haptics in robot-assisted surgery: challenges and benefits," *IEEE Engineering in Medicine and Biology Society*, vol. 9, pp. 49–65, 2016.
- [40] M. V. Ottermo, M. Ovstedal, T. Lango, O. Stavdahl, Y. Yavuz, T. a. Johansen, and R. Marvik, "The role of tactile feedback in laparoscopic surgery." *Journal of Surgical Laparoscopy, Endoscopy & Percutaneous Techniques*, vol. 16, no. 6, pp. 390–400, 2006.

- [41] E. P. Westebring-van der Putten, M. C. Berben, R. H. Goossens, J. J. Jakimowicz, and J. Dankelman, "The opinion and experience of surgeons with laparoscopic bowel grasper haptics," *Journal of Biomedical Science and Engineering*, vol. 3, no. 04, p. 422, 2010.
- [42] V. Gupta, N. P. Reddy, and P. Batur, "Forces in surgical tools: comparison between laparoscopic and surgical forceps," in *International Conference of Engineering in Medicine and Biology Society*, Amsterdam, Netherlands, Oct. 31-Nov. 3, 1996, pp. 223–224.
- [43] J. J. Van Den Dobbelsteen, A. Schooleman, and J. Dankelman, "Friction dynamics of trocars," *Surgical Endoscopy and Other Interventional Techniques*, vol. 21, no. 8, pp. 1338–1343, 2007.
- [44] C. Grimbergen, J. E. N. Jaspers, J. L. Herder, and H. G. Stassen, "Development of laparoscopic instruments." *Journal of the Society for Minimally Invasive Therapy*, vol. 10, no. 3, pp. 145–54, 2001.
- [45] K. T. Den Boer, J. L. Herder, W. Sjoerdsma, D. W. Meijer, D. J. Gouma, and H. G. Stassen, "Sensitivity of laparoscopic dissectors: What can you feel?" *Journal of Surgical Endoscopy*, vol. 13, no. 9, pp. 869–873, 1999.
- [46] J. Herder, M. Horward, and W. Sjoerdsma, "A laparoscopic grasper with force perception," *Minimally Invasive Therapy & Allied Technologies*, vol. 6, no. 4, pp. 279–286, 1997.
- [47] P. Breedveld, H. G. Stassen, D. W. Meijer, and J. J. Jakimowicz, "Observation in laparoscopic surgery: overview of impeding effects and supporting aids," *Journal of Laparoendoscopic & Advanced Surgical Techniques*, vol. 10, no. 5, pp. 231–241, 2000.
- [48] J. Barrie, D. G. Jayne, A. Neville, L. Hunter, A. J. Hood, and P. R. Culmer, "Real-time measurement of the tool-tissue interaction in minimally invasive abdominal surgery: The first step to developing the next generation of smart laparoscopic instruments," *Journal of Surgical Innovation*, vol. 23, no. 5, pp. 463–468, 2016.
- [49] P. Dubois, Q. Thommen, and A.-C. Jambon, "In vivo measurement of surgical gestures," *IEEE Transactions on Biomedical Engineering*, vol. 49, no. 1, pp. 49–54, 2002.

- [50] G. Tholey, A. Pillarisetti, W. Green, and J. Desai, "Design, development, and testing of an automated laparoscopic grasper with 3-D force measurement capability," *International Symposium of Medical Simulation (ISMS)*, Cambridge, MA, USA, June 17-18, 2004, pp. 38–48.
- [51] R. Ahmadi, J. Dargahi, M. Packirisamy, and R. Cecere, "A new mri-compatible optical fiber tactile sensor for use in minimally invasive robotic surgery systems," *Proc. SPIE 7653, Fourth European Workshop on Optical Fibre Sensors*, vol. 7653, p. 76532Z, September 9, 2010.
- [52] R. Ahmadi, M. Packirisamy, J. Dargahi, and R. Cecere, "Discretely loaded beam-type optical fiber tactile sensor for tissue manipulation and palpation in minimally invasive robotic surgery," *IEEE Sensors Journal*, vol. 12, no. 1, pp. 22–32, 2012.
- [53] J. Back, P. Dasgupta, L. Seneviratne, K. Althoefer, and H. Liu, "Feasibility study-novel optical soft tactile array sensing for minimally invasive surgery," *International Conference on Intelligent Robots and Systems (IROS)*, Hamburg, Germany, Sept. 28-Oct. 2, 2015, pp. 1528–1533.
- [54] D. J. Callaghan, G. Rajan, M. M. McGrath, E. Coyle, Y. Semenova, and G. Farrell, "Investigation and experimental measurement of scissor blade cutting forces using fiber Bragg grating sensors," *Smart Materials and Structures*, vol. 20, no. 10, p. 105004, 2011.
- [55] D. Callaghan, "Force Measurement & Evaluation for Surgical Cutting Applications: Development of an Effective Characterisation Testbed," *11th Annual Sir Bernard Crossland Symposium and Post-graduate Research Workshop*, University of Limerick, March 12 - 13, 2008.
- [56] D. J. Callaghan, M. M. McGrath, and E. Coyle, "Force Measurement Methods in Telerobotic Surgery : Implications for End-Effector Manufacture," *International Manufacturing Conference (IMC25)*, Dublin Institute of Technology, 2008, pp. 389-398.
- [57] D. J. Callaghan, M. M. McGrath, G. Rajan, E. Coyle, Y. Semenova, and G. Farrell, "Analysis of Strain Transfer to FBG's for Sensorized Telerobotic End-Effector Applications," *Advances in Robotics Research*, pp. 65–75, 2009.

- [58] U. Kim, D.-H. Lee, W. J. Yoon, B. Hannaford, and H. R. Choi, "Force sensor integrated surgical forceps for minimally invasive robotic surgery," *IEEE Transactions on Robotics*, vol. 31, no. 5, pp. 1214–1224, 2015.
- [59] C. H. King, M. O. Culjat, M. L. Franco, J. W. Bisley, G. P. Carman, E. P. Dutson, and W. S. Grundfest, "A Multielement Tactile Feedback System for Robot-Assisted Minimally Invasive Surgery," *IEEE Transactions on Haptics*, vol. 2, no. 1, pp. 52–56, 2009.
- [60] G. Rajan, D. Callaghan, Y. Semenova, M. McGrath, E. Coyle, and G. Farrell, "A fiber Bragg grating-based all-fiber sensing system for telerobotic cutting applications," *IEEE Sensors Journal*, vol. 10, no. 12, pp. 1913–1920, 2010.
- [61] B. Kubler, U. Seibold, and G. Hirzinger, "Development of actuated and sensor integrated forceps for minimally invasive robotic surgery," *The International Journal of Medical Robotics and Computer Assisted Surgery*, vol. 1, no. 3, pp. 96–107, 2005.
- [62] S. Saha, "Appropriate degrees of freedom of force sensing in robot-assisted minimally invasive surgery," *Johns Hopkins University*, Baltimore, MD, 2005.
- [63] A. Wroblewska, "Methods of the force measurement for robotic surgical tools," in *International Workshop on Robot Motion and Control*, Dymaczewo, Poland, June 23-25, 2005, pp. 51–54.
- [64] M. B. Hong and Y. H. Jo, "Design and evaluation of 2-DOF compliant forceps with force-sensing capability for minimally invasive robot surgery," *IEEE Transactions on Robotics*, vol. 28, no. 4, pp. 932–941, 2012.
- [65] K. Vakili, M. S. Flander, T. R. Sepp, M. Corral, J. D. Diaz, A. Slocum, and G. S. Teo, "Design and testing of a pressure sensing laparoscopic grasper," in *International Conference on Design of Medical Devices*, Minneapolis, MN, USA, April 12-14, 2011.
- [66] M. A. Qasaimeh, S. Sokhanvar, J. Dargahi, and M. Kahrizi, "Pvdf-based microfabricated tactile sensor for minimally invasive surgery," *Journal of Microelectromechanical Systems*, vol. 18, no. 1, pp. 195–207, 2009.

- [67] U. Kim, D.-H. Lee, W. J. Yoon, B. Hannaford, and H. R. Choi, "Force sensor integrated surgical forceps for minimally invasive robotic surgery," *IEEE Transactions on Robotics*, vol. 31, no. 5, pp. 1214–1224, 2015.
- [68] D.-H. Lee, U. Kim, H. Moon, J. C. Koo, W. J. Yoon, and H. R. Choi, "Preliminary design of multi-axial contact force sensor for minimally invasive robotic surgery grasper," in *IEEE Conf. on Robotics and Automation (ICRA)*, Karlsruhe, Germany, May 6-10, 2013, pp. 1019–1024.
- [69] K. Li, B. Pan, J. Zhan, W. Gao, Y. Fu, and S. Wang, "Design and performance evaluation of a 3-axis force sensor for mis palpation," *Sensor Review*, vol. 35, no. 2, pp. 219–228, 2015.
- [70] X. He, J. Handa, P. Gehlbach, R. Taylor, and I. Iordachita, "A submillimetric 3-dof force sensing instrument with integrated fiber bragg grating for retinal microsurgery," *IEEE Transactions on Biomedical Engineering*, vol. 61, no. 2, pp. 522–534, 2014.
- [71] Z. Yang, H. Liu, Y. Zhou, A. Gao, and H. Li, "A miniature force sensor for catheter based on optical micro deformation detection," in *International Conf. on Cyber Technology in Automation, Control, and Intelligent Systems (CYBER)*, Shenyang, China, 2015, pp. 441–445.
- [72] K. Yokoyama, H. Nakagawa, D. C. Shah, H. Lambert, G. Leo, N. Aeby, A. Ikeda, J. V. Pitha, T. Sharma, R. Lazzara, and W. M. Jackman, "Novel contact force sensor incorporated in irrigated radiofrequency ablation catheter predicts lesion size and incidence of steam pop and thrombus." *Circulation, Arrhythmia and Electrophysiology*, vol. 1, no. 5, pp. 354–362, 2008.
- [73] P. Polygerinos, T. Schaeffter, L. Seneviratne, and K. Althoefer, "A fibre-optic catheter-tip force sensor with MRI compatibility: A feasibility study," *International Conference of the IEEE Engineering in Medicine and Biology Society*, Minneapolis, MN, USA, Sept. 3-6, 2009, pp. 1501–1504.
- [74] P. Polygerinos, A. Ataollahi, T. Schaeffter, R. Razavi, L. D. Seneviratne, and K. Althoefer, "MRI-compatible intensity-modulated force sensor for cardiac catheterization procedures," *IEEE Transactions on Biomedical Engineering*, vol. 58, no. 3, pp. 721–726, 2011.

- [75] P. Z. Polygerinos D.; Schaeffter, T.; Razavi, R.; Seneviratne, L.D.; Althoefer, K., “MRI-Compatible Fiber-Optic Force Sensors for Catheterization Procedures,” *Sensors Journal*, vol. 10, no. 10, pp. 1598–1608, 2010.
- [76] P. Polygerinos, L. D. Seneviratne, R. Razavi, T. Schaeffter, and K. Althoefer, “Triaxial catheter-tip force sensor for MRI-guided cardiac procedures,” *IEEE/ASME Transactions on Mechatronics*, vol. 18, no. 1, pp. 386–396, 2013.
- [77] P. Puangmali, P. Dasgupta, L. D. Seneviratne, and K. Althoefer, “Miniaturized triaxial optical fiber force sensor for MRI-guided minimally invasive surgery,” *IEEE Conf. on Robotics and Automation (ICRA)*, Anchorage, AK, USA, May 3-7, 2010, pp. 2592–2597.
- [78] R. C. Hibbeler, *Statics and Mechanics of Materials*, Pearson Higher Ed, 2013.
- [79] L. Kruger, P. L. Swart, A. A. Chtcherbakov, and A. Van Wyk, “Non-contact torsion sensor using fibre bragg gratings,” *Measurement Science and Technology*, vol. 15, no. 8, p. 1448, 2004.
- [80] Y. Hwang and J. Lee, “Online non-contact torsion sensing method using fiber bragg grating sensors and optical coupling method,” *International Conference on Sound and Vibration (ICSV)*, Cairns, Australia, 2007, pp. 9–12.
- [81] a. J. van Wyk and M. C. S. Snyman, “Optical fibre Bragg sensor torque transducer,” *Third European Workshop on Optical Fibre Sensors*, Napoli, Italy, 2007, pp. 66190T–66190T–4.
- [82] S. Fu, Y. Huang, and X. Li, “Experimental study of torque measurement based on fbg,” in *International Conference on Communications, Signal Processing, and Systems*, Switzerland, 2014, pp. 255–261.
- [83] X. Tian and X. Taa, “Torsion measurement by using fbg sensors,” *Jounral of Experimental Mechanics*, vol. 41, no. 3, pp. 248–253, 2000.
- [84] C. G. Askins, G. A. Miller, and E. J. Friebele, “Bend and twist sensing in a multiple-core optical fiber,” in *Conference on Optical Fiber Communication (OFC)*, San Diego, CA, USA, Feb. 24-28, 2008, pp. 1–3.

- [85] L. A. Fernandes, J. R. Grenier, J. S. Aitchison, and P. R. Herman, "Fiber optic stress-independent helical torsion sensor," *Optics letters*, vol. 40, no. 4, pp. 657–660, 2015.
- [86] S. C. Ryu and P. E. Dupont, "FBG-based shape sensing tubes for continuum robots," *IEEE Conf. on Robotics and Automation (ICRA)*, Hong Kong, China, May 31-June 7, 2014, pp. 3531–3537.
- [87] R. Xu, A. Yurkewich, and R. V. Patel, "Curvature, Torsion, and Force Sensing in Continuum Robots Using Helically Wrapped FBG Sensors," *IEEE Robotics and Automation Letters*, vol. 1, no. 2, pp. 1052–1059, 2016.
- [88] M. I. Tiwana, S. J. Redmond, and N. H. Lovell, "A review of tactile sensing technologies with applications in biomedical engineering," *Sensors and Actuators*, vol. 179, pp. 17–31, 2012.
- [89] P. Roriz, L. Carvalho, O. Frazao, J. L. Santos, and J. A. Simoes, "From conventional sensors to fibre optic sensors for strain and force measurements in biomechanics applications: A review," *Journal of Biomechanics*, no. 6, pp. 1251–1261, 2014.
- [90] H. Yousef, M. Boukallel, and K. Althoefer, "Tactile sensing for dexterous in-hand manipulation in robotics - A review," *Sensors and Actuators*, vol. 167, pp. 171–187, 2011.
- [91] J. Rosen, M. MacFarlane, C. Richards, B. Hannaford, and M. Sinanan, "Surgeon-tool force/torque signatures—evaluation of surgical skills in minimally invasive surgery." *Studies in Health Technology and Informatics*, January 1999, pp. 290–6.
- [92] G. P. Moustiris, S. C. Hiridis, K. Deliparaschos, and K. Konstantinidis, "Evolution of autonomous and semi-autonomous robotic surgical systems: a review of the literature," *The International Journal of Medical Robotics and Computer Assisted Surgery (MRCAS)*, vol. 7, no. 3, pp. 375–392, 2011.
- [93] Y. Hu, R. B. Katragadda, H. Tu, Q. Zheng, Y. Li, and Y. Xu, "Bioinspired 3-d tactile sensor for minimally invasive surgery," *Journal of Microelectromechanical Systems*, vol. 19, no. 6, pp. 1400–1408, 2010.
- [94] G. B. Hanna, T. Drew, G. Arnold, M. Fakhry, and A. Cuschieri, "Development of force measurement system for clinical use in minimal access surgery," *Journal of Surgical Endoscopy*, vol. 22, no. 2, pp. 467–471, 2008.



- [95] K. J. Rebello, "Applications of MEMS in surgery," *Proceedings of the IEEE*, vol. 92, no. 1, pp. 43–55, 2004.
- [96] I. M. Koc, T. Eray, B. Sumer, and N. Cervi, "An active force controlled laparoscopic grasper by using a smart material actuation," *Tribology International*, vol. 100, pp. 1–11, 2016.
- [97] A. Bakar, "Advances in bio-tactile sensors for minimally invasive surgery using the fibre Bragg grating force sensor technique: a survey," *Sensors*, vol. 14, no. 4, pp. 6633–6665, 2014.
- [98] F. Taffoni, D. Formica, P. Saccomandi, G. Di Pino, and E. Schena, "Optical fiber-based MR-compatible sensors for medical applications: an overview." *Sensors*, vol. 13, no. 10, pp. 14 105–14 120, 2013.
- [99] Y.-L. Park, S. Elayaperumal, B. L. Daniel, E. Kaye, K. B. Pauly, R. J. Black, and M. R. Cutkosky, "MRI-Compatible Haptics: Feasibility of using optical fiber Bragg grating strain-sensors to detect deflection of needles in an MRI environment," *International Society for Magnetic Resonance in Medicine ISMRM 16th Annual Scientific Meeting*, vol. 16, p. 4, 2008.
- [100] S. J. Mihailov, "Fiber bragg grating sensors for harsh environments," *Sensors*, vol. 12, no. 2, pp. 1898–1918, 2012.
- [101] R. Ahmadi, S. Arbatani, J. Ozhikandathil, M. Packirisamy, and J. Dargahi, "A multi-purpose optical microsystem for static and dynamic tactile sensing," *Sensors and Actuators*, vol. 235, pp. 37–47, 2015.
- [102] Y. Zhao, Y. Zhao, and M. Zhao, "Novel force sensor based on a couple of fiber Bragg gratings," *Journal of the International Measurement*, vol. 38, no. 1, pp. 30–33, 2005.
- [103] H. Xie, H. Liu, Y. Noh, J. Li, S. Wang, and K. Althoefer, "A fiber-optics-based body contact sensor for a flexible manipulator," *IEEE Sensors Journal*, vol. 15, no. 6, pp. 3543–3550, 2015.
- [104] G. Rajan, S. Mathews, D. Callaghan, G. Farrell, and G.-D. Peng, "Polymer fiber Bragg grating force sensors for minimally invasive surgical devices," *International Conference on Optical Fiber Sensors (OFS)*, 2015, pp. 96551E-1-96551E-4.

- [105] Z. Mo, W. Xu, and N. Broderick, "A Fabry-Perot optical fiber force sensor based on intensity modulation for needle tip force sensing," *International Conference on Automation, Robotics and Applications (ICARA)*, Queenstown, New Zealand, Feb. 17-19, 2015, pp. 376–380.
- [106] H. Xie, A. Jiang, H. A. Wurdemann, H. Liu, L. D. Seneviratne, and K. Althoefer, "Magnetic resonance-compatible tactile force sensor using fiber optics and vision sensor," *IEEE Sensors Journal*, vol. 14, no. 3, pp. 829–838, 2014.
- [107] H. Xie, H. Liu, L. D. Seneviratne, and K. Althoefer, "An optical tactile array probe head for tissue palpation during minimally invasive surgery," *IEEE Sensors Journal*, vol. 14, no. 9, pp. 3283–3291, 2014.
- [108] K. M. Moerman, A. M. J. Sprengers, A. J. Nederveen, and C. K. Simms, "A novel MRI compatible soft tissue indenter and fibre Bragg grating force sensor," *Medical Engineering and Physics*, vol. 35, no. 4, pp. 486–499, 2013.
- [109] H. Song, K. Kim, and J. Lee, "Development of optical fiber Bragg grating force-reflection sensor system of medical application for safe minimally invasive robotic surgery," *Review of Scientific Instruments*, vol. 82, no. 7, p. 074301, 2011.
- [110] D. A. Jaffray, "World congress on medical physics and biomedical engineering," *IFMBE Proceedings*, vol. 51, Toronto, Canada, June 7-12, 2015, pp. 866–869.
- [111] C. Doyle, "Fibre Bragg Grating Sensors-An Introduction to Bragg gratings and interrogation techniques," *Smart Fibres Ltd*, vol. 1, pp. 1–5, 2003.
- [112] E. Al-Fakih, N. A. A. Osman, and F. R. M. Adikan, "The use of fiber bragg grating sensors in biomechanics and rehabilitation applications: The state-of-the-art and ongoing research topics," *Sensors*, vol. 12, no. 10, pp. 12 890–12 926, 2012.
- [113] J.-S. Heo, J.-H. Chung, and J.-J. Lee, "Tactile sensor arrays using fiber bragg grating sensors," *Sensors and Actuators*, vol. 126, no. 2, pp. 312–327, 2006.
- [114] V. Mishra, N. Singh, U. Tiwari, and P. Kapur, "Fiber grating sensors in medicine: Current and emerging applications," *Sensors and Actuators*, vol. 167, no. 2, pp. 279–290, 2011.

- [115] D. Callaghan, "Force sensing surgical scissor blades using fibre bragg grating sensors," *Dublin Institute of Technology*, Dublin, Ireland, 2013.
- [116] Z. Mo, W. Xu, N. Broderick, and H. Chen, "A temperature-compensated optical fiber force sensor for minimally invasive surgeries," *SPIE Micro-Nano Materials, Devices, and Applications*, Sydney, New South Wales, Australia, December 22, 2015, pp. 966850–966850.
- [117] Z. Wang, Y. Jiang, H. Peng, X. Ma, and L. Cui, "A temperature-compensated fibre optic extrinsic fabry–perot interferometric displacement sensor for fault measurement in geomechanics," *Measurement Science and Technology*, vol. 24, no. 2, p. 025104, 2012.
- [118] Z. Ran, Y. Rao, J. Zhang, Z. Liu, and B. Xu, "A miniature fiber-optic refractive-index sensor based on laser-machined fabry–perot interferometer tip," *Journal of Lightwave Technology*, vol. 27, no. 23, pp. 5426–5429, 2009.
- [119] M. E. H. Eltaib and J. R. Hewit, "Tactile sensing technology for minimal access surgery - A review," *Mechatronics*, vol. 13, no. 10, pp. 1163–1177, 2003.
- [120] D. Callaghan, M. Mcgrath, G. Rajan, Y. Semenova, G. Farrell, and E. Coyle, "Comparing FBG and PCF Force Sensors in a Laparoscopic Smart Surgical Scissor Instrument," *Electrical Engineering*, pp. 1–4, 2011.
- [121] O. Frazao, J. M. Baptista, and J. L. Santos, "Temperature-independent strain sensor based on a hi-bi photonic crystal fiber loop mirror," *IEEE Sensors Journal*, vol. 7, no. 10, pp. 1453–1455, 2007.
- [122] S. Mathews, D. Callaghan, Y. Semenova, G. Rajan, and G. Farrell, "Photonic crystal fiber strain sensors for laparoscopic surgical devices," *Photonics Global Conference (PGC)*, Singapore, Dec. 13-16, 2012, pp. 1–4.
- [123] G. Rajan, D. Callaghan, Y. Semenova, and G. Farrell, "Photonic crystal fiber sensors for minimally invasive surgical devices," *IEEE Transactions on Biomedical Engineering*, vol. 59, no. 2, pp. 332–338, 2012.

- [124] S. Qing, L. Fuyun, W. Zhi, J. Long, H. Juan, L. Zhanyuan, K. Guiyun, and D. Xiaoyi, “Environmentally Stable FabryProt-Type Strain Sensor Based On Hollow-Core Photonic Bandgap Fiber,” *IEEE Photonics Technology Letters*, vol. 20, no. 4, pp. 2008–2010, 2008.
- [125] X. Li, “Embedded sensors in layered manufacturing,” *Stanford University Stanford, CA*, 2001.
- [126] Y.-I. Park, K. Chau, R. J. Black, and M. R. Cutkosky, “Force Sensing Robot Fingers using Embedded Fiber Bragg Grating Sensors and Shape Deposition Manufacturing,” *IEEE Conf. on Robotics and Automation (ICRA)*, Roma, Italy, April 10-14, 2007.
- [127] A. M. Dollar, C. R. Wagner, and R. D. Howe, “Embedded sensors for biomimetic robotics via shape deposition manufacturing,” *International Conference on Biomedical Robotics and Biomechanics (BioRob)*, Pisa, Italy, Feb. 20-22, 2006, pp. 763–768.
- [128] G. S. Fischer, T. Akinbiyi, S. Saha, J. Zand, M. Talamini, M. Marohn, and R. Taylor, “Ischemia and force sensing surgical instruments for augmenting available surgeon information,” in *International Conference on Biomedical Robotics and Biomechanics (BioRob)*, Pisa, Italy, Feb. 20-22, 2006, pp. 1030–1035.
- [129] M. Kitagawa, D. Dokko, A. M. Okamura, and D. D. Yuh, “Effect of sensory substitution on suture-manipulation forces for robotic surgical systems,” *Journal of Thoracic and Cardiovascular Surgery*, vol. 129, no. 1, pp. 151–158, 2005.
- [130] W. McMahan, J. Gewirtz, D. Standish, P. Martin, J. A. Kunkel, M. Lilavois, A. Wedmid, D. I. Lee, and K. J. Kuchenbecker, “Tool contact acceleration feedback for telerobotic surgery,” *IEEE Transactions on Haptics*, vol. 4, no. 3, pp. 210–220, 2011.
- [131] S. V. Jackman, P. A. Jarzemeski, S. M. Listopadzki, B. R. Lee, D. Stoianovici, R. Demaree, T. W. Jarrett, and L. R. Kavoussi, “The EndoHand: comparison with standard laparoscopic instrumentation.” *Journal of Laparoendoscopic & Advanced Surgical Techniques. Part A*, vol. 9, no. 3, pp. 253–258, 1999.
- [132] C. Payne, “Ungrounded haptic-feedback for hand-held surgical robots,” *Imperial College, London, UK*, 2015.

- [133] U. Matern and P. Waller, "Instruments for minimally invasive surgery," *Journal of Surgical Endoscopy*, vol. 13, no. 2, pp. 174–182, 1999.
- [134] A. Ramani, M. Braasch, A. Botnaru, A. Lavers, S. Herrera, R. Nardi Pedro, and M. Monga, "Evaluation of efficacy of four laparoscopic needle drivers," *JSLs : Journal of the Society of Laparoendoscopic Surgeons / Society of Laparoendoscopic Surgeons*, vol. 12, no. 1, pp. 77–80, 2008.
- [135] Z. Li, G. Wang, J. Tan, X. Sun, H. Lin, and S. Zhu, "Building a framework for ergonomic research on laparoscopic instrument handles," *International Journal of Surgery*, vol. 30, pp. 74–82, 2016.
- [136] Tuijthof, van Engelen, Herder, Goossens, Snijders, and van Dijk, "Ergonomic handle for an arthroscopic cutter." *Journal of the Society for Minimally Invasive Therapy*, vol. 12, no. 1, pp. 82–90, 2003.
- [137] D. Gossot and G. Lange, "Deflectable and rotatable endoscopic instrument with intuitive control." *Journal of the Society for Minimally Invasive Therapy*, vol. 10, no. 6, pp. 295–9, 2001.
- [138] A. Melzer, K. Kipfmüller, and B. Halfar, "Deflectable endoscopic instrument system DENIS." *Journal of Surgical Endoscopy*, vol. 11, no. 10, pp. 1045–1051, 1997.
- [139] J. J. Abbott and A. M. Okamura, "Virtual fixture architectures for telemanipulation," in *IEEE Conf. on Robotics and Automation (ICRA)*, Taipei, Taiwan, Sep. 14-19, 2003, pp. 2798–2805.
- [140] H. Yamashita, A. Iimura, E. Aoki, T. Suzuki, T. Nakazawa, E. Kobayashi, M. Hashizume, I. Sakuma, and T. Dohi, "Development of Endoscopic Forceps Manipulator Using Multi-Slider Linkage Mechanisms," *International Symposium on Computer Aided Surgery - Robotic and Image guided Surgery*, Ibaraki, Japan, April 28, 2005, pp. 3–6.
- [141] A. H. Zahraee, J. K. Paik, J. Szewczyk, and G. Morel, "Toward the development of a hand-held surgical robot for laparoscopy," *IEEE/ASME Transactions on Mechatronics*, vol. 15, no. 6, pp. 853–861, 2010.
- [142] C. D. Hinman and D. J. Danitz, "Tool with rotation lock," 2007, uS Patent App. 11/787,607.

- [143] A. Hassan-Zahraee, B. Herman, and J. Szewczyk, "Mechatronic design of a hand-held instrument with active trocar for laparoscopy," *IEEE Conf. on Robotics and Automation (ICRA)*, Shanghai, China, May 9-13, 2011, pp. 1890–1895.
- [144] M. Piccigallo, F. Focacci, O. Tonet, G. Megali, C. Quaglia, and P. Dario, "Hand-held robotic instrument for dextrous laparoscopic interventions," *The International Journal of Medical Robotics and Computer Assisted Surgery*, vol. 4, no. 4, pp. 331–338, 2008.
- [145] J. T. Wen, "EndoBot: a robotic assistant in minimally invasive surgeries," *IEEE Conf. on Robotics and Automation (ICRA)*, Seoul, South Korea, May 21-26, 2001, pp. 2031–2036.
- [146] S. Leonard, K. L. Wu, Y. Kim, A. Krieger, and P. C. W. Kim, "Smart tissue anastomosis robot (STAR): A vision-guided robotics system for laparoscopic suturing," *IEEE Transactions on Biomedical Engineering*, vol. 61, no. 4, pp. 1305–1317, 2014.
- [147] *Food and Drug Administration regulatory: New Section 513(f)(2) Evaluation of Automatic Class III Designation, Guidance for Industry and CDRH Staff.*
- [148] T. R. Kucklick, *The Medical Device R&D Handbook*, CRC Press, 2012.
- [149] P. H. King, R. C. Fries, and A. T. Johnson, *Design of Biomedical Devices and Systems*, CRC Press, 2014.
- [150] "Device classification under section 513(a)(1)(de novo) : Reclassification order for den110016."
- [151] "Device classification under section 513(a)(1)(de novo) : Decision summary (fda review) for den110016."
- [152] D. D. Masaya Kitagawa and A. M. Okamura, "Effect of sensory substitution on suture manipulation forces for surgical teleoperation," *Medicine Meets Virtual Reality 12: Building a Better You: the Next Tools for Medical Education, Diagnosis, and Care*, vol. 98, p. 157, 2004.
- [153] P. S. Zarrin, A. Escoto, R. Xu, R. V. Patel, M. D. Naish, and A. L. Trejos, "Development of an optical fiber-based sensor for grasping and axial force sensing," in *IEEE Conf. on Robotics and Automation (ICRA)*, Singapore, May 29-June 3, 2017, pp. 939–944.

- 
- [154] *CES EduPack software*, Granta Design Limited, Cambridge, UK, 2009.
- [155] R. Xu, A. Yurkewich, and R. V. Patel, “Shape sensing for torsionally compliant concentric-tube robots,” *Optical Fibers and Sensors for Medical Diagnostics and Treatment*, San Francisco, California, USA, February 13-18, 2016, pp. 97020V–1.
- [156] P. S. Zarrin, A. Escoto, R. Xu, R. V. Patel, M. D. Naish, and A. L. Trejos, “Development of a 2-dof sensorized surgical grasper for grasping and axial force measurements,” *Submitted paper to IEEE Sensors Journal*, (revision requested).

## **Appendix A**

# **Expanded Views and Technical Drawings**



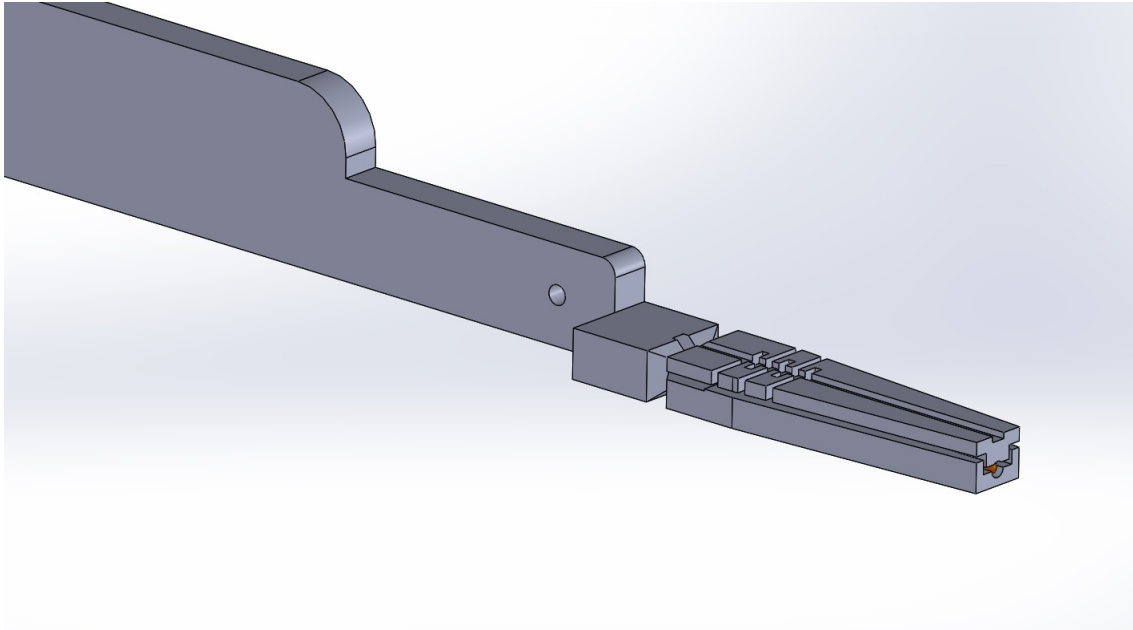


Figure A.1: 1st prototype of the sensorized grasper

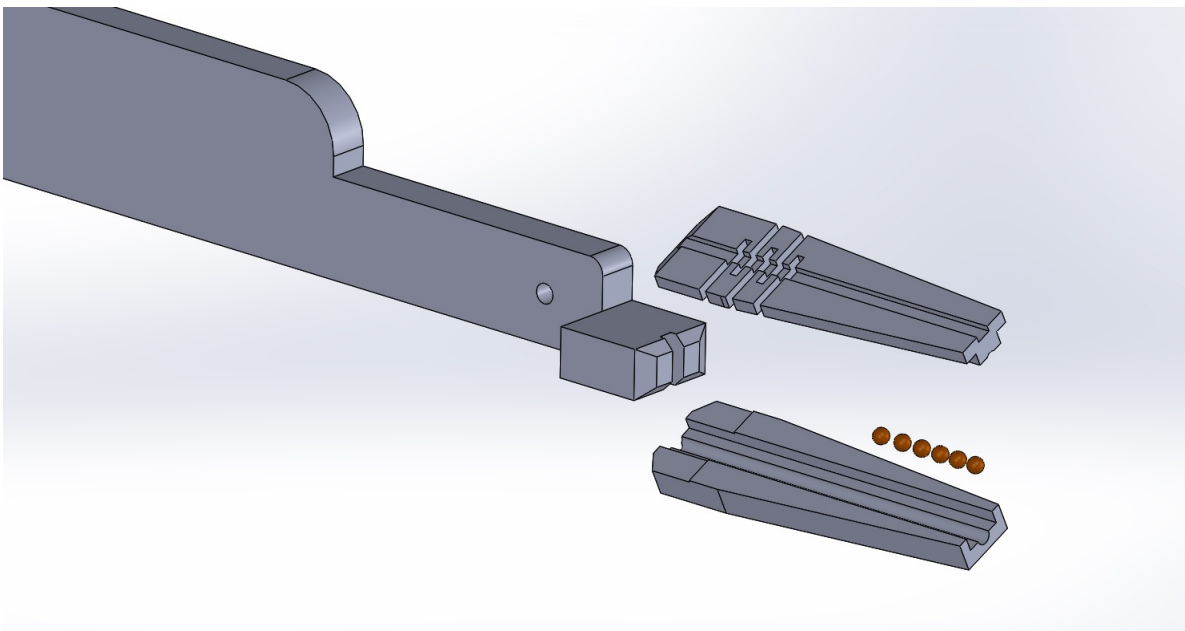


Figure A.2: Expanded view of the 1st prototype of the sensorized grasper

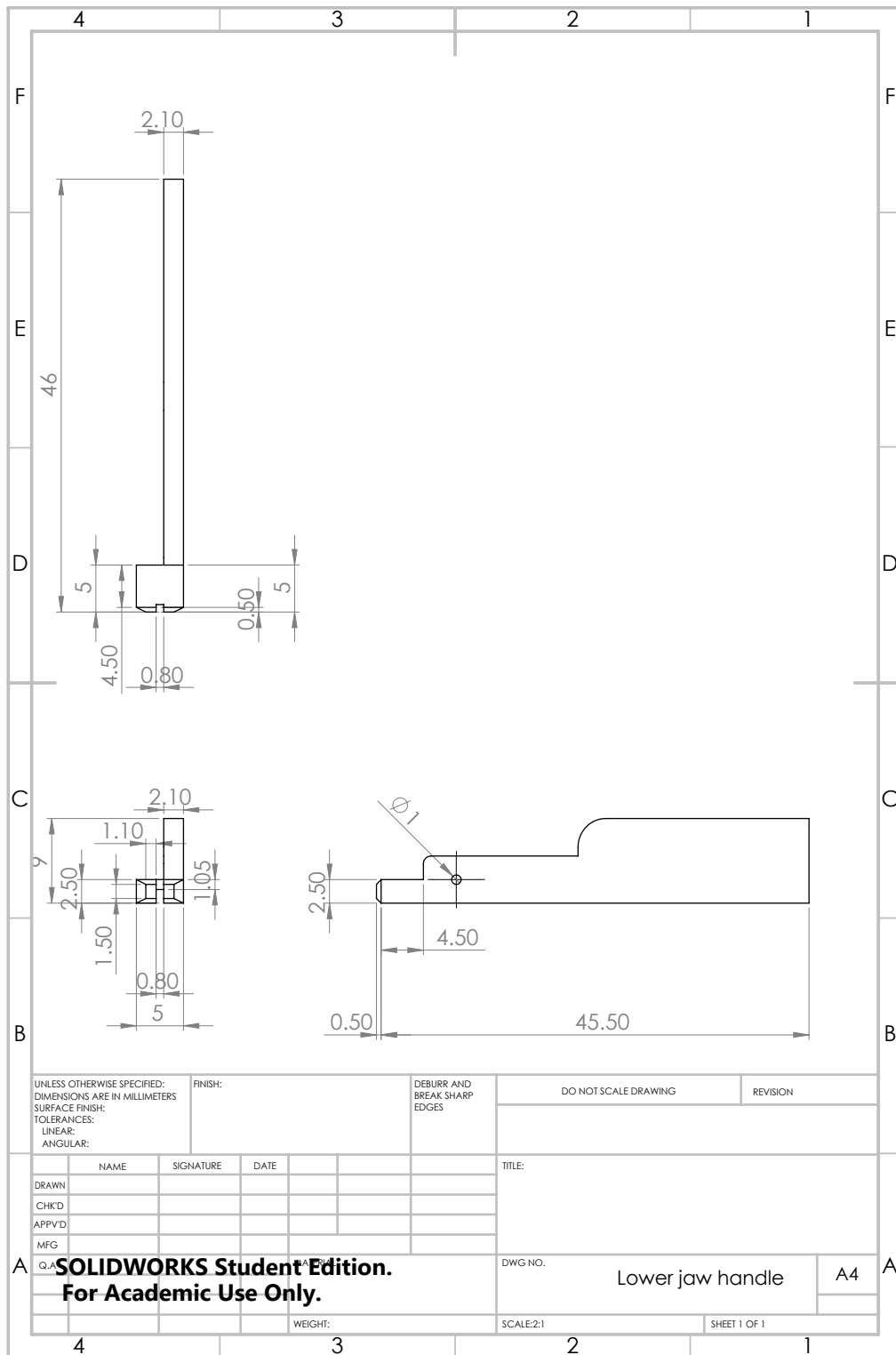


Figure A.3: Lower jaw handle of 1st sensorized grasper

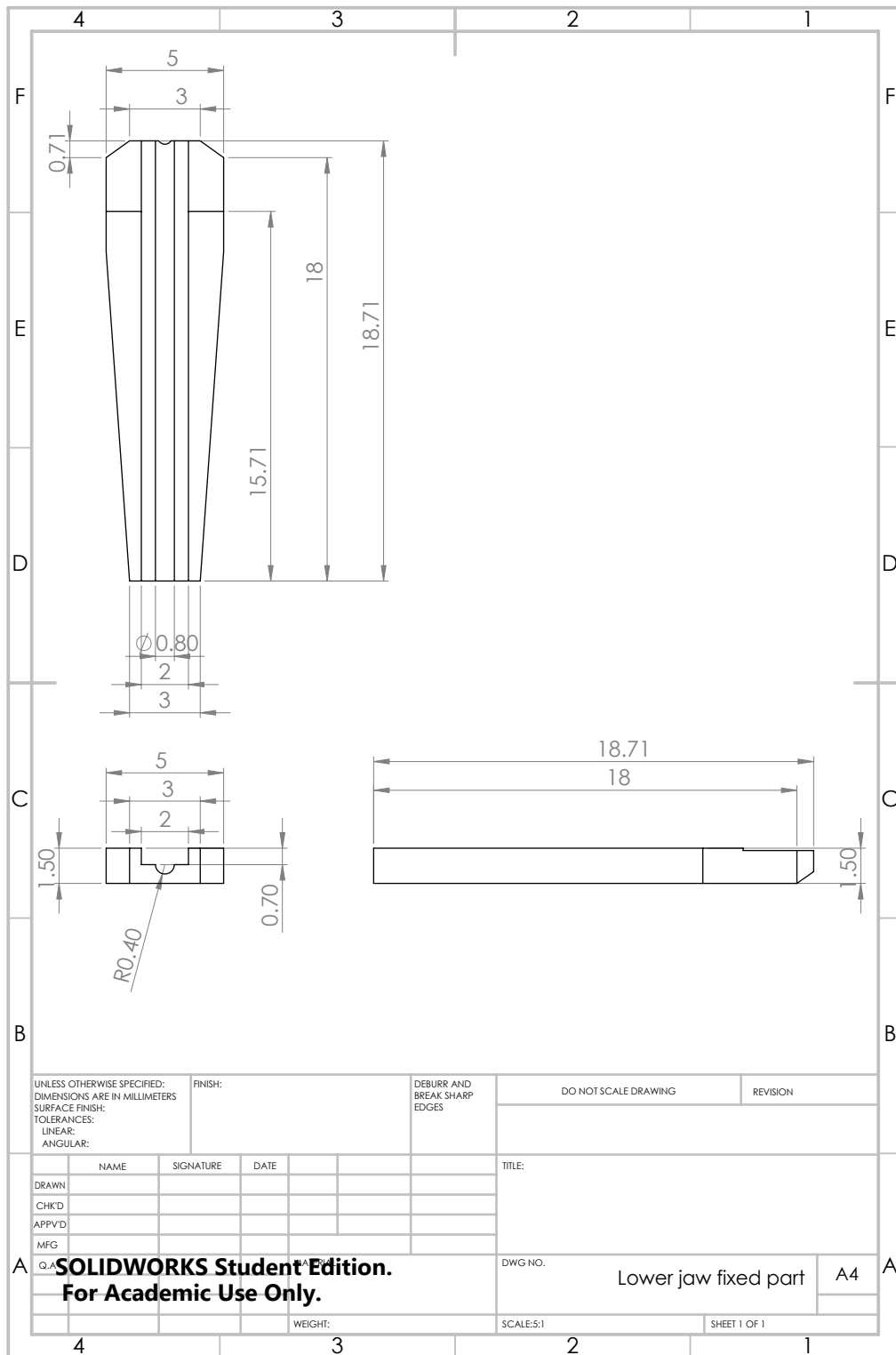


Figure A.4: Fixed part of the lower jaw of the 1st sensorized grasper

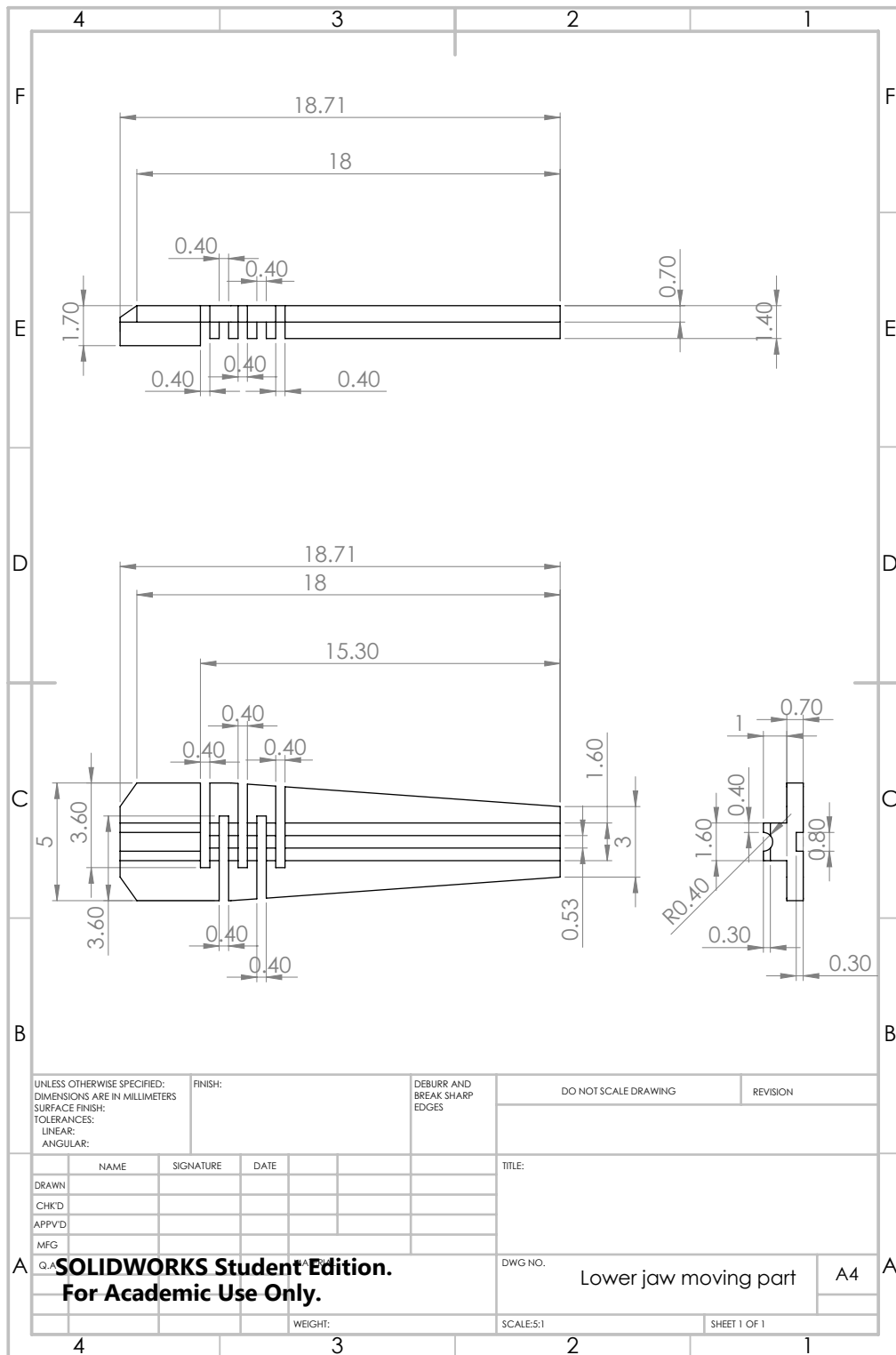


Figure A.5: Moving part of the lower jaw of the 1st sensorized grasper

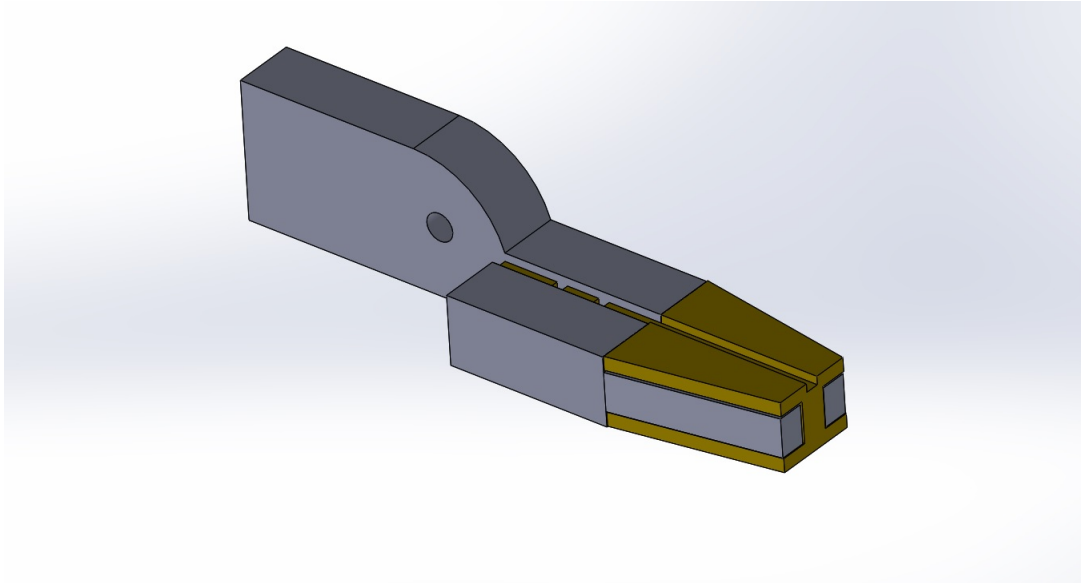


Figure A.6: 2nd prototype of the sensorized grasper

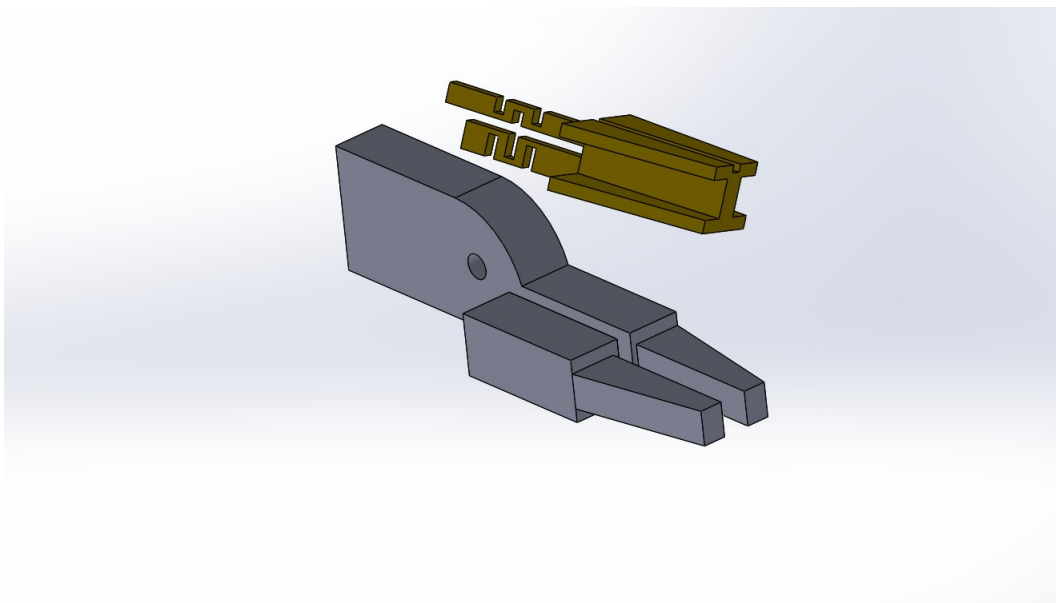


Figure A.7: Expanded view of the 2nd prototype of the sensorized grasper

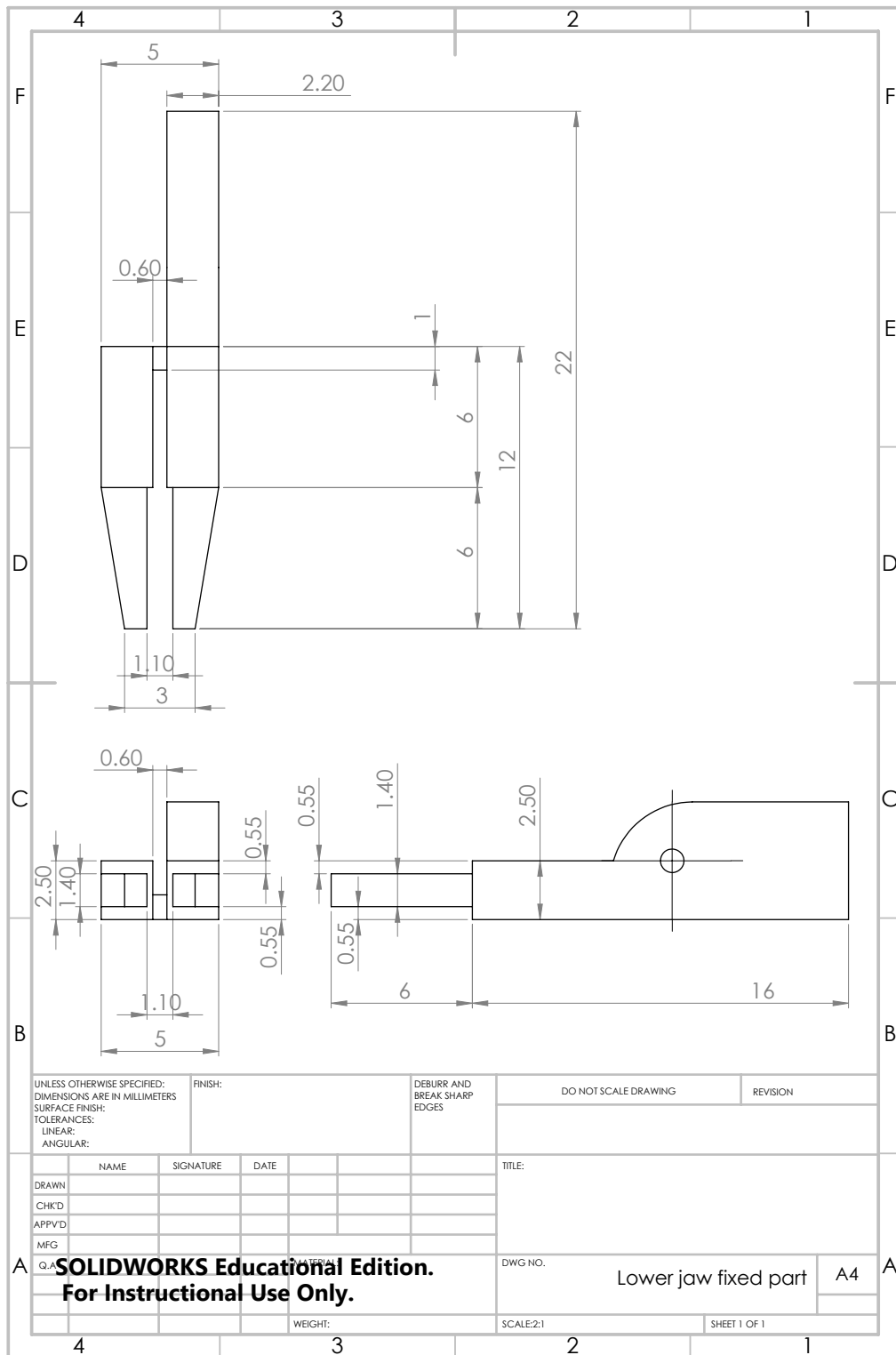


Figure A.8: Fixed part of the lower jaw of the 2nd sensorized grasper

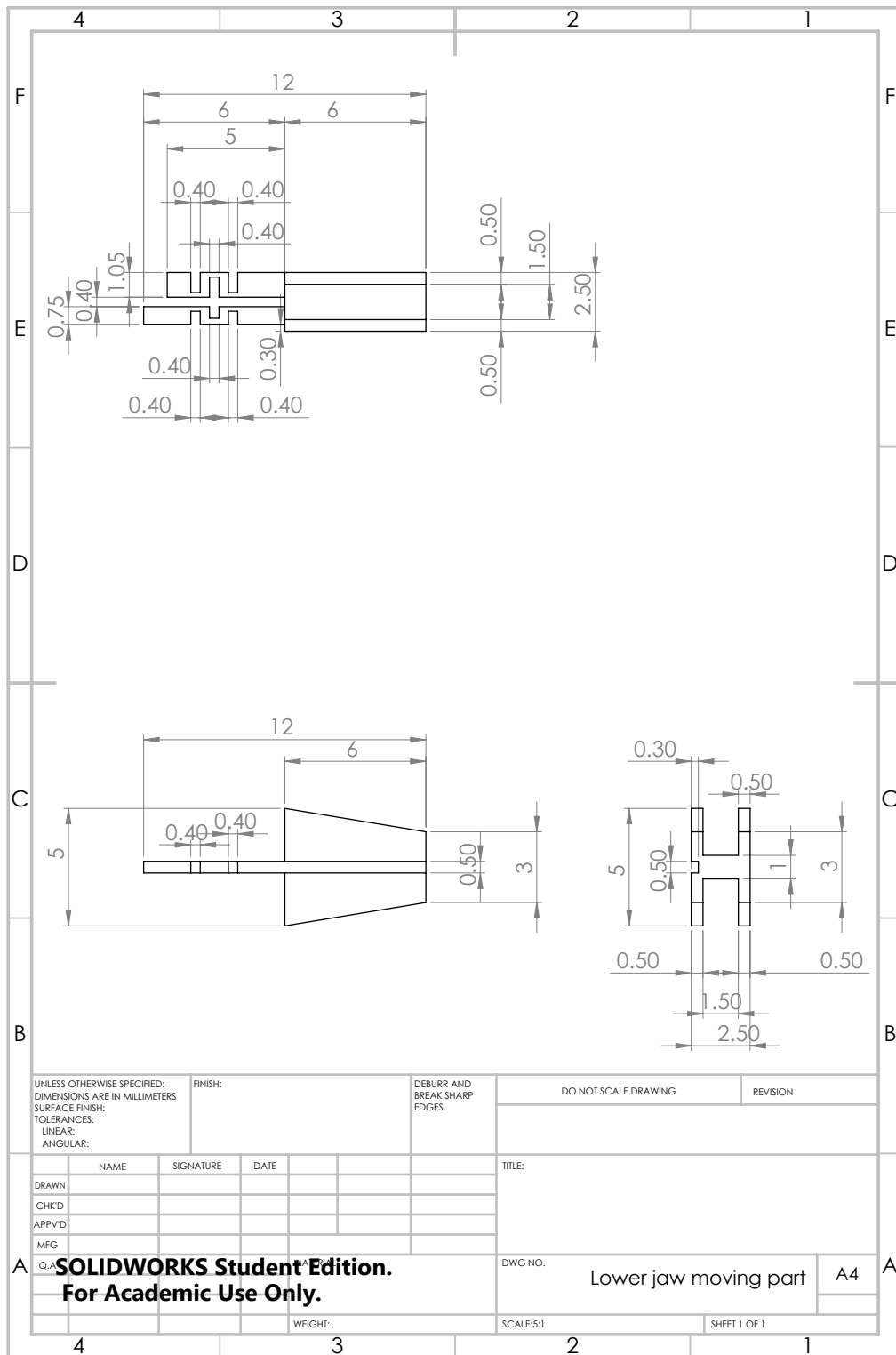


Figure A.9: Moving part of the lower jaw of the 2nd sensorized grasper

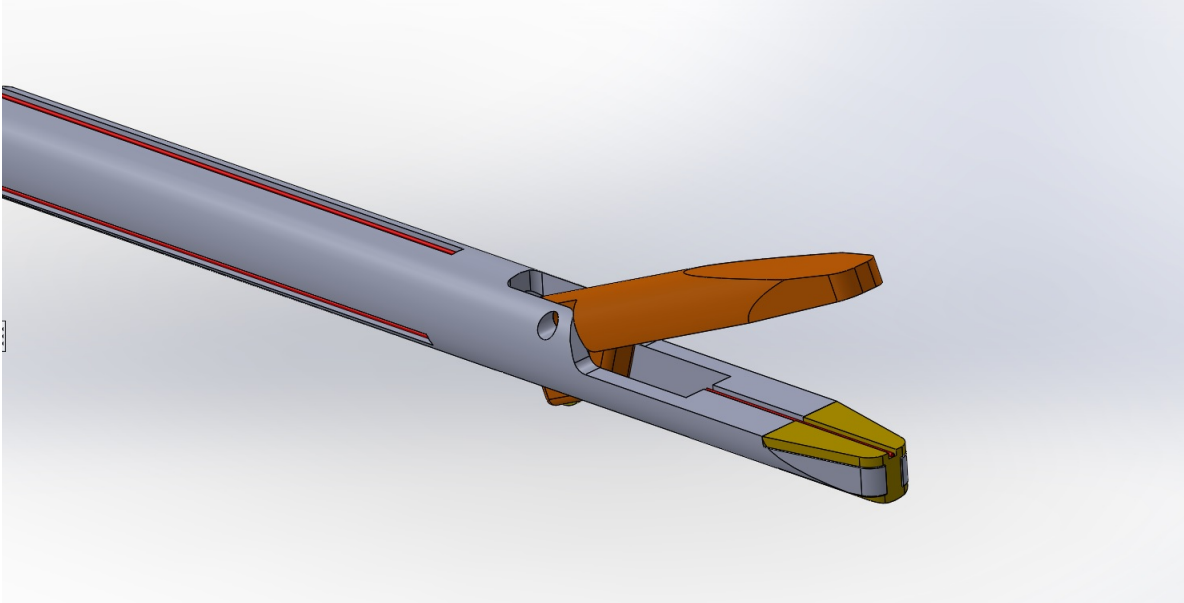


Figure A.10: Final prototype of the sensorized instrument

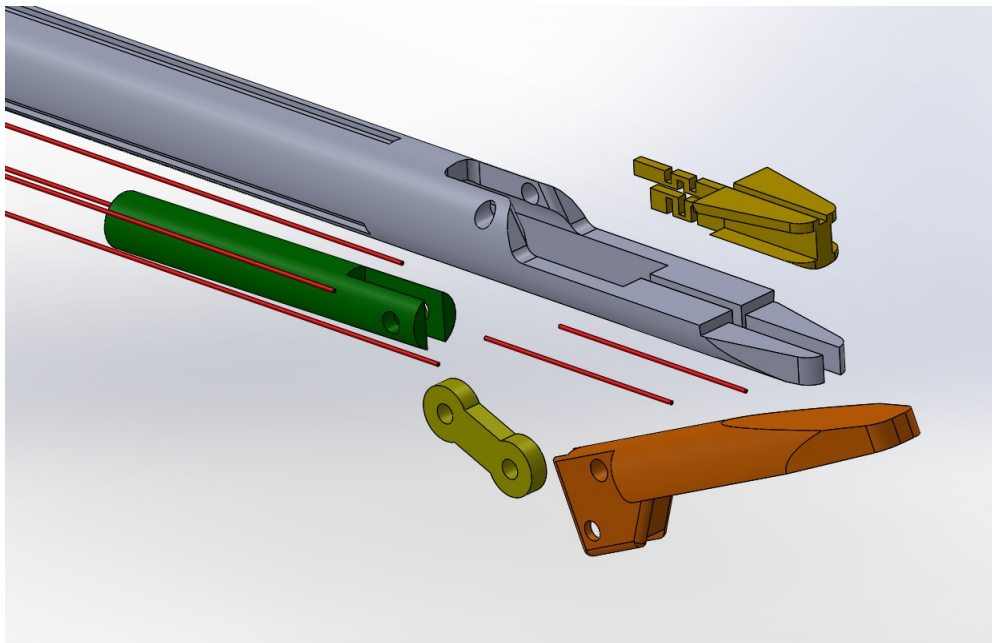


Figure A.11: Expanded view of the final prototype of the sensorized instrument



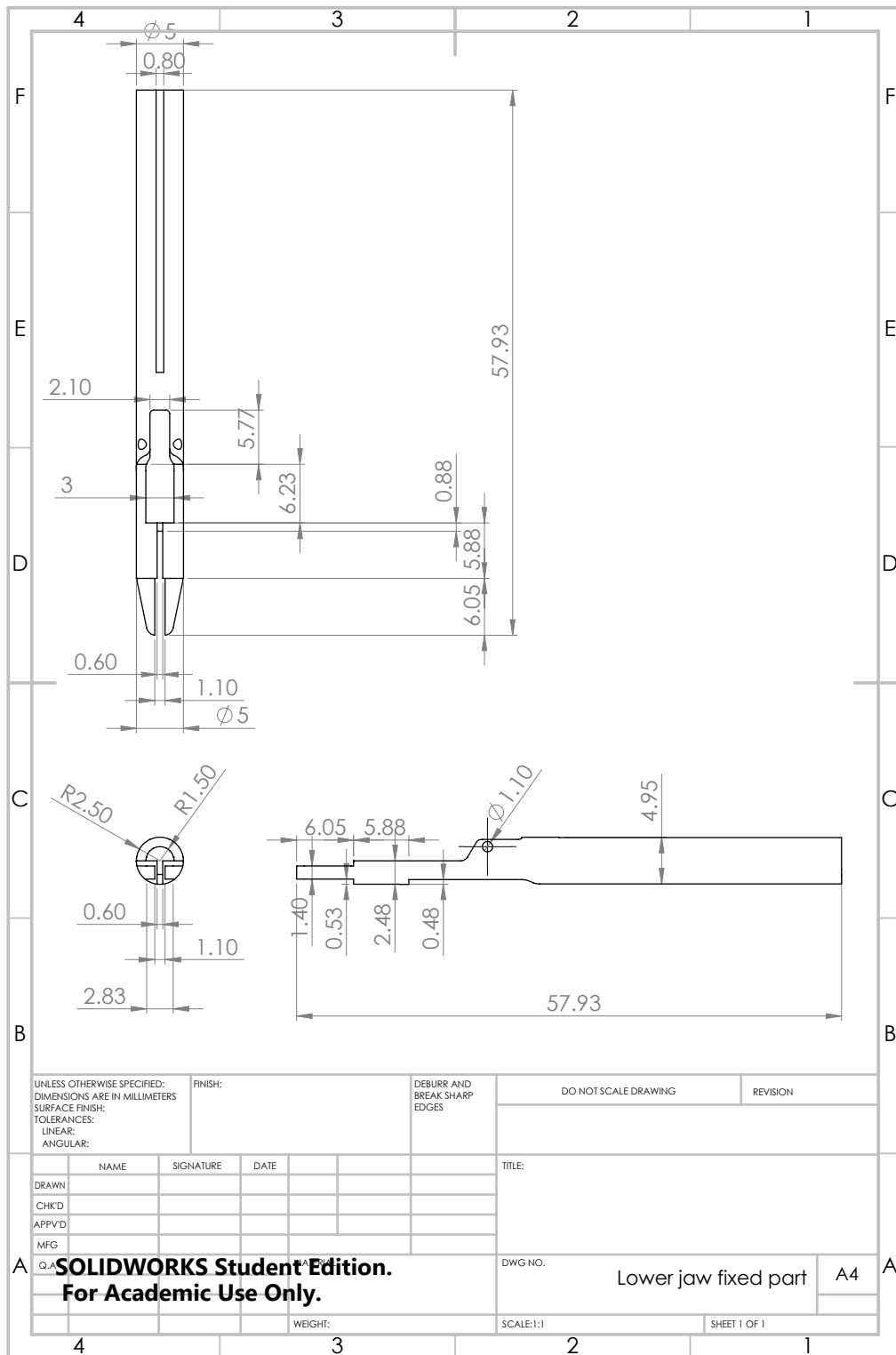


Figure A.12: Fixed part of the lower jaw of the final sensorized instrument

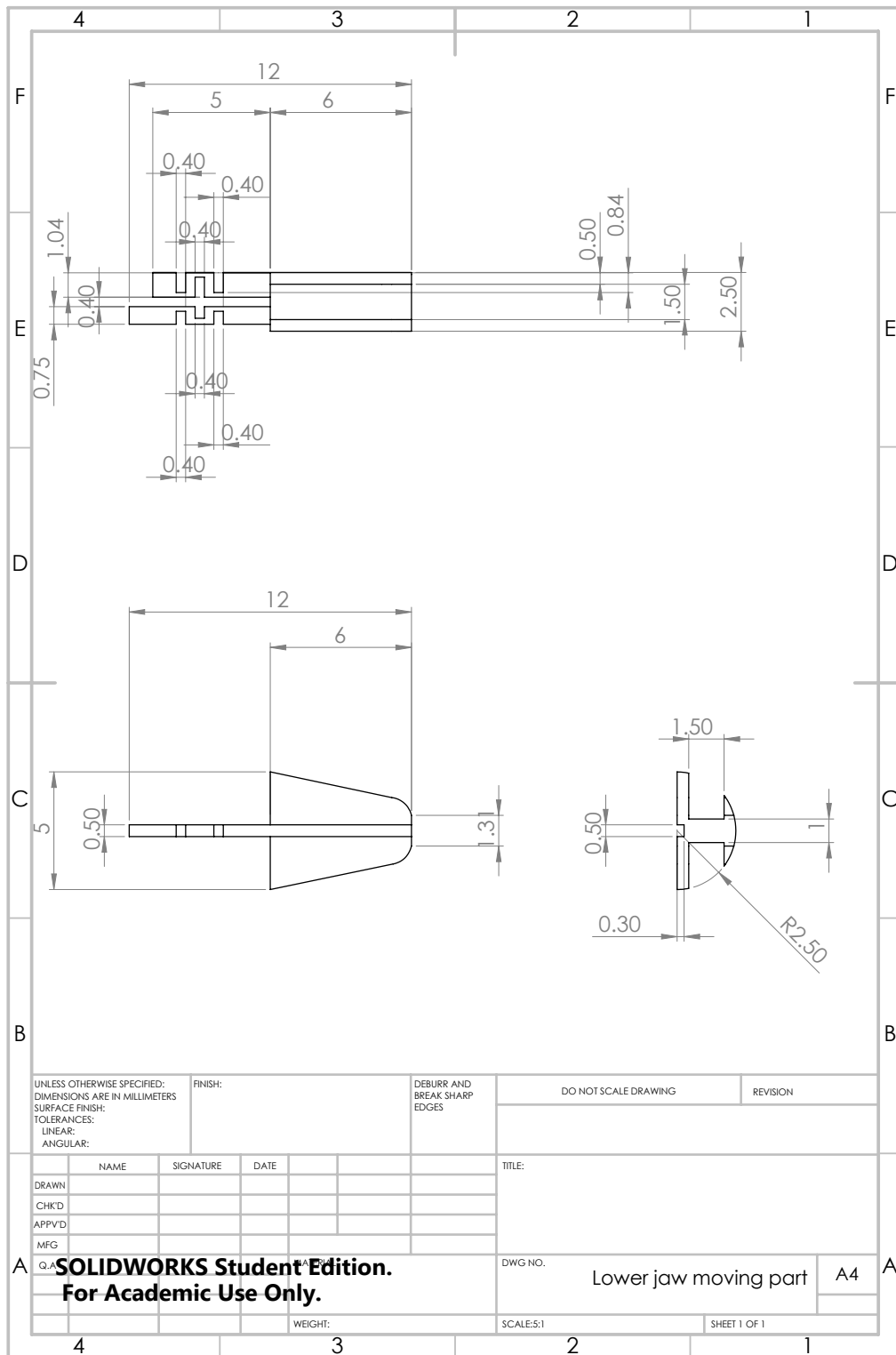


Figure A.13: Moving part of the lower jaw of the final sensorized instrument

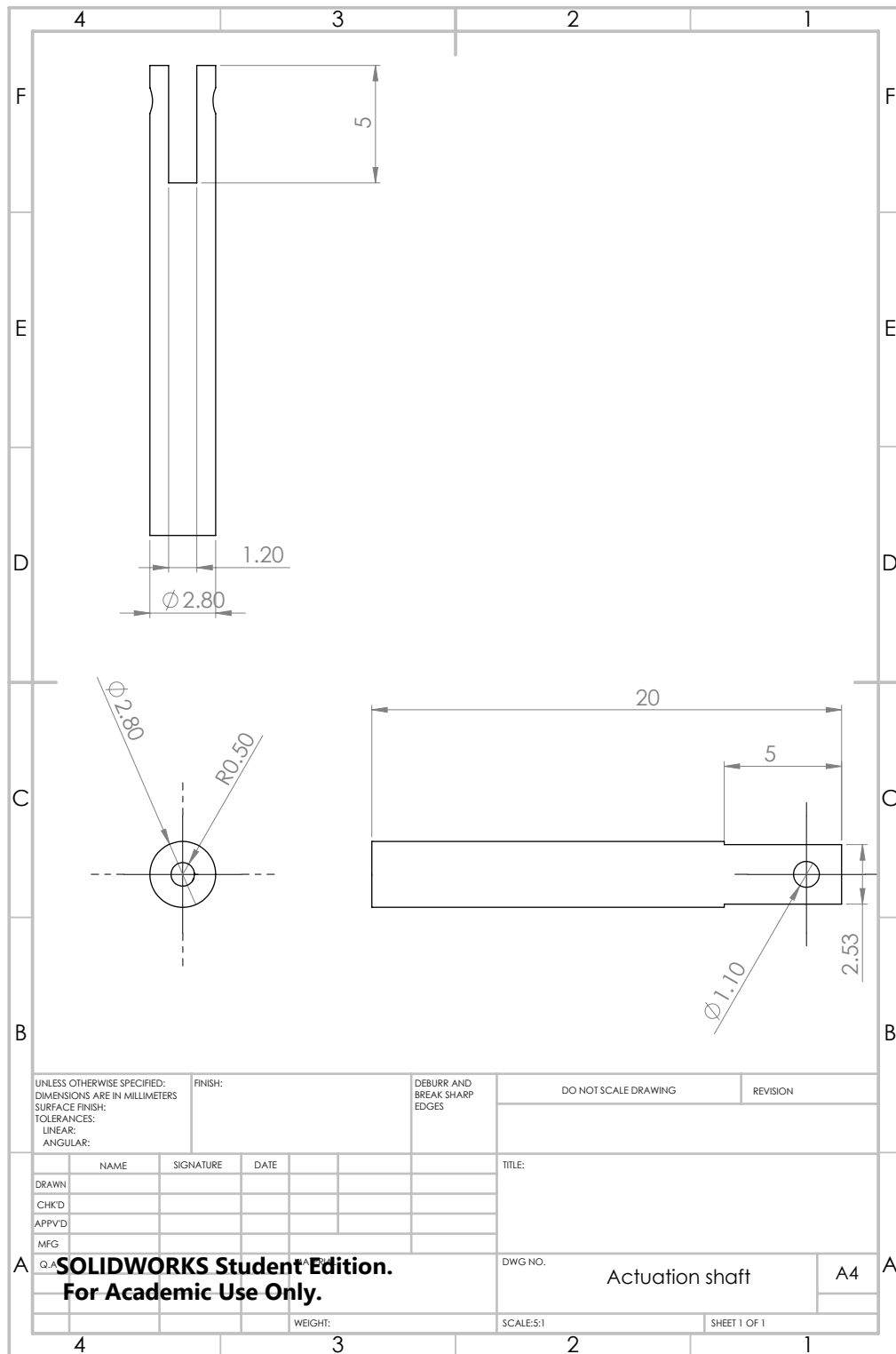


Figure A.14: Actuation shaft of the lower jaw of the final sensorized instrument

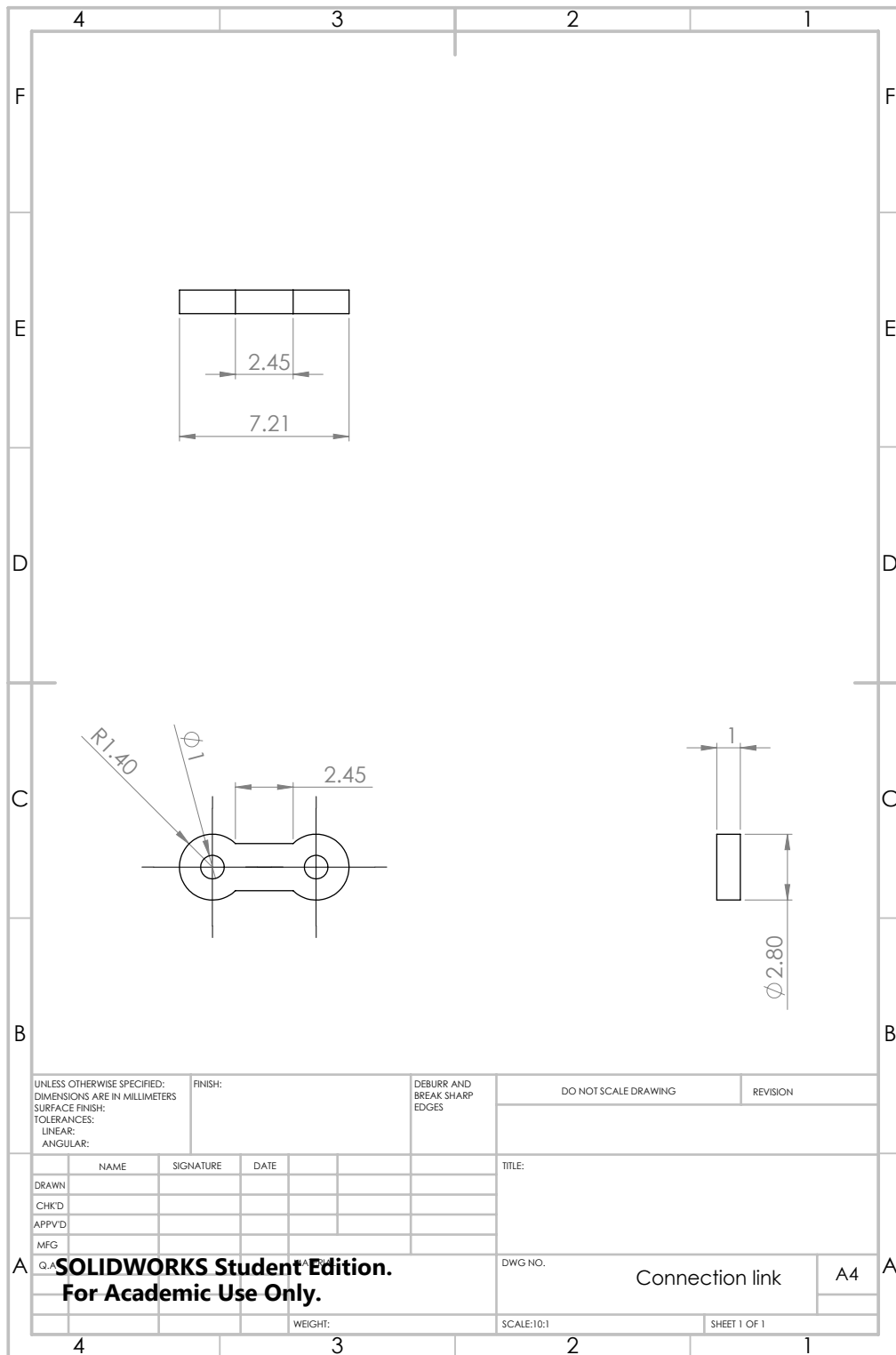


Figure A.15: Connection link for the crank-slider mechanism

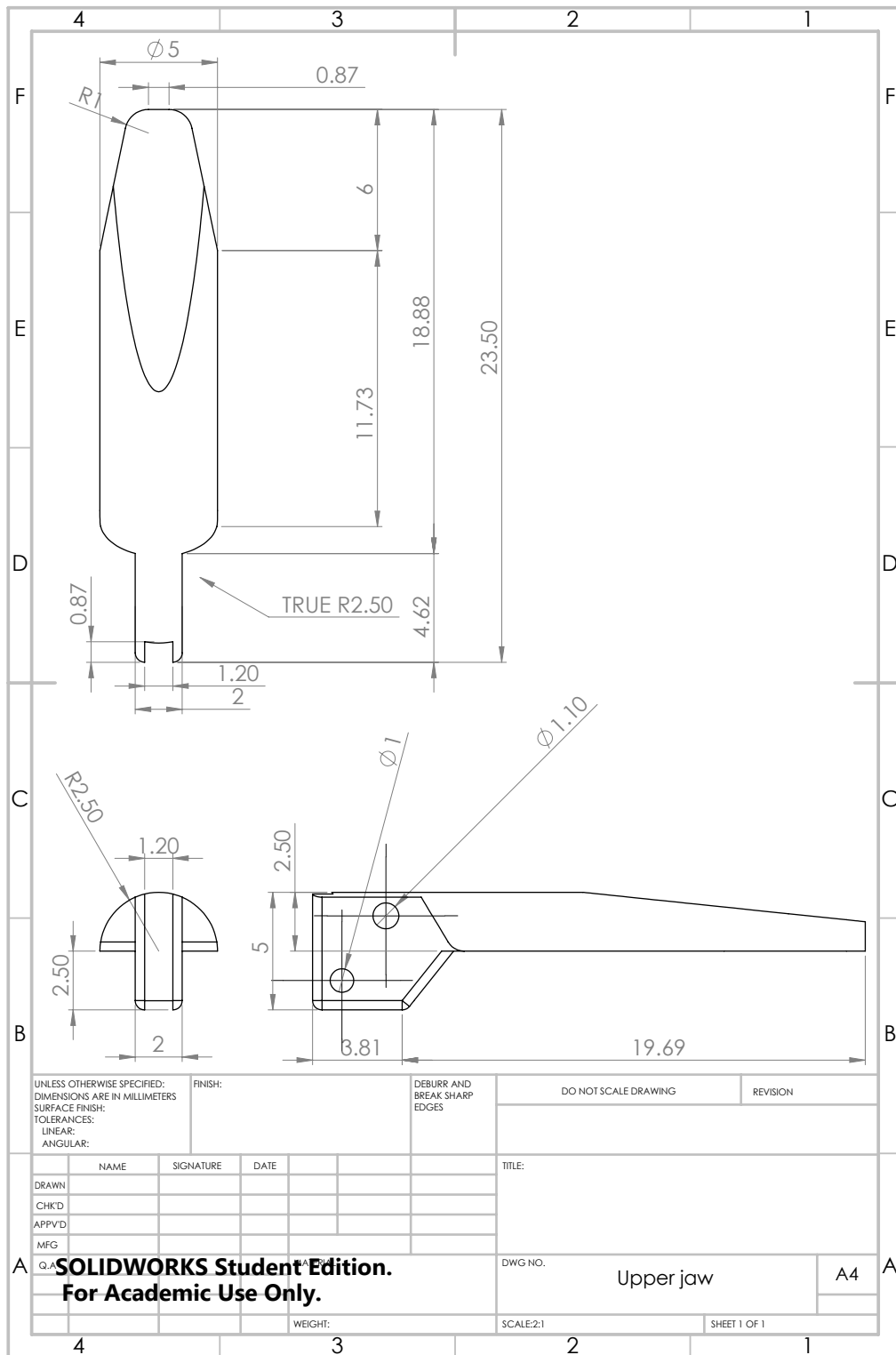


Figure A.16: Upper jaw of the final sensorized instrument

## **Appendix B**

# **Permissions and Approvals**

Copyright Clearance Center **RightsLink®** [Home](#) [Create Account](#) [Help](#) 



**Title:** Use of 3 mm percutaneous instruments with 5 mm end effectors during different laparoscopic procedures

**Author:** Giulia David, Luigi Boni, Stefano Rausei, Elisa Cassinotti, Gianlorenzo Dionigi, Francesca Rovera, Sebastiano Spampatti, Elisabetta Marta Colombo, Renzo Dionigi

**Publication:** International Journal of Surgery

**Publisher:** Elsevier

**Date:** December 2013



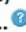



Copyright © 2013 Elsevier Ltd and Surgical Associates Ltd. All rights reserved.

**LOGIN**

If you're a **copyright.com** user, you can login to RightsLink using your copyright.com credentials. Already a RightsLink user or want to [learn more?](#)

#### Quick Price Estimate

**This reuse request is free of charge although you are required to obtain a license through Rightslink and comply with the license terms and conditions. You will not be charged for this order. To complete this transaction, click the Continue button below.**

<b>I would like to...</b> 	<input type="text" value="reuse in a thesis/dissertation"/>	<p><b>This service provides permission for reuse only.</b> If you do not have a copy of the content, you may be able to purchase a copy using RightsLink as an additional transaction. Simply select 'I would like to...' 'Purchase this content'.</p> <p>Unclear about <a href="#">who you are?</a></p>
<b>I would like to use...</b> 	<input type="text" value="figures/tables/illustrations"/>	
<b>My number of figures/tables/illustrations ...</b> 	<input type="text" value="1"/>	
<b>My format is...</b> 	<input type="text" value="electronic"/>	
<b>I am the author of this Elsevier article...</b> 	<input type="text" value="No"/>	
<b>I will be translating...</b> 	<input type="text" value="No"/>	
<b>My currency is...</b>	<input type="text" value="CAD - \$"/>	
<b>Quick Price</b>	0.00 CAD	<div style="display: flex; justify-content: center; gap: 10px;"> <div style="background-color: #0056b3; color: white; padding: 5px 15px; border-radius: 3px;">QUICK PRICE</div> <div style="background-color: #0056b3; color: white; padding: 5px 15px; border-radius: 3px;">CONTINUE</div> </div>

Exchange rates under license from [XE.com](#).  
To request permission for a type of use not listed, please contact [Elsevier](#) Global Rights Department.

Are you the [author](#) of this Elsevier journal article?

Copyright © 2017 Copyright Clearance Center, Inc. All Rights Reserved. [Privacy statement](#). [Terms and Conditions](#).  
Comments? We would like to hear from you. E-mail us at [customercare@copyright.com](mailto:customercare@copyright.com)

Figure B.1: Online permission for Figure 2.1



The screenshot shows the IEEE RightsLink interface. At the top left is the Copyright Clearance Center logo. To its right is the RightsLink logo. Further right are navigation buttons for Home, Account Info, Help, and an email icon. Below the navigation is a box with the IEEE logo and the text: "Requesting permission to reuse content from an IEEE publication". To the right of this box, the following information is displayed:

**Title:** Design of a sensorized instrument for skills assessment and training in minimally invasive surgery

**Conference Proceedings:** Biomedical Robotics and Biomechanics, 2008. BioRob 2008. 2nd IEEE RAS & EMBS International Conference on

**Author:** Ana Luisa Trejos

**Publisher:** IEEE

**Date:** Oct. 2008

Copyright © 2008, IEEE

On the right side of the page, there is a "Logged in as:" section showing the user "Pouya Soltani Zarrin" and a "LOGOUT" button.

#### Thesis / Dissertation Reuse

**The IEEE does not require individuals working on a thesis to obtain a formal reuse license, however, you may print out this statement to be used as a permission grant:**

*Requirements to be followed when using any portion (e.g., figure, graph, table, or textual material) of an IEEE copyrighted paper in a thesis:*

- 1) In the case of textual material (e.g., using short quotes or referring to the work within these papers) users must give full credit to the original source (author, paper, publication) followed by the IEEE copyright line © 2011 IEEE.
- 2) In the case of illustrations or tabular material, we require that the copyright line © [Year of original publication] IEEE appear prominently with each reprinted figure and/or table.
- 3) If a substantial portion of the original paper is to be used, and if you are not the senior author, also obtain the senior author's approval.

*Requirements to be followed when using an entire IEEE copyrighted paper in a thesis:*

- 1) The following IEEE copyright/ credit notice should be placed prominently in the references: © [year of original publication] IEEE. Reprinted, with permission, from [author names, paper title, IEEE publication title, and month/year of publication]
- 2) Only the accepted version of an IEEE copyrighted paper can be used when posting the paper or your thesis on-line.
- 3) In placing the thesis on the author's university website, please display the following message in a prominent place on the website: In reference to IEEE copyrighted material which is used with permission in this thesis, the IEEE does not endorse any of [university/educational entity's name goes here]'s products or services. Internal or personal use of this material is permitted. If interested in reprinting/republishing IEEE copyrighted material for advertising or promotional purposes or for creating new collective works for resale or redistribution, please go to [http://www.ieee.org/publications\\_standards/publications/rights/rights\\_link.html](http://www.ieee.org/publications_standards/publications/rights/rights_link.html) to learn how to obtain a License from RightsLink.

If applicable, University Microfilms and/or ProQuest Library, or the Archives of Canada may supply single copies of the dissertation.

BACK

CLOSE WINDOW

Copyright © 2017 Copyright Clearance Center, Inc. All Rights Reserved. [Privacy statement](#). [Terms and Conditions](#).  
Comments? We would like to hear from you. E-mail us at [customercare@copyright.com](mailto:customercare@copyright.com)

Figure B.2: Online permission for Figure 2.2 (a)



10/26/2017

Rightslink® by Copyright Clearance Center



RightsLink®

Home

Create Account

Help



**Title:** Prototype of Instrument for Minimally Invasive Surgery with 6-Axis Force Sensing Capability

**Conference Proceedings:** Robotics and Automation, 2005. ICRA 2005. Proceedings of the 2005 IEEE International Conference on

**Author:** U. Seibold

**Publisher:** IEEE

**Date:** 2005

Copyright © 2005, IEEE

LOGIN

If you're a **copyright.com** user, you can login to RightsLink using your copyright.com credentials. Already a **RightsLink** user or want to [learn more?](#)

### Thesis / Dissertation Reuse

**The IEEE does not require individuals working on a thesis to obtain a formal reuse license, however, you may print out this statement to be used as a permission grant:**

*Requirements to be followed when using any portion (e.g., figure, graph, table, or textual material) of an IEEE copyrighted paper in a thesis:*

- 1) In the case of textual material (e.g., using short quotes or referring to the work within these papers) users must give full credit to the original source (author, paper, publication) followed by the IEEE copyright line © 2011 IEEE.
- 2) In the case of illustrations or tabular material, we require that the copyright line © [Year of original publication] IEEE appear prominently with each reprinted figure and/or table.
- 3) If a substantial portion of the original paper is to be used, and if you are not the senior author, also obtain the senior author's approval.

*Requirements to be followed when using an entire IEEE copyrighted paper in a thesis:*

- 1) The following IEEE copyright/ credit notice should be placed prominently in the references: © [year of original publication] IEEE. Reprinted, with permission, from [author names, paper title, IEEE publication title, and month/year of publication]
- 2) Only the accepted version of an IEEE copyrighted paper can be used when posting the paper or your thesis on-line.
- 3) In placing the thesis on the author's university website, please display the following message in a prominent place on the website: In reference to IEEE copyrighted material which is used with permission in this thesis, the IEEE does not endorse any of [university/educational entity's name goes here]'s products or services. Internal or personal use of this material is permitted. If interested in reprinting/republishing IEEE copyrighted material for advertising or promotional purposes or for creating new collective works for resale or redistribution, please go to [http://www.ieee.org/publications\\_standards/publications/rights/rights\\_link.html](http://www.ieee.org/publications_standards/publications/rights/rights_link.html) to learn how to obtain a License from RightsLink.

If applicable, University Microfilms and/or ProQuest Library, or the Archives of Canada may supply single copies of the dissertation.

BACK

CLOSE WINDOW

Copyright © 2017 [Copyright Clearance Center, Inc.](#) All Rights Reserved. [Privacy statement.](#) [Terms and Conditions.](#) Comments? We would like to hear from you. E-mail us at [customer-care@copyright.com](mailto:customer-care@copyright.com)

Figure B.3: Online permission for Figure 2.2 (b)

The screenshot displays the Copyright Clearance Center RightsLink interface. At the top left is the Copyright Clearance Center logo. To its right is the RightsLink logo. Further right are navigation buttons for Home, Account Info, and Help, along with a chat icon. Below the navigation is a Taylor & Francis logo and a 'Journal Reprints' button. The main content area lists article details: Title (Fiber Bragg Grating-Based Force-Torque Sensor with Six Degrees of Freedom), Author (Mathias Stefan Müller, Lars Hoffmann, Thorbjörn Christopher Buck, et al), Publication (International Journal of Optomechatronics), Publisher (Taylor & Francis), and Date (Sep 8, 2009). A 'Logged in as: Pouya Soltani Zarrin' box with a 'LOGOUT' button is also visible. At the bottom, there is a 'Thesis/Dissertation Reuse Request' section with a paragraph of text and two buttons: 'BACK' and 'CLOSE WINDOW'. A footer contains copyright information and contact details.

Copyright Clearance Center RightsLink<sup>®</sup> Home Account Info Help

Taylor & Francis Taylor & Francis Group Journal Reprints

**Title:** Fiber Bragg Grating-Based Force-Torque Sensor with Six Degrees of Freedom  
**Author:** Mathias Stefan Müller, Lars Hoffmann, Thorbjörn Christopher Buck, et al  
**Publication:** International Journal of Optomechatronics  
**Publisher:** Taylor & Francis  
**Date:** Sep 8, 2009  
Copyright © 2009 Taylor & Francis

Logged in as: Pouya Soltani Zarrin  
LOGOUT

**Thesis/Dissertation Reuse Request**

Taylor & Francis is pleased to offer reuses of its content for a thesis or dissertation free of charge contingent on resubmission of permission request if work is published.

BACK CLOSE WINDOW

Copyright © 2017 Copyright Clearance Center, Inc. All Rights Reserved. [Privacy statement](#). [Terms and Conditions](#). Comments? We would like to hear from you. E-mail us at [customer@copyright.com](mailto:customer@copyright.com)

Figure B.4: Online permission for Figure 2.2 (c)



Copyright Clearance Center RightsLink®

Home Account Info Help

Logged in as: Pouya Soltani Zarrin LOGOUT

**IEEE**  
Requesting permission to reuse content from an IEEE publication

**Title:** A Submillimetric 3-DOF Force Sensing Instrument With Integrated Fiber Bragg Grating for Retinal Microsurgery

**Author:** Xingchi He

**Publication:** Biomedical Engineering, IEEE Transactions on

**Publisher:** IEEE

**Date:** Feb. 2014

Copyright © 2014. IEEE

### Thesis / Dissertation Reuse

**The IEEE does not require individuals working on a thesis to obtain a formal reuse license, however, you may print out this statement to be used as a permission grant:**

*Requirements to be followed when using any portion (e.g., figure, graph, table, or textual material) of an IEEE copyrighted paper in a thesis:*

- 1) In the case of textual material (e.g., using short quotes or referring to the work within these papers) users must give full credit to the original source (author, paper, publication) followed by the IEEE copyright line © 2011 IEEE.
- 2) In the case of illustrations or tabular material, we require that the copyright line © [Year of original publication] IEEE appear prominently with each reprinted figure and/or table.
- 3) If a substantial portion of the original paper is to be used, and if you are not the senior author, also obtain the senior author's approval.

*Requirements to be followed when using an entire IEEE copyrighted paper in a thesis:*

- 1) The following IEEE copyright/ credit notice should be placed prominently in the references: © [year of original publication] IEEE. Reprinted, with permission, from [author names, paper title, IEEE publication title, and month/year of publication]
- 2) Only the accepted version of an IEEE copyrighted paper can be used when posting the paper or your thesis on-line.
- 3) In placing the thesis on the author's university website, please display the following message in a prominent place on the website: In reference to IEEE copyrighted material which is used with permission in this thesis, the IEEE does not endorse any of [university/educational entity's name goes here]'s products or services. Internal or personal use of this material is permitted. If interested in reprinting/republishing IEEE copyrighted material for advertising or promotional purposes or for creating new collective works for resale or redistribution, please go to [http://www.ieee.org/publications\\_standards/publications/rights/rights\\_link.html](http://www.ieee.org/publications_standards/publications/rights/rights_link.html) to learn how to obtain a License from RightsLink.

If applicable, University Microfilms and/or ProQuest Library, or the Archives of Canada may supply single copies of the dissertation.

BACK

CLOSE WINDOW

Copyright © 2017 Copyright Clearance Center, Inc. All Rights Reserved. [Privacy statement](#). [Terms and Conditions](#). Comments? We would like to hear from you. E-mail us at [customer-care@copyright.com](mailto:customer-care@copyright.com)

Figure B.5: Online permission for Figure 2.2 (d)



The screenshot shows the IEEE RightsLink interface. At the top left is the Copyright Clearance Center logo. To its right is the RightsLink logo. Further right are navigation buttons for Home, Account Info, and Help, along with a chat icon. Below the navigation is a box with the IEEE logo and the text: "Requesting permission to reuse content from an IEEE publication". To the right of this box, the following information is displayed:

**Title:** Design of 3-DOF force sensing micro-forceps for robot assisted vitreoretinal surgery

**Conference Proceedings:** Engineering in Medicine and Biology Society (EMBC), 2013 35th Annual International Conference of the IEEE

**Author:** Berk Gonenc

**Publisher:** IEEE

**Date:** July 2013

Copyright © 2013, IEEE

On the right side, there is a "Logged in as:" section showing the user "Pouya Soltani Zarrin" and a "LOGOUT" button.

#### Thesis / Dissertation Reuse

**The IEEE does not require individuals working on a thesis to obtain a formal reuse license, however, you may print out this statement to be used as a permission grant:**

*Requirements to be followed when using any portion (e.g., figure, graph, table, or textual material) of an IEEE copyrighted paper in a thesis:*

- 1) In the case of textual material (e.g., using short quotes or referring to the work within these papers) users must give full credit to the original source (author, paper, publication) followed by the IEEE copyright line © 2011 IEEE.
- 2) In the case of illustrations or tabular material, we require that the copyright line © [Year of original publication] IEEE appear prominently with each reprinted figure and/or table.
- 3) If a substantial portion of the original paper is to be used, and if you are not the senior author, also obtain the senior author's approval.

*Requirements to be followed when using an entire IEEE copyrighted paper in a thesis:*

- 1) The following IEEE copyright/ credit notice should be placed prominently in the references: © [year of original publication] IEEE. Reprinted, with permission, from [author names, paper title, IEEE publication title, and month/year of publication]
- 2) Only the accepted version of an IEEE copyrighted paper can be used when posting the paper or your thesis on-line.
- 3) In placing the thesis on the author's university website, please display the following message in a prominent place on the website: In reference to IEEE copyrighted material which is used with permission in this thesis, the IEEE does not endorse any of [university/educational entity's name goes here]'s products or services. Internal or personal use of this material is permitted. If interested in reprinting/republishing IEEE copyrighted material for advertising or promotional purposes or for creating new collective works for resale or redistribution, please go to [http://www.ieee.org/publications\\_standards/publications/rights/rights\\_link.html](http://www.ieee.org/publications_standards/publications/rights/rights_link.html) to learn how to obtain a License from RightsLink.

If applicable, University Microfilms and/or ProQuest Library, or the Archives of Canada may supply single copies of the dissertation.

BACK

CLOSE WINDOW

Copyright © 2017 Copyright Clearance Center, Inc. All Rights Reserved. [Privacy statement](#). [Terms and Conditions](#).  
Comments? We would like to hear from you. E-mail us at [customercare@copyright.com](mailto:customercare@copyright.com)

Figure B.6: Online permission for Figure 2.2 (e)





Copyright Clearance Center  
RightsLink®

Home Account Info Help

Logged in as:  
Pouya Soltani Zarrin  
LOGOUT

**IEEE**  
Requesting permission to reuse content from an IEEE publication

**Title:** Miniature 3-Axis Distal Force Sensor for Minimally Invasive Surgical Palpation  
**Author:** Pinyo Puangmali  
**Publication:** Mechatronics, IEEE/ASME Transactions on  
**Publisher:** IEEE  
**Date:** Aug. 2012  
Copyright © 2012, IEEE

#### Thesis / Dissertation Reuse

**The IEEE does not require individuals working on a thesis to obtain a formal reuse license, however, you may print out this statement to be used as a permission grant:**

*Requirements to be followed when using any portion (e.g., figure, graph, table, or textual material) of an IEEE copyrighted paper in a thesis:*

- 1) In the case of textual material (e.g., using short quotes or referring to the work within these papers) users must give full credit to the original source (author, paper, publication) followed by the IEEE copyright line © 2011 IEEE.
- 2) In the case of illustrations or tabular material, we require that the copyright line © [Year of original publication] IEEE appear prominently with each reprinted figure and/or table.
- 3) If a substantial portion of the original paper is to be used, and if you are not the senior author, also obtain the senior author's approval.

*Requirements to be followed when using an entire IEEE copyrighted paper in a thesis:*

- 1) The following IEEE copyright/ credit notice should be placed prominently in the references: © [year of original publication] IEEE. Reprinted, with permission, from [author names, paper title, IEEE publication title, and month/year of publication]
- 2) Only the accepted version of an IEEE copyrighted paper can be used when posting the paper or your thesis on-line.
- 3) In placing the thesis on the author's university website, please display the following message in a prominent place on the website: In reference to IEEE copyrighted material which is used with permission in this thesis, the IEEE does not endorse any of [university/educational entity's name goes here]'s products or services. Internal or personal use of this material is permitted. If interested in reprinting/republishing IEEE copyrighted material for advertising or promotional purposes or for creating new collective works for resale or redistribution, please go to [http://www.ieee.org/publications\\_standards/publications/rights/rights\\_link.html](http://www.ieee.org/publications_standards/publications/rights/rights_link.html) to learn how to obtain a License from RightsLink.

If applicable, University Microfilms and/or ProQuest Library, or the Archives of Canada may supply single copies of the dissertation.

BACK

CLOSE WINDOW

Copyright © 2017 Copyright Clearance Center, Inc. All Rights Reserved. [Privacy statement](#). [Terms and Conditions](#).  
Comments? We would like to hear from you. E-mail us at [customercare@copyright.com](mailto:customercare@copyright.com)

Figure B.7: Online permission for Figure 2.2 (f)

1/6/2017

RightsLink Printable License

**ELSEVIER LICENSE  
TERMS AND CONDITIONS**

Jan 06, 2017

This Agreement between Pouya Soltani Zarrin ("You") and Elsevier ("Elsevier") consists of your license details and the terms and conditions provided by Elsevier and Copyright Clearance Center.

License Number	4023221202341
License date	Jan 06, 2017
Licensed Content Publisher	Elsevier
Licensed Content Publication	Sensors and Actuators A: Physical
Licensed Content Title	A micro optical force sensor for force feedback during minimally invasive robotic surgery
Licensed Content Author	Jan Peirs,Joeri Clijnen,Dominiek Reynaerts,Hendrik Van Brussel,Paul Herijgers,Brecht Corteville,Sarah Boone
Licensed Content Date	21 September 2004
Licensed Content Volume Number	115
Licensed Content Issue Number	2-3
Licensed Content Pages	9
Start Page	447
End Page	455
Type of Use	reuse in a thesis/dissertation
Intended publisher of new work	other
Portion	figures/tables/illustrations
Number of figures/tables/illustrations	1
Format	both print and electronic
Are you the author of this Elsevier article?	No
Will you be translating?	No
Order reference number	
Original figure numbers	Figure 1
Title of your thesis/dissertation	Optical Fiber-based MIS Instruments
Expected completion date	Dec 2017
Estimated size (number of pages)	150
Elsevier VAT number	GB 494 6272 12
Requestor Location	Pouya Soltani Zarrin

Figure B.8: Online permission for Figure 2.2 (g)



Copyright Clearance Center RightsLink®

Home Account Info Help

Logged in as: Pouya Soltani Zarrin  
LOGOUT

**IEEE**  
Requesting permission to reuse content from an IEEE publication

**Title:** Preliminary design of multi-axial contact force sensor for minimally invasive robotic surgery grasper

**Conference Proceedings:** Robotics and Automation (ICRA), 2013 IEEE International Conference on

**Author:** Dong-Hyuk Lee

**Publisher:** IEEE

**Date:** May 2013

Copyright © 2013, IEEE

#### Thesis / Dissertation Reuse

**The IEEE does not require individuals working on a thesis to obtain a formal reuse license, however, you may print out this statement to be used as a permission grant:**

*Requirements to be followed when using any portion (e.g., figure, graph, table, or textual material) of an IEEE copyrighted paper in a thesis:*

- 1) In the case of textual material (e.g., using short quotes or referring to the work within these papers) users must give full credit to the original source (author, paper, publication) followed by the IEEE copyright line © 2011 IEEE.
- 2) In the case of illustrations or tabular material, we require that the copyright line © [Year of original publication] IEEE appear prominently with each reprinted figure and/or table.
- 3) If a substantial portion of the original paper is to be used, and if you are not the senior author, also obtain the senior author's approval.

*Requirements to be followed when using an entire IEEE copyrighted paper in a thesis:*

- 1) The following IEEE copyright/ credit notice should be placed prominently in the references: © [year of original publication] IEEE. Reprinted, with permission, from [author names, paper title, IEEE publication title, and month/year of publication]
- 2) Only the accepted version of an IEEE copyrighted paper can be used when posting the paper or your thesis on-line.
- 3) In placing the thesis on the author's university website, please display the following message in a prominent place on the website: In reference to IEEE copyrighted material which is used with permission in this thesis, the IEEE does not endorse any of [university/educational entity's name goes here]'s products or services. Internal or personal use of this material is permitted. If interested in reprinting/republishing IEEE copyrighted material for advertising or promotional purposes or for creating new collective works for resale or redistribution, please go to [http://www.ieee.org/publications\\_standards/publications/rights\\_link.html](http://www.ieee.org/publications_standards/publications/rights_link.html) to learn how to obtain a License from RightsLink.

If applicable, University Microfilms and/or ProQuest Library, or the Archives of Canada may supply single copies of the dissertation.

BACK CLOSE WINDOW

Copyright © 2017 Copyright Clearance Center, Inc. All Rights Reserved. [Privacy statement](#). [Terms and Conditions](#). Comments? We would like to hear from you. E-mail us at [customer@copyright.com](mailto:customer@copyright.com)

Figure B.9: Online permission for Figure 2.2 (h)



The screenshot displays the Copyright Clearance Center RightsLink interface. At the top left is the Copyright Clearance Center logo. To its right is the RightsLink logo. Further right are navigation buttons for Home, Account Info, and Help, along with a chat icon. The main content area features the SAGE Publishing logo on the left and a list of article details on the right. The article details include the title, author, publication information, publisher, and date. A user is logged in as Pouya Soltani Zarrin, with a Logout button. Below the article details is a 'Gratis Reuse' section with a paragraph of text and two buttons: BACK and CLOSE WINDOW. At the bottom, there is a copyright notice and contact information.

**Copyright Clearance Center** RightsLink®

Home Account Info Help Chat

**SAGE** Publishing

**Title:** Force sensing and its application in minimally invasive surgery and therapy: A survey

**Author:** A L Trejos, R V Patel, M D Naish

**Publication:** Proceedings of the Institution of Mechanical Engineers, Part C: Journal of Mechanical Engineering Science

**Publisher:** SAGE Publications

**Date:** 07/01/2010

Copyright © 2010, © SAGE Publications

Logged in as: Pouya Soltani Zarrin

LOGOUT

**Gratis Reuse**

Permission is granted at no cost for use of content in a Master's Thesis and/or Doctoral Dissertation. If you intend to distribute or sell your Master's Thesis/Doctoral Dissertation to the general public through print or website publication, please return to the previous page and select 'Republish in a Book/Journal' or 'Post on intranet/password-protected website' to complete your request.


BACK CLOSE WINDOW

Copyright © 2017 Copyright Clearance Center, Inc. All Rights Reserved. [Privacy statement](#). [Terms and Conditions](#). Comments? We would like to hear from you. E-mail us at [customercare@copyright.com](mailto:customercare@copyright.com)

Figure B.10: Online permission for Figure 2.3



MDPI Journals A-Z Information & Guidelines About Editorial Process



Title / Keyword  Journal   
 Author  Section   
 Article Type  Special Issue

---

**MDPI Contact**

### MDPI Open Access Information and Policy

All articles published by MDPI are made immediately available worldwide under an open access license. This means:

- everyone has free and unlimited access to the full-text of *all* articles published in MDPI journals, and
- everyone is free to re-use the published material if proper accreditation/citation of the original publication is given.
- open access publication is supported by the authors' institutes or research funding agencies by payment of a comparatively low [Article Processing Charge \(APC\)](#) for accepted articles.

---

#### External Open Access Resources

MDPI is a [RoMEO green publisher](#) — RoMEO is a database of Publishers' copyright and self-archiving policies hosted by the [University of Nottingham](#)

Those who are new to the concept of open access might find the following websites or 'Open Access 101' video informative:

[Wikipedia article on 'Open Access'](#)  
[Peter Suber's 'Open Access Overview'](#)  
[Information Platform Open Access](#) [in [English](#), in [German](#)]  
[SHERPA's 'Authors and Open Access'](#)

---

#### Meaning of Open Access

In accordance with major definitions of open access in scientific literature (namely the Budapest, Berlin, and Bethesda declarations), MDPI defines *open access* by the following conditions:

- peer-reviewed literature is freely available without subscription or price barriers,
- literature is immediately released in open access format (no embargo period), and
- published material can be re-used without obtaining permission as long as a correct citation

#### Open Access Explained!



Figure B.11: Online permission for Figure 2.4

25/10/2017

Rightslink® by Copyright Clearance Center



RightsLink®

Home

Create Account

Help



**Title:** Development of an optical fiber-based sensor for grasping and axial force sensing

**Conference Proceedings:** Robotics and Automation (ICRA), 2017 IEEE International Conference on

**Author:** Pouya Soltani Zarrin

**Publisher:** IEEE

**Date:** May 2017

Copyright © 2017, IEEE

LOGIN

If you're a **copyright.com** user, you can login to RightsLink using your copyright.com credentials. Already a **RightsLink** user or want to [learn more?](#)

### Thesis / Dissertation Reuse

**The IEEE does not require individuals working on a thesis to obtain a formal reuse license, however, you may print out this statement to be used as a permission grant:**

*Requirements to be followed when using any portion (e.g., figure, graph, table, or textual material) of an IEEE copyrighted paper in a thesis:*

- 1) In the case of textual material (e.g., using short quotes or referring to the work within these papers) users must give full credit to the original source (author, paper, publication) followed by the IEEE copyright line © 2011 IEEE.
- 2) In the case of illustrations or tabular material, we require that the copyright line © [Year of original publication] IEEE appear prominently with each reprinted figure and/or table.
- 3) If a substantial portion of the original paper is to be used, and if you are not the senior author, also obtain the senior author's approval.

*Requirements to be followed when using an entire IEEE copyrighted paper in a thesis:*

- 1) The following IEEE copyright/ credit notice should be placed prominently in the references: © [year of original publication] IEEE. Reprinted, with permission, from [author names, paper title, IEEE publication title, and month/year of publication]
- 2) Only the accepted version of an IEEE copyrighted paper can be used when posting the paper or your thesis on-line.
- 3) In placing the thesis on the author's university website, please display the following message in a prominent place on the website: In reference to IEEE copyrighted material which is used with permission in this thesis, the IEEE does not endorse any of [university/educational entity's name goes here]'s products or services. Internal or personal use of this material is permitted. If interested in reprinting/republishing IEEE copyrighted material for advertising or promotional purposes or for creating new collective works for resale or redistribution, please go to [http://www.ieee.org/publications\\_standards/publications/rights/rights\\_link.html](http://www.ieee.org/publications_standards/publications/rights/rights_link.html) to learn how to obtain a License from RightsLink.

If applicable, University Microfilms and/or ProQuest Library, or the Archives of Canada may supply single copies of the dissertation.

BACK

CLOSE WINDOW

Copyright © 2017 [Copyright Clearance Center, Inc.](#) All Rights Reserved. [Privacy statement](#). [Terms and Conditions](#). Comments? We would like to hear from you. E-mail us at [customer-care@copyright.com](mailto:customer-care@copyright.com)

Figure B.12: Online permission for Figures 3.2 – 3.14

## CURRICULUM VITAE

**Name:** Pouya Soltani Zarrin

**Post-secondary Education and Degrees:** The University of Western Ontario  
London, Ontario, Canada  
2015–2017 M.E.Sc.,  
Biomedical Engineering

The University of Tabriz  
Tabriz, E.Azerbaijan, IRAN  
2011–2015 B.Sc.,  
Mechanical Engineering

**Membership and Affiliation:** Canadian Surgical Technologies and Advanced Robotics (CSTAR)  
Lawson Health Research Institute  
University of Western Ontario

**Honours and Awards:** German academic exchange scholarship (DAAD)  
Ranked among top 10 students of Mechanical Engineering students (9 out of 133)  
Ranked among top 0.1% of applicants of the nation-wide university entrance exam

**Related Work Experience:** Research Assistant  
Canadian Surgical Technologies and Advanced Robotics  
The University of Western Ontario, London, Canada  
2015-2017

Design Engineer Intern  
The Innovations for High Performances  
IHP GmbH, Frankfurt (Oder), Germany  
2017

Teaching Assistant

*Fall 2017 – Engineering Thermodynamics*

*Winter 2017 – Electric Circuits and Electromechanics*

*Summer 2016 – Risk Assessment and Management in Engineering Systems*

*Fall & Winter 2016 – C++ Programming Fundamentals for Engineers*

*Fall 2015 – Materials Selection and Manufacturing Process*

The University of Western Ontario

2015–2017

**Related Publications:**

**P. S. Zarrin**, A. Escoto, R. Xu, M. D. Naish, R. V. Patel, and A. L. Trejos. Development of an optical fiber-based sensor for grasping and axial force sensing. In IEEE International Conference on Robotics and Automation (ICRA), Singapore, May, 2017, pp. 939-944.

**P. S. Zarrin**, A. Escoto, R. Xu, M. D. Naish, R. V. Patel, and A. L. Trejos. Development of a 2-DOF sensorized surgical grasper for grasping and axial force measurements, Submitted paper to IEEE Sensors Journal; (revision requested).